AD _____

ENVIRONMENTAL FATE OF WHITE PHOSPHORUS/FELT AND RED PHOSPHORUS/BUTYL RUBBER MILITARY SCREENING SMOKES

FINAL REPORT

RONALD J. SPANGGORD
ROBERT REWICK
TSONG-WEN CHOU
ROBERT WILSON
R. THOMAS PODOLL
THEODORE MILL
RICHARD PARNAS
ROBERT PLATZ
DARYL ROBERTS

APRIL 1985

Supported by

U.S. ARMY MEDICAL RESEARCH AND DEVELOPMENT COMMAND
Fort Detrick, Frederick, Maryland 21701-5012

Contract No. DAMD17-82-C-2320
SRI Project PYU-4937

SRI International
333 Ravenswood Avenue
Menlo Park, California 94025-3493

Jesse J. Barkley, Contracting Officer Technical Representative
U.S. Army Medical Bioengineering Research and Development Laboratory
Fort Detrick, Frederick, Maryland 21701-5010

Approved for public release; distribution unlimited

The findings in this report are not to be construed as an official Department of the Army position unless so designated by other authorized documents.

SECURITY CLASSIFICATION OF THIS PAGE AD-A176 922

REPORT DOCUMENTATION PAGE

1a. REPORT SECURITY CLASSIFICATION Unclassified	1b. RESTRICTIVE MARKINGS
2a. SECURITY CLASSIFICATION AUTHORITY	3. DISTRIBUTION / AVAILABILITY OF REPORT Approved for public release; distribution unlimited
2b. DECLASSIFICATION / DOWNGRADING SCHEDULE	
4. PERFORMING ORGANIZATION REPORT NUMBER(S) PYU-4937	5. MONITORING ORGANIZATION REPORT NUMBER(S)
6a. NAME OF PERFORMING ORGANIZATION SRI International 6b. OFFICE SYMBOL (If applicable)	7a. NAME OF MONITORING ORGANIZATION U.S. Army Medical Bioengineering R&D Laboratory Environmental Protection Research Divison
6c. ADDRESS (City, State, and ZIP Code) Menlo Park, CA 94025	7b. ADDRESS (City, State, and ZIP Code) Fort Detrick, Frederick, MD 21701-5010
8a. NAME OF FUNDING / SPONSORING ORGANIZATION U.S. Army Medical Research & Development Com. 8b. OFFICE SYMBOL (If applicable)	9. PROCUREMENT INSTRUMENT IDENTIFICATION NUMBER DAMD17-82-C-2320
8c. ADDRESS (City, State, and ZIP Code) Fort Detrick, Frederick, MD 21701-5012	10. SOURCE OF FUNDING NUMBERS PROGRAM ELEMENT NO. 62720A; PROJECT NO. 3E162720A835; TASK NO. AA; WORK UNIT ACCESSION NO. 075

11. TITLE (Include Security Classification)
Environmental Fate of White Phosphorus/Felt and Red Phosphorus/Butyl Rubber Military Screening Smokes

12. PERSONAL AUTHOR(S) Ronald J. Spanggord, Robert Rewick, Tsong-wen Chou, Robert Wilson, R. Thomas Podoll, Theodore Mill, Richard Parnas, Robert Platz, Daryl Roberts

13a. TYPE OF REPORT	13b. TIME COVERED	14. DATE OF REPORT (Year, Month, Day)	15. PAGE COUNT
Final Report	FROM 82/9/30 TO 85/1/31	1985 April	187

16. SUPPLEMENTARY NOTATION

17. COSATI CODES			18. SUBJECT TERMS (Continue on reverse if necessary and identify by block number)
FIELD	GROUP	SUB-GROUP	Environmental fate; Phosphorus; Screening smoke; Chemical transformation; Biodegradation
07	02		
07	03		

19. ABSTRACT (Continue on reverse if necessary and identify by block number)

Investigations were conducted to identify those processes that control the loss and movement of WP/F, RP/BR, and their combustion products in air, soil, and aquatic environments. (WP/F = white phosphorus / felt; RP/BR = Red phosphorus / Butyl Rubber)

The fate of RP/BR will be controlled by oxidative transformation. In air, half-lives of 1.8 years were found while in aerated water, the half-life approach 3 years and was found to be dependent on both particle size and oxygen concentration. In soil, the transformation was limited by oxygen diffusion and half-lives into the thousands of years were projected. cont'd

WP/F was found to react extremely rapidly with air ($t_{1/2}$ ~5 min) while it was found to be quite persistent as a suspension in water ($t_{1/2}$ = 2.4 years. Dissolution rates for WP/F

20. DISTRIBUTION / AVAILABILITY OF ABSTRACT	21. ABSTRACT SECURITY CLASSIFICATION
☐ UNCLASSIFIED/UNLIMITED ☒ SAME AS RPT. ☐ DTIC USERS	UNCLASSIFIED
22a. NAME OF RESPONSIBLE INDIVIDUAL Mrs. Virginia Miller	22b. TELEPHONE (Include Area Code) 301/663-7325
22c. OFFICE SYMBOL SGRD-RMS	

DD FORM 1473, 84 MAR 83 APR edition may be used until exhausted. All other editions are obsolete.

SECURITY CLASSIFICATION OF THIS PAGE

19. (Continued)

In water were measured to be 1 x 10^{-7} g hr^{-1} cm^{-2}. Soluble WP will be lost to the atmosphere through volatilization ($t_{1/2}$ = 48 min) in shallow and turbulent streams while both oxidative and hydrolytic processes will equally control the loss of WP in deep water bodies ($t_{1/2}$ = 42 hrs). Humic materials in natural waters were found to have a stability effect on soluble WP. In soil, WP will be highly persistent and its transformation will be limited by oxygen diffusion. A minimum life-time of 10 years was projected for a 1 cm^3 chunk of WP buried 12 cm beneath the surface. Longer life-times are projected at deeper depths and the buildup of surface oxide layers will add to the persistence.

cont'd

The oxidative transformation and combustion of WP/F and RP/BR lead to the formation of linear condensed polyphosphates, (P_1-P_{22}), phosphoric acid, phosphorous acid, hypophosphorous acid, and phosphine. The linear polyphosphates hydrolyze rapidly at low pH ($t_{1/2}$ = 2 days) which is expected in the aerosol phase. In a neutralized state, the polyphosphates are subject to slow chemical hydrolysis ($t_{1/2}$ = 100 days). Microorganisms will hydrolyze linear polyphosphates in soils and water with half lives of 15 days in systems containing 1 x 10^5 organisms/ml (gm). Cyclic meta-phosphates (tri-, tetra-, and (hexa-) are formed from the linear polyphosphates in aqueous solution and are stable to chemical hydrolysis ($t_{1/2}$ = 3 years). However, microorganisms can utilize these compounds as a phosphate source with a half-life of 20 days.

100,000

Phosphorous acid is stable to chemical transformation under environmental conditions, however microorganisms will biotransform this chemical to orthophosphoric acid with a half-life of 25-35 days. Phosphine is rapidly transported to the vapor phase where reactions with ozone and hydroxyl radical will limit its persistence to half-lives of 2-3 hours.

Using laboratory generated transport and transformation rates constants, computer models for aquatic, terrestrial, and atmospheric environments were constructed to simulate the loss and movement of WP/F, RP/BR and their combustion products under selected environmental senarios.

DISTRIBUTION

25 copies	Commander US Army Medical Bioengineering Research and Development Laboratory ATTN: SGRD-UBG-M Fort Detrick Frederick, MD 21701
1 copy	Commander US Army Medical Research and Development Command ATTN: SGRD-RMI-S Fort Detrick Frederick, MD 21701-5012
1 copy	Defense Technical Information Center (DTIC) ATTN: DTIC-DDA Cameron Station Alexandria, VA 22304-6145
1 copy	Dean School of Medicine Uniformed Services University of the Health Sciences 4301 Jones Bridge Road Bethesda, MD 20814-4799
1 copy	Commandant Academy of Health Sciences, US Army ATTN: AHS-CDM Fort Sam Houston, TX 78234-6100
1 copy	Commander US Army Medical Bioengineering Research and Development Laboratory ATTN: SGRD-UBD-A/Librarian Fort Detrick Frederick, MD 21701-5010
1 copy	Commander US Army Materiel Command ATTN: AMCEN-A 5001 Eisenhower Ave. Alexandria, VA 22333-0001

CONTENTS

FIGURES

TABLES

ACKNOWLEDGEMENTS

We are again indebted to our staff of scientists who provided the data that were key to the assessment of the fate of smoke re[illegible]ed products in the environment. They are Philip Alferness and [illegible]man Lau (Analytical Chemistry), Doris Tse, Karen Sundback, and Ann-Marie Liu (Chemical Transformations), Kathy Irwin, James Harper, and Barbara Kingsley (Physical Transport), Justine Whaley and Julie Parker (Biotransformation), and Russel Gates and Walter Johnson (Scale Model Deployment). We also thank the Contracting Officer's Technical Representatives, Kathryn Kenyon and Jesse Barkley, Jr., for their support throughout this project.

EXECUTIVE SUMMARY

Investigations were conducted to identify those processes that control the loss and movement of WP/F, RP/BR, and their combustion products in air, soil, and aquatic environments.

The fate of RP/BR will be controlled by oxidative transformation. In air, half-lives of 1.8 years were found while in aerated water, the half-life approached 3 years and was found to be dependent on both particle size and oxygen concentration. In soil, the transformation was limited by oxygen diffusion and half-lives into the thousands of years were projected.

WP/F was found to react extremely rapidly with air ($t_{1/2} \sim 5$ min) while it was found to be quite persistent as a suspension in water ($t_{1/2} = 2.4$ years). Dissolution rates for WP/F in water were measured to be 1×10^{-7} g hr^{-1} cm^{-2}. Soluble WP will be lost to the atmosphere through volatilization ($t_{1/2} = 48$ min) in shallow and turbulent streams while both oxidative and hydrolytic processes will equally control the loss of WP in deep water bodies ($t_{1/2} = 42$ hrs). Humic materials in natural waters were found to have a stability effect on soluble WP. In soil, WP will be highly persistent and its transformation will be limited by oxygen diffusion. A minimum life-time of 10 years was projected for a 1 cm^3 chunk of WP buried 12 cm beneath the surface. Longer life-times are projected at deeper depths and the buildup of surface oxide layers will add to the persistence.

The oxidative transformations and combustion of WP/F and RP/BR lead to the formation of linear condensed polyphosphates, (P_1-P_{22}), phosphoric acid, phosphorous acid, hypophosphorous acid, and phosphine. The linear polyphosphates hydrolyze rapidly at low pH ($t_{1/2} = 2$ days) which is expected in the aerosol phase. In a neutralized state, the polyphosphates are subject to slow chemical hydrolysis ($t_{1/2} = 100$ days). Microorganisms will hydrolyze linear polyphosphates in soils and water with half lives of

15 days in systems containing 1 x 10^5 organisms/ml (gm). Cyclic meta-phosphates (tri-, tetra-, and hexa-) are formed from the linear polyphosphates in aqueous solution and are stable to chemical hydrolysis ($t_{1/2}$ = 3 years). However, microorganisms can utilize these compounds as a phosphate source with a half-life of 20 days.

Phosphorous acid is stable to chemical transformations under environmental conditions, however microorganisms will biotransform this chemical to orthophosphoric acid with a half-life of 25-35 days. Phosphine is rapidly transported to the vapor phase where reactions with ozone and hydroxyl radical will limit its persistence to half-lives of 2-3 hours.

Using laboratory generated transport and tranformation rates constants, computer models for aquatic (SRI aquatic model), terrestrial (SRI terrestrial model), and atmospheric (MAEROS) environments were constructed to simulate the loss and movement of WP/F, RP/BR and their combustion products under selected environmental senarios.

I INTRODUCTION

The increased use of smokes and obscurants in military training exercises has brought about a concern for the effects of both combusted and uncombusted smoke products on the environment and human health. In training exercises, smoke is generated to simulate actual battlefield conditions. This results in potentially significant contamination of terrestrial, aquatic, and atmospheric environments in training areas. The persistence of such smoke in these environments is not well understood. Also, the deposition of smoke products into the environment from the incomplete combustion of smoke devices and because of past and present smoke materials manufacturing practices of smoke has led to further concern as to the fate of these agents in the environment.

Two such agents used in training exercises are white phosphorus/felt (WP/F) and red phosphorus/butyl rubber (RP/BR). WP/F is currently manufactured by Pine Bluff Arsenal (PBA) in Pine Bluff, Arkansas. RP/BR is currently produced in Great Britian and shipped to PBA for incorporation into smoke devices. Because of a paucity of information available to estimate the persistence of these agents in the environment, the magnitude of potential environmental effects is difficult to estimate.

To help increase the knowledge and understanding within this area, this report describes the efforts of SRI International to assess the dominant processes that affect the loss and movement of WP/F and RP/BR when dispersed into the environment in both their combusted and uncombusted forms. After initial identification and compositional studies of smoke components, investigational studies were conducted into the transport and transformation processes that affect the persistence of each component. These studies included solubility measurements, dissolution studies, Henry's Constant determinations, sorption and octanol-water partition coefficients, and volatilization rate constant measurements to describe physical transport processes. Transformation processes studied were

chemical oxidation in soil and water, hydrolysis, biotransformation, and transformation by the tropospheric agents, hydroxyl radical and ozone.

We conducted kinetic investigations of dominant processes, from which rate constants were established. From these data, we projected half-lives for specific components in terrestrial, aquatic, and atmospheric environments. These data were then incorporated into computer simulation models to project the overall behavior and persistence of phosphorus smoke products in the environment.

II BACKGROUND

The use of screening smoke in military operations is effective in visually concealing personnel and materiel, screening targets, and creating confusion and deception among enemy troops. Two such smokes used in military tactics are WP/F and RP/BR. They are usually deployed from field artillery, grenades, mortars, and smoke pots. WP/F consists of 75-80% elemental phosphorus solidified into a cellulose (felt) matrix. RP/BR consists of a mixture of red phosphorus and butyl rubber (isobutylenes, BR) mixed in the ratio of 95 RP to 5 BR. RP is an amorphous material that is not readily characterized. Although there are many forms of RP, it is generally represented as polymeric units.

The forms of elemental phosphorus shown in Figure 1 can enter the environment through manufacturing processes and practices, spillage of material from smoke devices, and the incomplete combustion of material from smoke devices. Also, the combustion of such smoke generating materials produces a complex mixture of phosphorus oxides and condensed linear and cyclic polyphosphates that deposits on land and water from an aerosolized state. Berkowitz et al (1981) have reported the compounds shown below as resulting from WP and RP combustion.

$$\begin{matrix} P_4 \\ \text{or} \\ RP \end{matrix} \xrightarrow{[O]} H_3PO_4 + P_4O_{10} + P_4O_6 + H_3PO_3 + PH_3 +$$

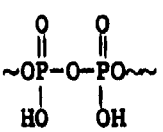

Thus, from this partial list of tranformation products, it is obvious that many forms of phosphorus, ranging in oxidation state from -3 (PH_3)

WP/F

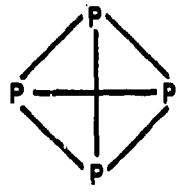

75-80% P_4

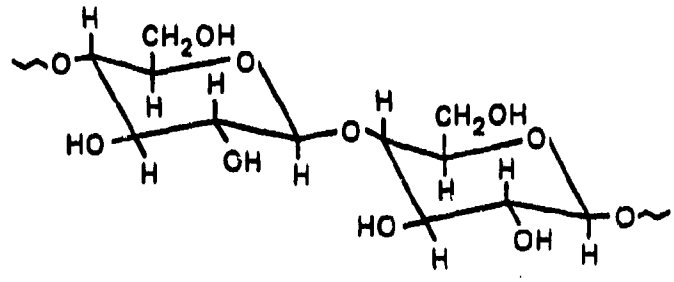

20-25% Cellulose

RP/BR

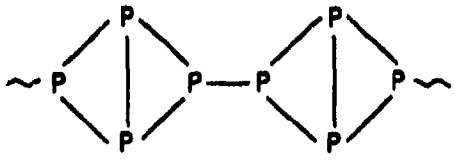

95% Phosphorus

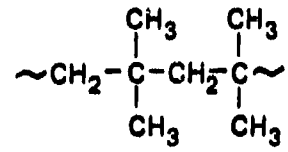

5% Polyisobutylene

FIGURE 1 COMPOSITION OF PHOSPHORUS SMOKES

to 0 (P_4) to +5 (PO_4^{-3}), will be present in the environment. For this study, we consider the transformation of phosphorus species to orthophosphoric acid (H_3PO_4) to be the final end product. Orthophosphoric acid or its salts are ubiquitous in the environment and any contribution to the phosphoric acid pool from phosphorus smoke devices would be infinitesimally small when dispersed over a wide area (aerosol deposition). Elevated levels of phosphates are expected at specific points and will undergo neutralization reactions at rates governed by the buffering power of the environment at the point of contact.

In general, the processes that contribute to the loss and movement of phosphorus species in the aquatic environment are biotransformation, oxidation, reduction, hydrolysis, photoxidation, volatilization, and sediment sorption. A number of these processes also occur in the terrestrial environment and in the atmosphere. By identifying which processes dominate in a particular environment and establishing the pseudo-first-order rate constant for the process(es), we can determine environmental half-lives for specific chemicals and estimate their persistence. Specific uses of phosphorus smokes or smoke products can then be modeled using computer simulations of selected environments. These simulations provide the basis for environmental assessments that permit the prediction of the persistence of chemicals and their stable end products.

We estimated the persistence of WP/F and RP/BR and their products in aquatic, soil, and air environments. We determined deposition velocities for combustion aerosols and modeled the aerosol dynamics using computer simulations. From these results, we predicted the time required to convert WP/F, RP/BR, and their combustion products in selected environments to orthophosphoric acid.

III CHARACTERIZATION OF WP/F AND RP/BR AND AEROSOL PRODUCTS

A. WP/F

An actual WP/F 155 mm round, minus the burster charge was obtained from Aberdeen Proving Ground, MD. This item is a sealed metal cannister 155 mm in diameter and 200 cm in length. The cannister was placed in a wooden cradle submerged in water that was contained in a 55-gallon drum that had been cut lengthwise. The cannister was opened under water using a hacksaw, the felt wedges were pried from the cannister, and both were stored under water.

The phosphorus composition of the wedge was determined by drying 4-10 gm samples in an inert atmosphere for several days, weighing a sample into a glass apparatus, and sealing the system under vacuum. Then the apparatus was filled with 100% oxygen, sealed, and allowed to burn to completion. The residue was dissolved in water, boiled for 1 hour, and titrated potentiometrically with standardized sodium hydroxide. The results of these determinations showed the WP/F to contain 75.3 ± 3.5% elemental phosphorus. The high standard deviation is probably the result of a nonuniform distribution of P_4 in the felt matrix. The remaining 25% of the WP/F is believed to be cellulose, although combustion studies (see Section III-C) could not account for all material being converted to CO_2.

B. RP/BR

RP/BR was also obtained from Aberdeen Proving Grounds. This material is produced as pellets and is very spongy and hydroscopic. Analysis of eight samples for elemental phosphorus by combustion followed by boiling of the residue in water and potentiometric titration yielded a phosphorus content of 87.9 ± 3.0%. An additional 3.2% phosphorus is present as surface oxides, titratable by boiling the uncombusted RP/BR in water. Thus, surface oxides coat most RP/BR pellets. Combustion studies showed the butyl rubber to amount to 5.2% of the formulation (see Section III-C).

Samples of RP/BR pellets (~ 0.6 cm x 0.6 cm) and powder (~ 0.09 cm) were submitted to Omicron Technology Corporation (Berkeley Heights, New Jersey) for surface area measurements. As measured by a continuous volumetric method, the surface areas for powder and pellets were 0.2 m^2/g and 0.15 $m^2/g \pm 20\%$, respectively. A repeat of analysis using a one-point BET method (Brunaller, Emmett, Teller surface area determination) resulted in a value of 0.1 m^2/g for both samples, which is slightly lower that the volumetric result but within the uncertainty of the measurement.

Samples of RP/BR pellets and powder were examined by scanning electron microscopy (SEM). As shown in Figure 2, the surfaces of the pellets and powder are similarly rough, as is suggested by the surface area measurements. It is not possible to distinguish between individual BR and RP crystallites by this technique.

X-ray fluorescence (XRF) analysis of both powder and pellets showed the presence of phosphorus as the major component and trace amounts of silicon. Carbon was difficult to detect by this technique.

C. RP Combustion Studies to Generate CO_2

Samples of RP/BR and WP/F were combusted to examine the effects of oxygen partial pressure on the production of carbon monoxide and carbon dioxide. The gaseous species were monitored by gas chromatography (GC) using a thermal conductivity detector and a 0.31 cm x 1.8-m stainless steel column packed with 80/100 mesh Carbosphere.

RP/BR was ignited with a Nichrome fuse wire in a 92 cc Monel reactor sealed with a Teflon washer at different oxygen pressures. The solid residue following combustion was dissolved in water, heated to boiling for 1 hour, cooled, and titrated with standard 0.1 N NaOH to the pK_1 for H_3PO_4 (pH 4.4).

Figure 3 shows the formation of CO_2 and CO and the residual oxygen following RP/BR combustion under different oxygen pressures. As shown, CO passes through a maximum but is always an order of magnitude less

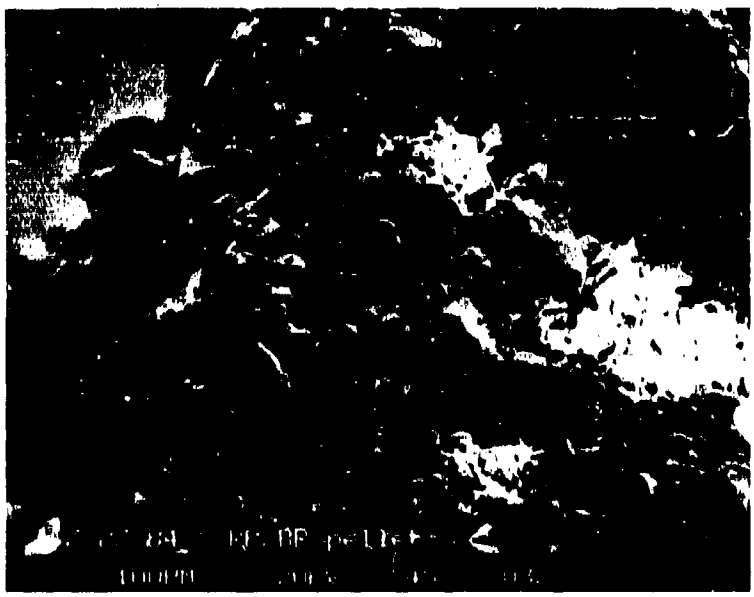

(a) SEM Photograph of RP/BR Pellets (230x)

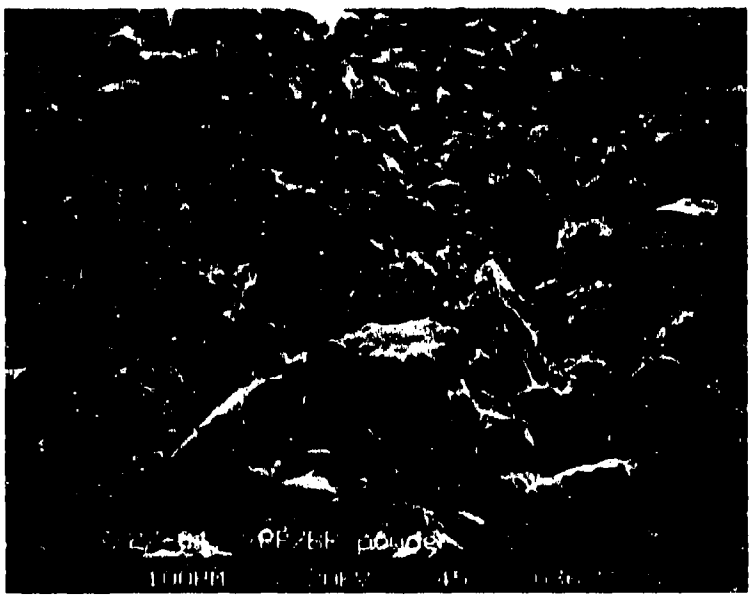

(b) SEM Photograph of RP/BR Powder (220x)

LP-4937-3

FIGURE 2 SCANNING ELECTRON MICROGRAPHS OF RP/BR PELLETS (TOP) AT 230x AND RP/BR POWDER (BOTTOM) AT 220x

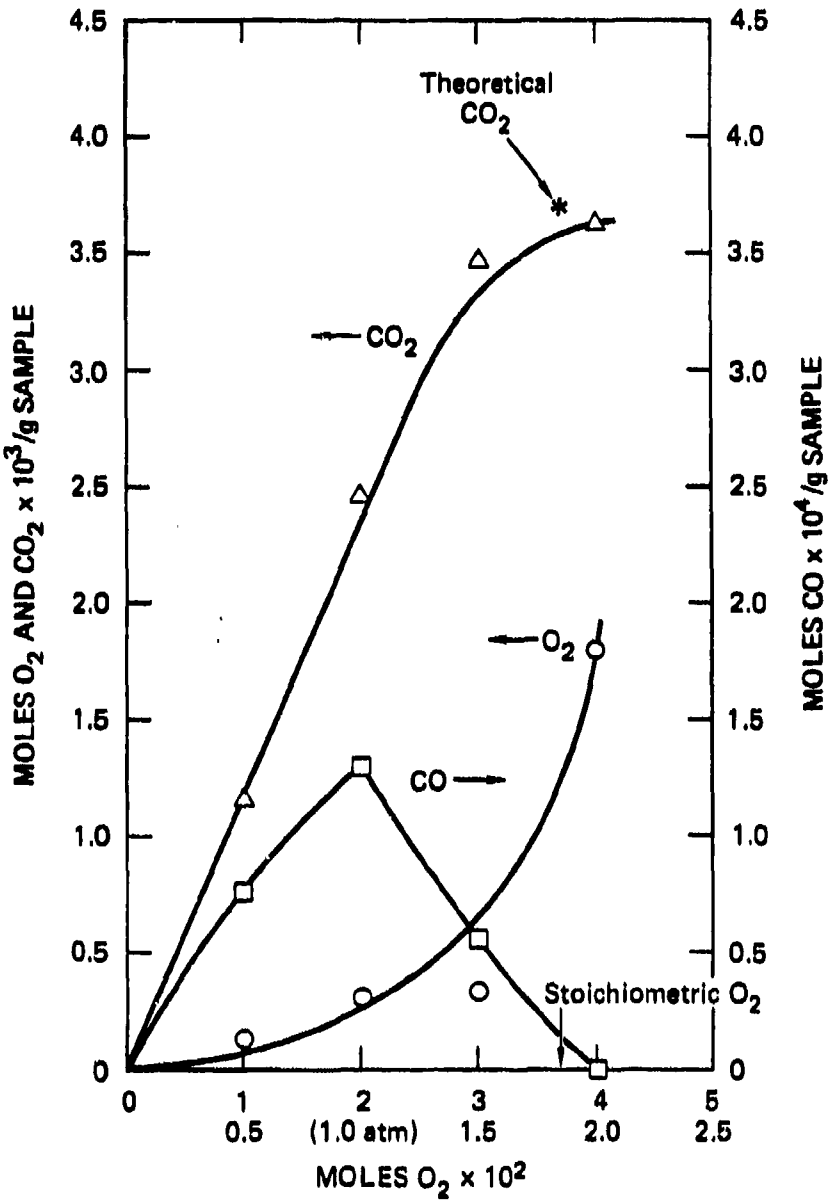

FIGURE 3 FORMATION OF CO_2 AND CO AND THE RESIDUAL O_2 FOLLOWING COMBUSTION OF RP/BR AS A FUNCTION OF OXYGEN PRESSURE

than CO_2 at the same initial O_2 pressure. As the O_2 pressure increases, the oxidation of carbon in BR (5.2%) proceeds nearly quantitatively (97%) to CO_2.

As shown in Table 1, we calculated the percent conversion of RP to P_4O_{10} based on the oxygen balance shown in Figure 3. The oxygen consumed is calculated from the difference between O_2 (initial O_2 concentration, abscissa) and the O_2 curve. If the oxygen consumption is corrected for CO_2 formation (CO can be neglected), the net value is that which has combined with RP. Because we can calculate the O_2 that is theoretically required to oxidize the available RP (87.9%) to P_4O_{10}, we can estimate the extent of this conversion.

As shown in Figure 4, the oxidation of RP in RP/BR to P_4O_{10} proceeds linearly with the initial oxygen pressure. The incomplete conversion at a stoichiometric oxygen pressure (88.5% conversion) and below is probably due to a protective shield of P_4O_{10} that forms initially on the RP surface. Also, our calculations do not take into account the presence of lower oxides such as P_4O_6, which undoubtedly form during incomplete combustion.

The combustion results for RP/BR are summarized in Table 2 in terms of RP and BR conversion and initial oxygen pressure.

RP conversion is generally lower than the oxidation of BR. However, the starting material contains an appreciably higher fraction of RP (RP/BR = 16.9). In 11% excess O_2, the oxidation of both components is nearly equal and close to 100%.

Using GC/AFID methods, we made some preliminary investigations of phosphorus-containing species being generated in the combustion process. Both P_4 (from the depolymerization of red phosphorus) and phosphine (PH_3) were observed. The latter product probably arises from the disproportionation of P_4O_6 in the presence of moisture, as shown in Equation 1.

$$P_4O_6 + 6H_2O \longrightarrow 3H_3PO_4 + PH_3 \qquad (1)$$

Table 1

CALCULATION OF RP/BR COMBUSTION BASED ON AVAILABLE OXYGEN CONSUMPTION

Initial (i) O_2 Concentration ($\times 10^2$ moles)	Final (f) O_2 Concentration ($\times 10^3$ moles)	$(O_{2i} - O_{2f} \times 10^2$	CO_2 Produced ($\times 10^3$) moles	O_2 for RP $\times 10^2$ $(O_{2i} - O_{2f} - CO_2)$	Conversion of RP $\rightarrow P_4O_{10}$ [a] %
1.0	0.19	10.0	1.16	0.86	24
2.0	0.32	2.0	2.44	1.7	49
3.0	0.36	3.0	3.4	2.6	74
4.0	1.8	3.8	3.6	3.5	98

[a] 3.55×10^{-2} moles O_2 are required for 100% P_4 oxidation.

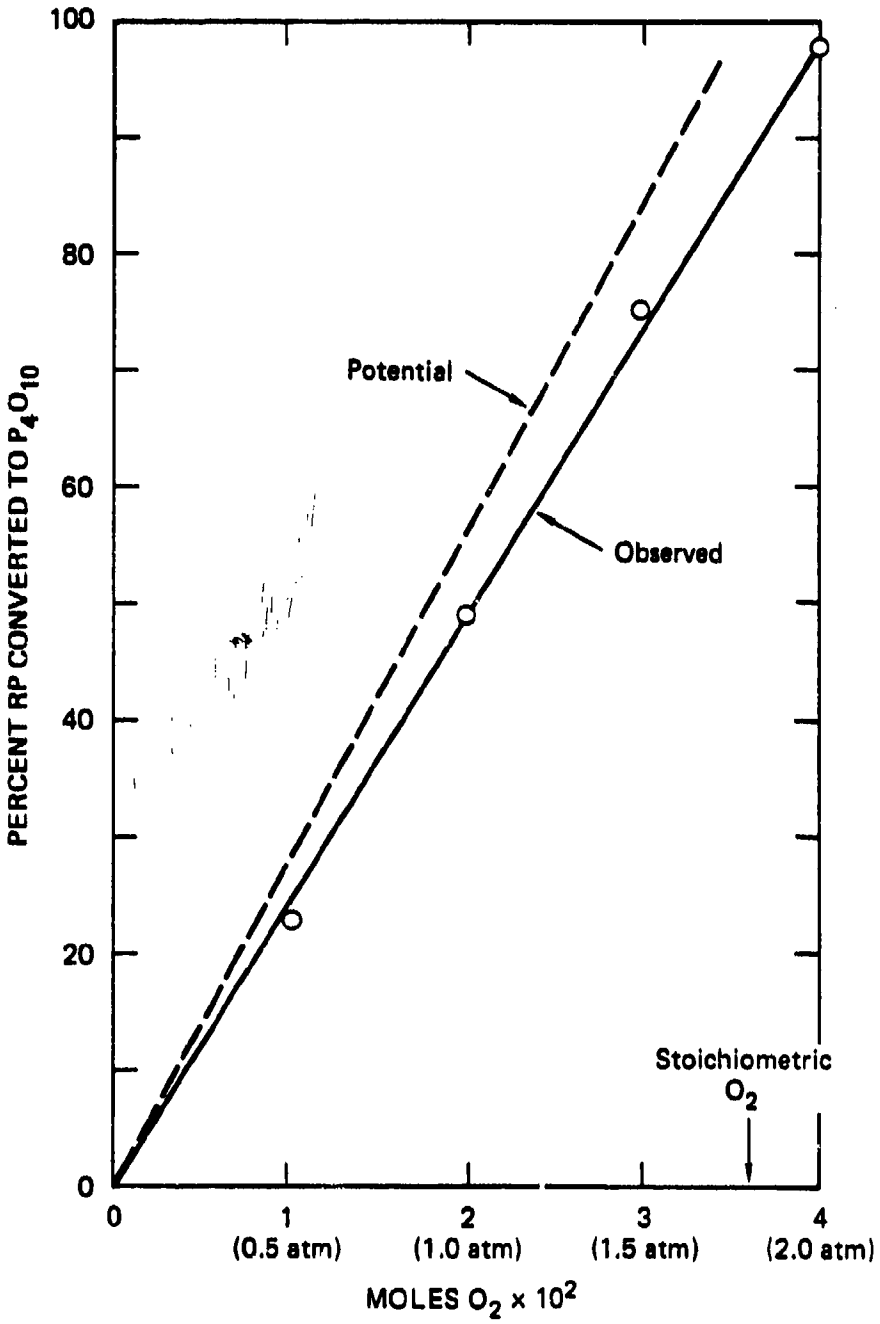

FIGURE 4 OBSERVED AND POTENTIAL CONVERSION OF RP TO P_4O_{10} AS A FUNCTION OF OXYGEN PRESSURE

Table 2

PERCENT CONVERSION OF BR AND P_4
AS A FUNCTION OF OXYGEN PRESSURE

O_2 Pressure (atm)	Percent Conversion	
	BR	RP
0.5	31	24
1.0	78	49
1.5	92	74
1.8 (stoichiometric)	96	89
2.0	97	98

D. WP/F Combustion Studies

Studies were performed to evaluate the combustion of WP/F as a function of initial oxygen pressure and to evaluate the formation of gaseous products. WP/F samples (~ 1 g each) were weighed into the Monel reactor in a dry box. The reactor was sealed and tranferred to a vacuum line. After removal of the N_2 atmosphere and cooling of the reactor to liquid nitrogen temperature (-195°C), O_2 was added from a calibrated volume. Reaction of WP/F with O_2 generally occurred when the reactor warmed to near room temperature.

Figure 5 shows the formation of CO and CO_2 from the combustion of 1 g of WP/F as a function of the initial O_2 pressure. CO, present at about two orders of magnitude less than CO_2, reaches a maximum concentration near 2.5 atm O_2, whereas CO_2 increases with pressure. As shown in the Figure, conversion of felt to CO_2 is far less than the theoretical value of 39.5×10^{-3} moles.

A comparison of the conversion of butyl rubber in RP/BR and felt in WP/F to CO_2 is shown in Figure 6. The results demonstrate a significant difference in the burning characteristics of the two munitions: at the

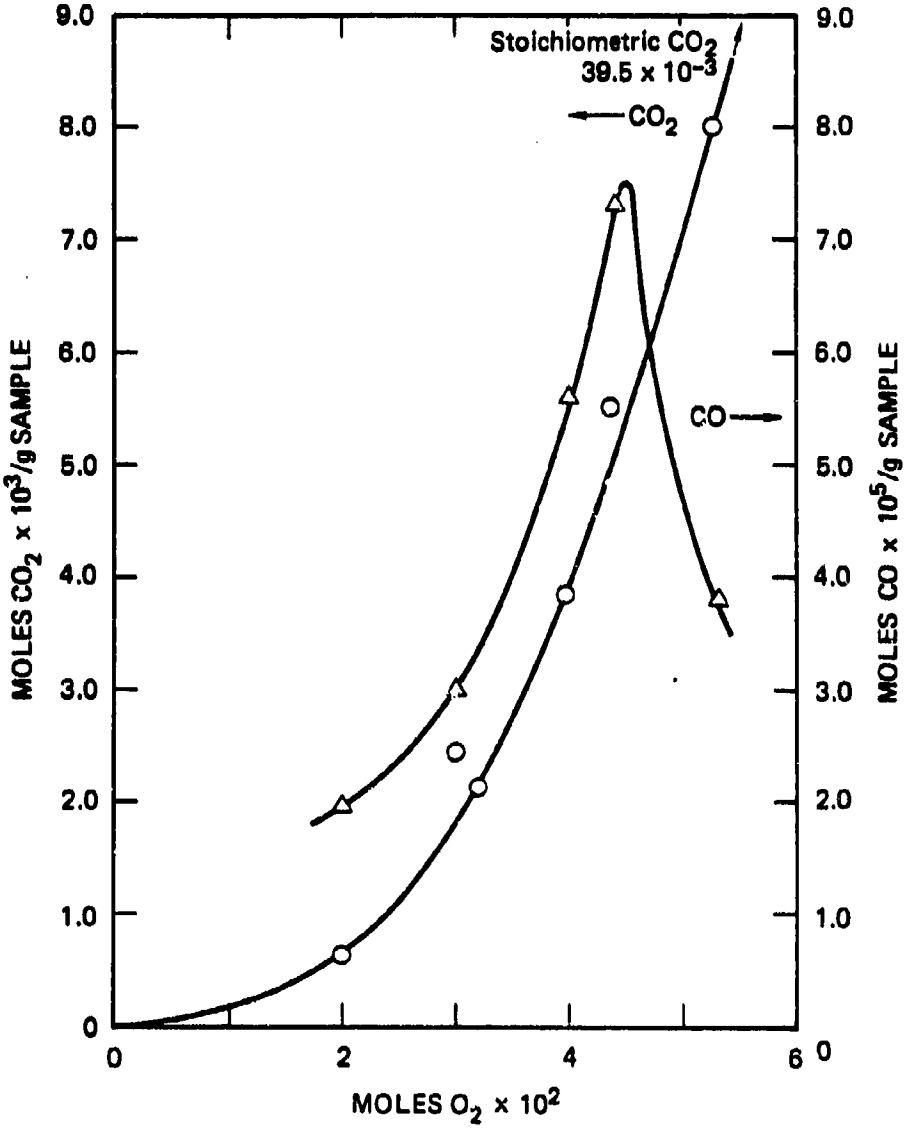

FIGURE 5 FORMATION OF CO AND CO_2 FROM THE COMBUSTION OF 1-g OF WP/F AS A FUNCTION OF O_2 CONCENTRATION

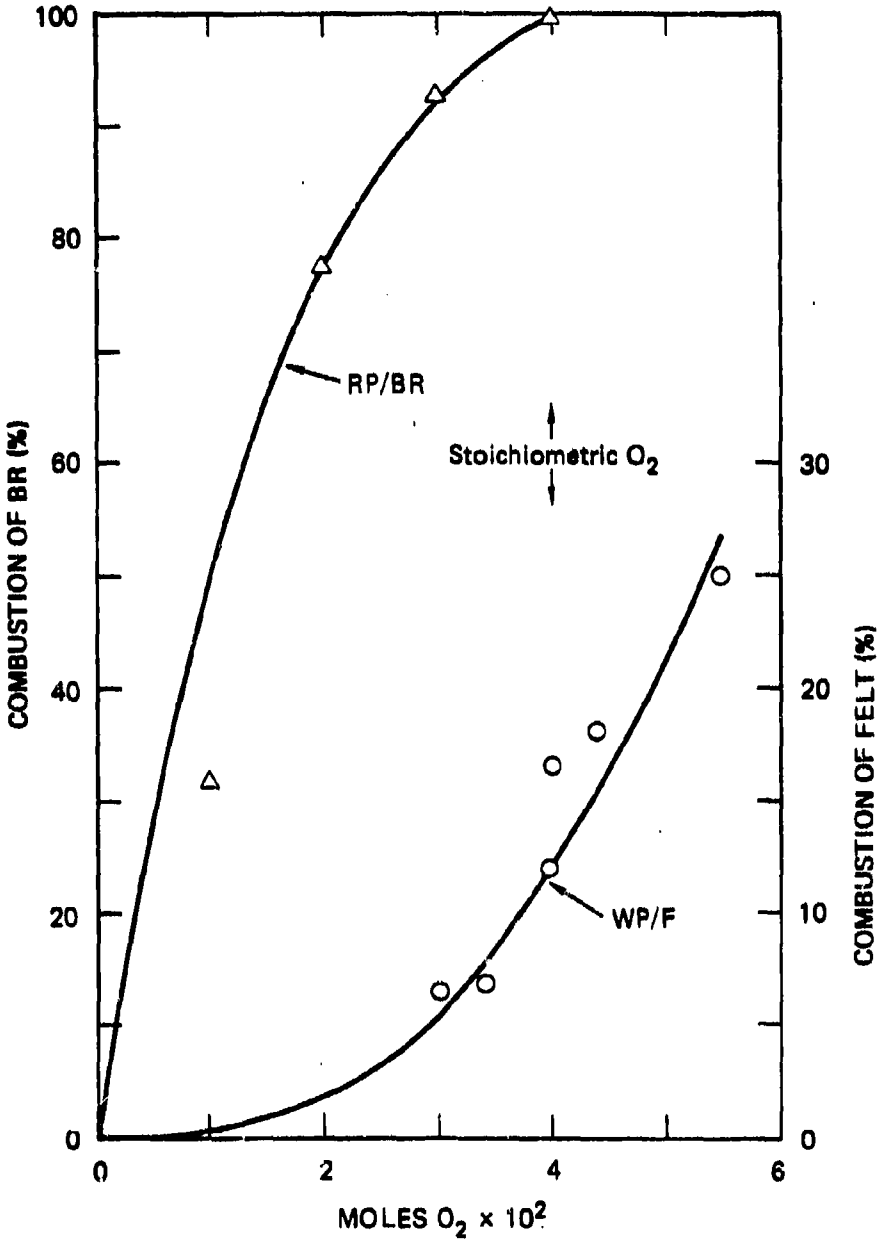

FIGURE 6 PERCENT COMBUSTION OF BUTYL RUBBER (BR) AND FELT (F) AS A FUNCTION OF O_2 CONCENTRATION FOR 1-g OF RP/BR AND WP/F

stoichiometric O_2 pressure for RP/BR, 98% of the butyl rubber is burned but only 11% of the felt is converted to CO_2. We estimate for WP/F that even in the presence of 50% excess O_2, only about 25% of the felt will burn completely.

The degree of oxidation of phosphorus to P_4O_{10} (assumed product) is similar for both munitions. As shown in Figure 7, about 90% of the P_4 in both munitions is converted to P_4O_{10} at the respective stoichiometric O_2 pressure. At higher O_2 pressures, however, a major difference is observed. The results suggest that nearly complete oxidation of red phosphorus can be achieved by increasing the oxygen pressure, whereas the upper limit of conversion of white phosphorus is about 92%. Thus, in the burning of WP/F in the environment, a significant amount of unreacted P_4 is expected to remain in the burned felt matrix.

E. Aerosol Components

The aerosol components of RP/BR and WP/F were characterized by ion-exchange chromatography followed by post-column hydrolysis and derivatization and detection at 660 nm. This procedure is similar to that described by Yamaguchi (1979). The following conditions were employed:

Instrument: Spectra-Physics 3500B Liquid Chromatograph

Column: Bio-Rad 150 x 10 mm Aminex A-14 ion-exchange column

Mobile Phase: A) 0.22 M NaCl in 5 mM EDTA (disodium)
B) 0.55 M NaCl in 5 mM EDTA (disodium)

Solvent Program: 0-100% B in A over a 6-hr convex gradient

Flow: 1.0 ml/min

Detection: Molybdate blue at 660 nm.

Samples of aerosol were collected by freeze-trapping on silanized glass wool at -20°C. The aerosols were washed from the traps (two in series) and 2.0 ml was injected into the HPLC using a Water's WISP autoinjector.

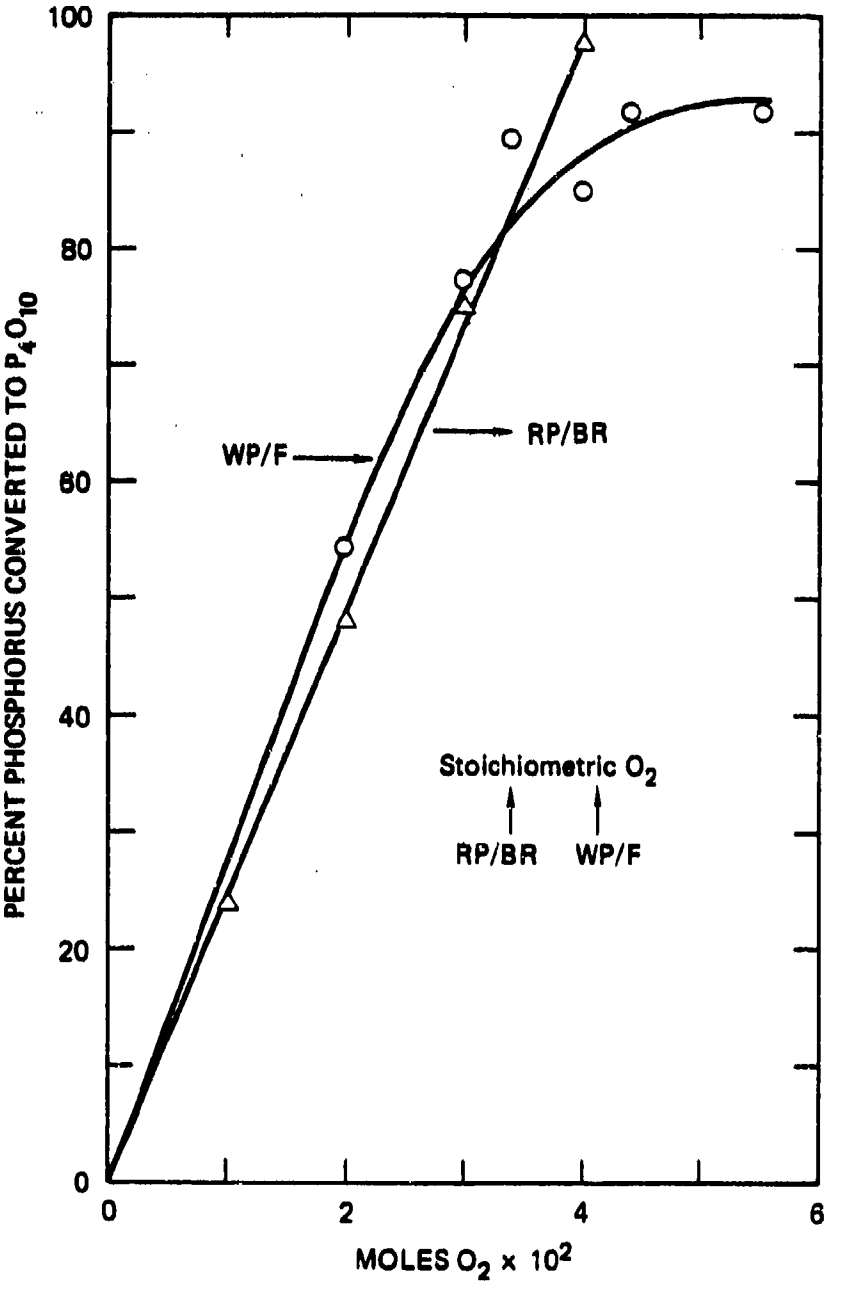

FIGURE 7 PERCENT CONVERSION OF RP/BR AND WP/F TO P_4O_{10} AS A FUNCTION OF OXYGEN CONCENTRATION

WP/F and RP/BR gave nearly identical profiles of phosphorus-containing species, identified as orthophosphoric acid (H_3PO_4), pyrophosphoric acid ($H_4P_2O_7$), triphosphoric acid ($H_5P_3O_{10}$), and tetrapolyphosphoric acid ($H_6P_4O_{13}$) by comparing retention times to authentic standards (Sigma Chemical Co., St. Louis, Mo), plus a homologous series of linear, condensed polyphosphates consisting of P_6-P_{16} polyphosphates tentatively identified on the basis of their chromatographic properties and their formation of the heteroblue-molybdate complex (Figure 8). On standing in water, the tri-, tetra-, and hexa-cyclic metapolyphosphates were formed, with the cyclic trimetapolyphosphate predominating.

The only lower oxidation state phosphorus compounds identified besides phosphine were hypophosphorous acid (H_3PO_2) and phosphorous acid (H_3PO_3). These compounds were identified by indirect photometric chromatography (Small, 1982) as compared to authentic standards (Figure 9). The structures of these components are shown in Figure 10. The products shown in Figure 10 and WP/F and RP/BR were therefore studied with respect to their persistence in selected environments.

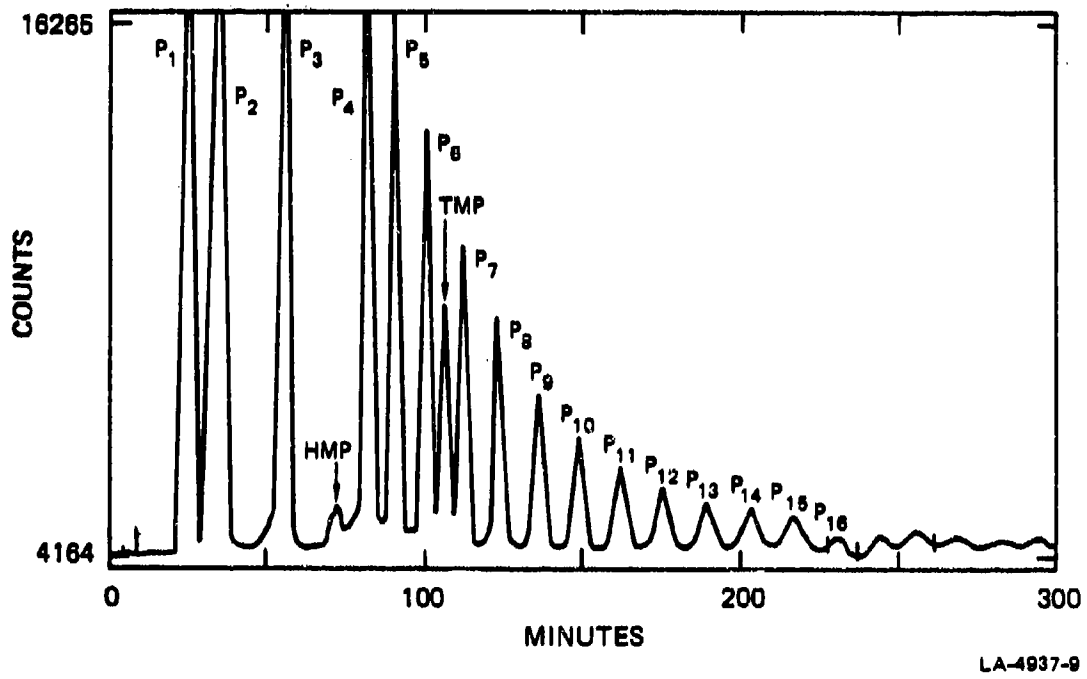

FIGURE 8 HPLC PROFILE OF WP BURN RESIDUE

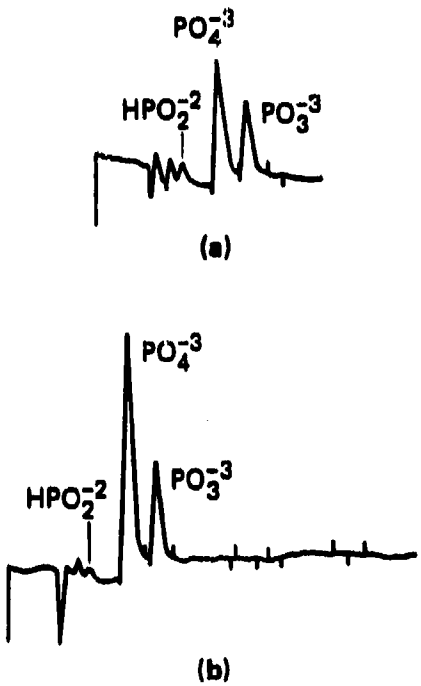

FIGURE 9 HPLC PROFILES OF PHOSPHOROUS SMOKE RESIDUE (BURN A) AND SMOKE CONDENSATE (BURN B) FOR HYPOPHOSPHITE, PHOSPHATE, AND PHOSPHINE

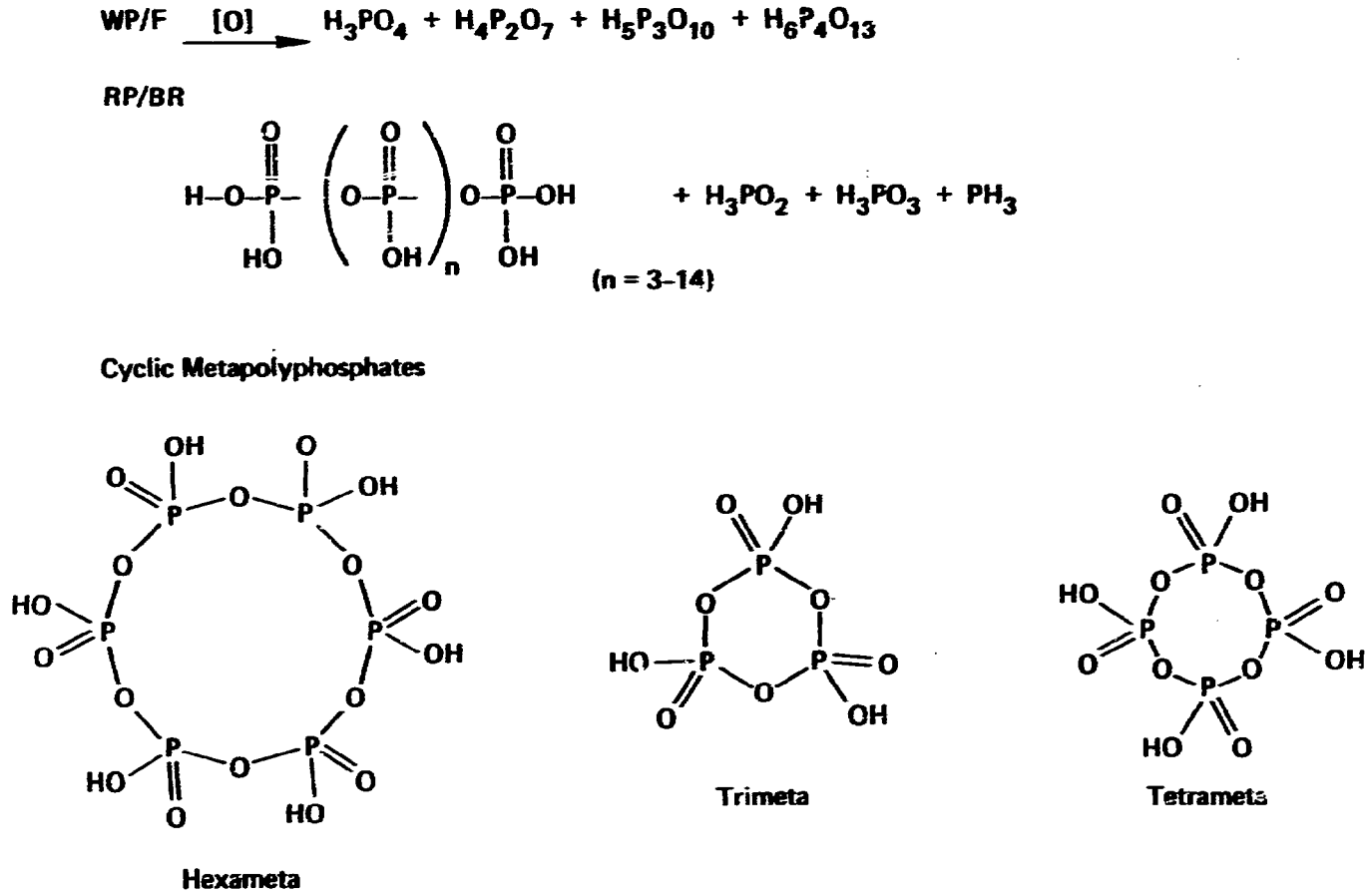

FIGURE 16 COMBUSTION PRODUCTS FROM WP/F AND RP/BR BURNS

IV PHYSICAL PROPERTIES AND TRANSPORT STUDIES

Research on physical and transport properties focused on white phosphorus and phosphine. The physical and transport properties of red phosphorus are briefly reviewed following discussion of this experimental work.

A. Aqueous Solubility of Red Phosphorus and P_4

The aqueous solubility of red phosphorus was considered negligible due to its polymeric nature and its lack of discreet unoxidized units detectable in the aqueous phase.

The aqueous solubility of P_4 was measured at 15, 25, and 35°C by placing excess P_4 and deoxygenated water in a 4-ml vial equipped with a teflon Mininert valve (no headspace). The sample was warmed to 45°C, sonicated for 30 min, then stirred for 48 hr in a temperature-controlled bath. The vial containing the sample was then centrifuged at 15, 25, or 35°C and 7000 rpm for 60 min. A 0.5-ml aliquot was withdrawn with a 1-ml gastight syringe and immediately added to an equal volume of hexane. The hexane extract was analyzed by GC using an alkali-flame ionization detector. The GC conditions were:

Column: Porapak P, glass (4 ft x 2mm ID)

Column temp: 200°C

Carrier gas: He, 40 ml/min

Retention time, P_4: 5.0 min.

Calibration standards were prepared in benzene with vacuum-dried P_4. The stock benzene solution of P_4 was prepared in a N_2-filled dry box and diluted for calibration standards. The calibration was linear for concentrations less than 10 ppm. Hexane or benzene solutions of P_4 were stable within detector sensitivity for several days. The calibration was checked daily.

Table 3 summarizes the solubility data.

Table 3

SOLUBILITY OF P_4 AS A FUNCTION OF TEMPERATURE

Temp (°C)	S_w[a] (ppm)	Relative Standard Deviation (%)
15	2.4	10
25	4.1	4.8
35	5.0	7.6

[a]Mean value of four determinations.

These values agree reasonably well with the solubility of 3 ppm at 15°C reported by Berkowitz et al. (1981). Figure 11 gives a plot of the aqueous solubility of P_4 versus the reciprocal of the absolute temperature. The enthalpy of solution (ΔH_s) of P_4 in water can be calculated from Equation 2.

$$d(\ln S_w)/d(1/T) = -\Delta H_s/R, \quad (2)$$

where S_w is the aqueous solubility and R is the ideal gas constant. The calculated value of ΔH_s is 6 Kcal/mol from the best fit of data through the three data points of Figure 11.

B. Soil Sorption and Stability of P_4 in Soil Water

1. Soil Characterization

A sandy loam (supplied by Woods Science, Monterey, CA), PBA soil, and a Menlo Park soil collected by SRI staff were used as test soils for white phosphorus sorption. Characterization included measurements of organic carbon content (TOC), particle size distribution, oxalate-extractable iron,

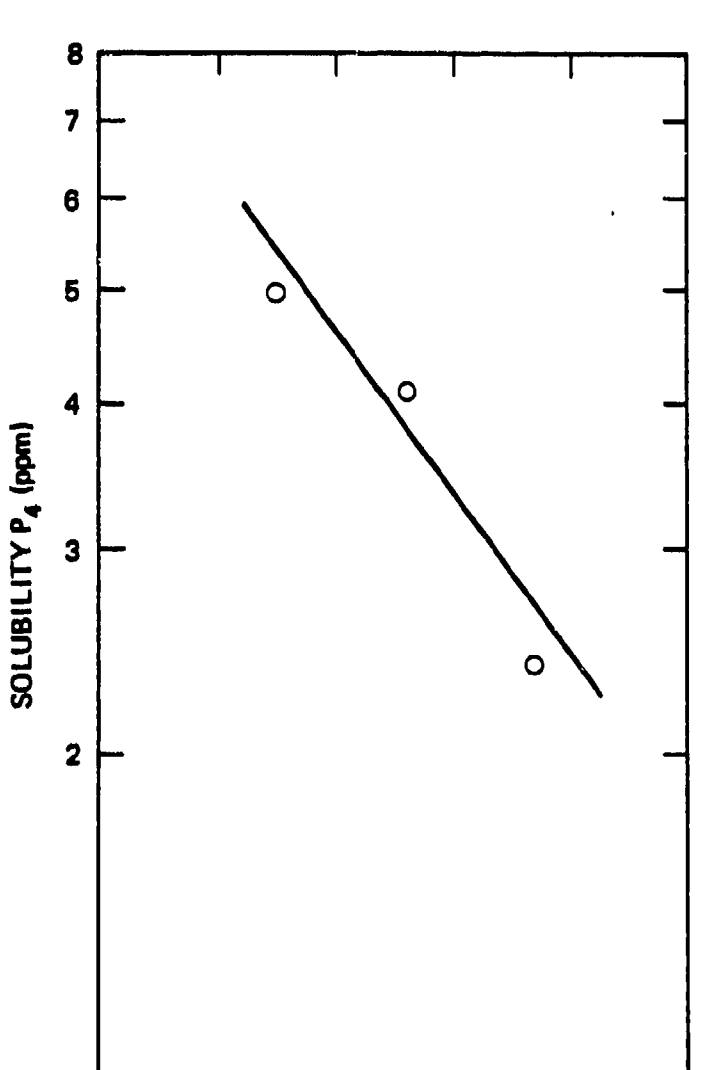

FIGURE 11 AQUEOUS P_4 SOLUBILITY AS A FUNCTION OF TEMPERATURE

pH, and porosity. The characterization methods used and the results obtained are summarized in Table 4.

2. Soil Sorption Partition Coefficient (K_p)

Studies were conducted to measure the soil partition coefficients for P_4 using soils both high (4.2%) and low (0.3%) in organic content. These studies were performed inside a glove bag under nitrogen to minimize oxidation of the P_4. Degassed soils were weighed into tared 25-ml centrifuge tubes and filled with aqueous P_4 solution (no headspace). Test samples ranging from 0.03 to 1.0 g for the high organic content soils (Menlo Park) and from 3 to 15 g for the low organic content soils (Sandy) were used in the batch experiments. Approximately 30 g of aqueous P_4 solution at 1 to 2 ppm was used in both sets of experiments. The tubes were weighed, wrapped in aluminum foil, placed in a rotating-arm mixer overnight, and then centrifuged at 10,000 rpm for 30 minutes. The supernatant was transferred to a septum-sealed vial in the glove bag. The soil was washed with clean deoxygenated water and the residue was extracted with hexane.

The aqueous supernatant and hexane extract were analyzed by GC with a nitrogen-phosphorus detector. Our first experiments indicated a K_p value of 20 $m\ell\ g^{-1}$ and a K_{oc} ($=K_p/OC$ where OC is the organic carbon content) value of 480 $m\ell\ g^{-1}$ for the Menlo Park soil and $K_p = 1$, $K_{oc} = 360$ for the sandy loam. The experiment with the high organic carbon Menlo Park soil was repeated because of poor mass balance recoveries by performing analyses of hexane extracts of the aqueous supernatant instead of direct aqueous injection to minimize loss of P_4 during this step. Because of unaccountable losses of P_4 (discussed below), the upper K_p limit that could be calculated for the Menlo Park soil was 25 ml g^{-1}. This estimate assumes that all P_4 not recovered from the supernatant is sorbed. The true value is thus equal to or lower than this value.

Our attempts to obtain reliable data for the soil partition coefficient for white phosphorus were confounded by significant losses

Table 4

MEASURED PROPERTIES OF TEST SOILS

Soil	TOC (%)	Particle Size Distribution (% 6 μ)	Oxalate Extractable Iron	Moisture	pH	Porosity (%)
Sandy	0.3	36/70 31/50 26/20 23/10 20/6	0.10	0.14	6.6	31
PBA	0.5	74/49 62/22 48/15 37/8 30/4 25/1	0.26	13.4	3.3	38
Menlo Park	4.2	62/50 50/15 43/10 39/6 32/1	0.22	4.9	5.7	52
Method	Walkley-Black wet dichromate digestion	Gravity settling column	Extraction with ammonium oxalate	Weight difference after drying	pH meter	Measure difference between volume wet and dry

of P_4 in the "no soil" controls. This uncertainty was too great to permit a reasonable attempt to determine whether the sorption isotherms were linear or whether sorption of P_4 significantly correlated with the organic carbon content of the soil, or to determine the leachability of P_4 in soil. Instead, efforts were directed toward resolving the problem of P_4 loss in the "no soil" controls.

A stability experiment was performed with white phosphorus in water under the best anaerobic conditions achievable in a glove bag. The bag itself was flushed with nitrogen (containing 0.1 ppm O_2 after passage through an oxytrap).

P_4 solutions were prepared by allowing water to stand over P_4 lumps for several days in a glove bag. The P_4 solution was then poured into four 5-ml glass vials (no headspace). The vials were sealed tightly with Mininert-valve caps, and the cap-glass interface was wrapped with Teflon tape. The vials remained in the glove bag at all times.

A fresh vial was sampled at intervals by removing P_4 solution through the valve and extracting this aliquot with an equal volume of hexane. The hexane extract was analyzed by GC/NPD. The results are presented in Table 5.

Table 5

OBSERVED LOSS OF P_4 FROM "NO SOIL" CONTROL

Vial #	Time (hr)	P_4 Concentration (ppm)	% Lost (Gain)
1	0	0.71	---
2	2.5	0.68	(4)
3	5.0	0.54	17
4	23	0.44	38

These data show that even under the best available conditions, approximately 40% of the P_4 disappears during the time required for

an adsorption isotherm experiment. Because these losses occur simultaneously with adsorption, the results of the sorption experiments are very uncertain and thus difficult to interpret.

3. Stability of Dissolved P_4 in Water

It was observed in the sorption measurements that the P_4 concentration in the "no soil" controls was significantly lower than that observed in the supernatant above the "low soil" controls. In one adsorption experiment performed over 16 hr, an initial P_4 concentration of 1.7 ppm was reduced to 0.38 ppm in the "no soil" controls, whereas concentrations of 1.5 ppm and 0.92 ppm were observed in "low soil" and "high soil" adsorption tube supernatants, respectively, under identical conditions. These data suggest that aqueous-extractable soil matter stabilizes P_4 in solution. Therefore, an experiment was performed to determine whether the increased stability of white phosphorus observed in the supernatant of soil adsorption studies is due to the aqueous-extractable soil matter.

A P_4 solution was prepared by allowing water to stand over P_4 lumps for several days in a glove bag filled with argon. The suspension was warmed and then sonicated to hasten dissolution of the P_4. The solution was filtered and an aliquot was diluted with deoxygenated water containing aqueous-extractable matter from Menlo Park soil (TOC: 4.2%). This soil extract was prepared by centrifuging and filtering a 10-wt% suspension of the soil. An aliquot of P_4 solution diluted with deoxygenated Milli-Q water was used as a control. A series of 2-ml vials were filled to overflowing with the diluted P_4 solutions. All solution manipulations were carried out in the glove bag in which the vials were stored. Aliquots (0.5 ml) were periodically removed and extracted with 0.5 ml of hexane for analysis by GC.

The experimental results, shown in Figure 12, indicate that aqueous-extractable soil matter stabilizes P_4 dissolved in deoxygenated water. After 24 hr, 70% of the dissolved P_4 remained in the distilled-water controls, whereas 100% remained in the solutions diluted

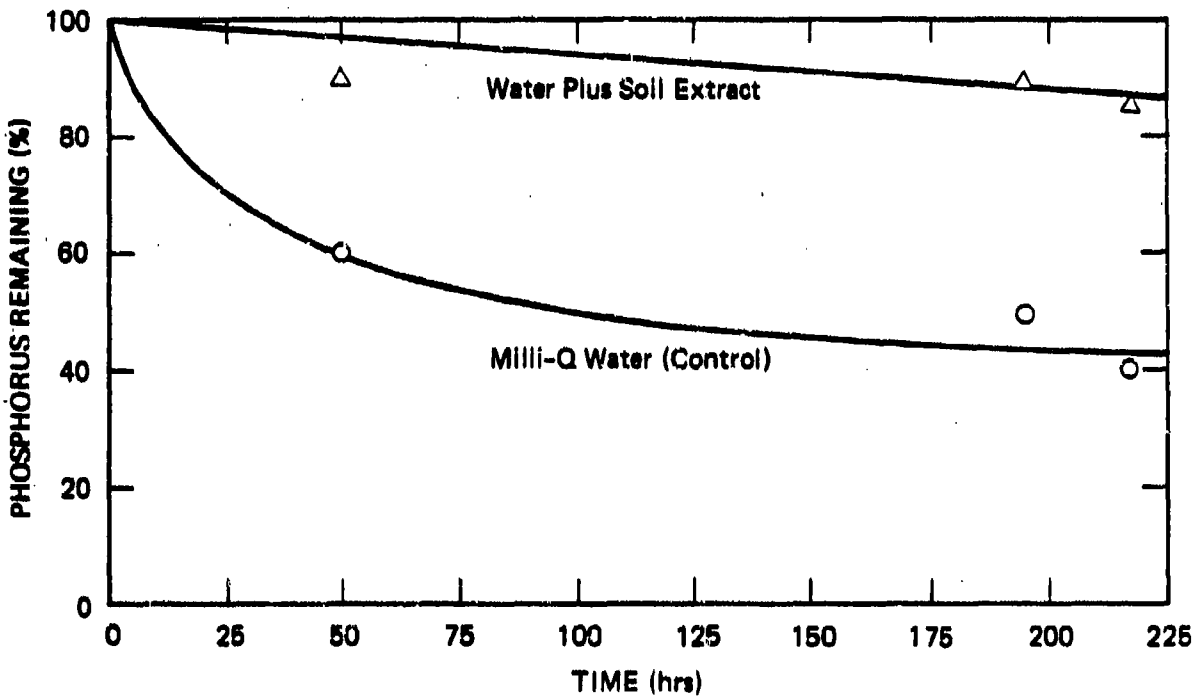

FIGURE 12 STABILITY OF P_4 IN AQUEOUS SOIL EXTRACT AND CONTROL WATER SOLUTIONS

with water containing soil extract. After 216 hr, 41% remained in the controls, but 86% remained in the solutions containing soil extract. However, after 100 hr, both solutions appeared to lose P_4 at the same rate.

C. Octanol/Water Partition Coefficient (K_{ow}) of P_4

The K_{ow} for P_4 was determined by the method of Leo et al. (1971). Under anaerobic conditions, a stock solution of P_4 in water-saturated octanol was prepared. Small volumes of this solution were equilibrated with various volumes of octanol-saturated water. After equilibration at ambient temperature, the phases were separated by centrifugation at 1000 rpm for 10 min. The concentration of sample in the octanol or aqueous phase was determined by GC. The GC conditions were:

Detector: Alkali-flame ionization/HP5880A

Column: 3% SP2100/Supelcoport, 2' x 2 mm 10 glass

Temp program:

Temp 1	33°C (1 min)
Rate	3 deg min^{-1}
Temp 2	60°C

Carrier: Helium, 50 ml min^{-1}

P_4 retention time: 1.53 min

The P_4 concentration was calculated using the external standard method. The results are summarized in Table 6.

Table 6

K_{ow} DETERMINATIONS FOR WHITE PHOSPHORUS (P_4)

Run No.	Volume Ratio (o/w)	P_4 (water) (mg)	P_4 (octanol) (mg)	K_{ow}
1	1/ 7.5	0.27	281	1000
2	1/10	0.37	484	1300
3	1/10	0.25	318	1300
4	1/10	0.32	394	1200
5	1/10	0.29	398	1400
6	1/20	0.55	669	1200
7	1/20	0.47	503	1100

Av. 1200 ± 100

It is interesting to note that several researchers--for example, Kenaga and Garing (1978) and Yalkowsky and Valvani (1980)--have reported good correlations between K_{ow} and S_w for a variety of organic compounds. The values of S_w predicted by substituting K_{ow} = 1200 into these equations are between one and two orders of magnitude higher than those we found experimentally. This is not surprising considering that the K_{ow}-S_w correlation is based on the assumption that octanol/solute interactions are similar in magnitude to solute/solute interactions. Our data indicate that, as expected, P_4/P_4 interactions are much stronger than octanol/P_4 interactions.

D. Vapor Pressure of P_4

The vapor pressure of P_4 was measured at 25°C by the gas saturation method. Briefly, a measured volume of N_2 gas is saturated by passing it through a U-tube containing glass beads coated with elemental phosphorus in a constant-temperature box. The vaporized phosphorus is trapped in xylene impingers and analyzed by GC. Assuming Dalton's law of partial pressures and the ideal-gas law, the partial pressure of the vapor is calculated by Equation 3.

$$P = \frac{g}{M} \frac{RT}{V} \quad , \qquad (3)$$

where P = partial pressure of phosphorus

g = grams of phosphorus

R = gas constant

T = temperature

M = molecular weight

V = total volume of gas passed through the impinger.

Figure 13 is a diagram of the apparatus that we used.

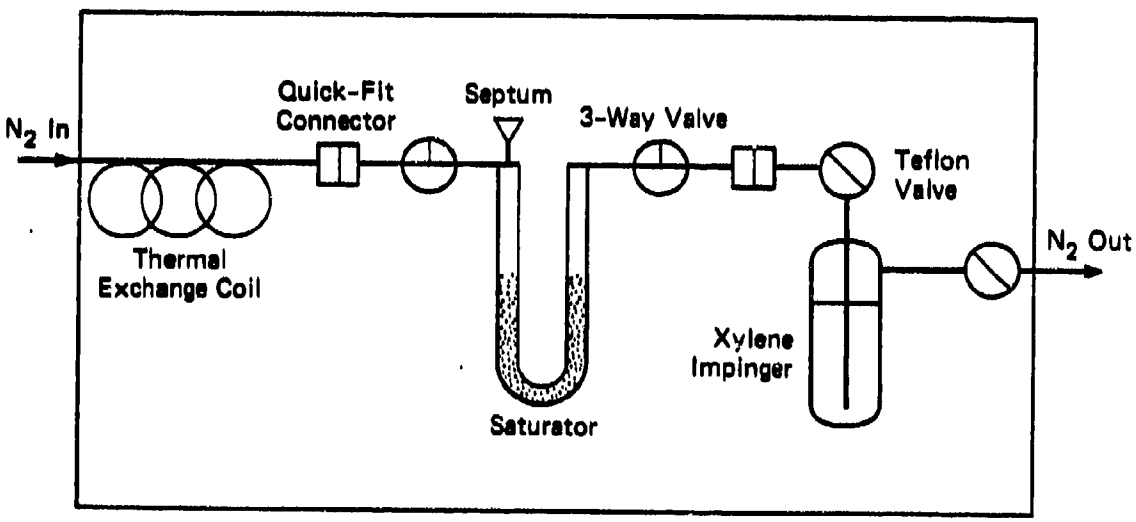

T = Temperature
M = Molecular Weight
V = Total Volume of Gas Passed Through The Impinger

FIGURE 13 GAS SATURATION APPARATUS

The observed vapor pressures for duplicate runs at 25 ± 0.5°C were 0.024 torr and 0.021 torr. The vapor pressure calculated from the Clausius-Clapeyron constants as reported in the CRC Handbook (1973) is 0.04 torr at 25°C. It should be noted that the white phosphorus coating on the glass beads in the generator turned red during these experiments. This indicates that the P_4 was being transformed and thus our measured vapor pressures are probably low.

E. Henry's Constant and Volatility of P_4

Henry's constant was measured at 25°C using the method of Mackay et al., 1979). The apparatus (Figure 14) consisted of a glass column fitted with a gas-dispersion tube. Nitrogen was passed through an Oxysorb trap and then saturated with water before bubbling into the Henry's apparatus. Nitrogen flow, water volume, and chemical (P_4) concentration were measured periodically. A plot of ln concentration vs purge volume produced a straight line, from which Henry's constant was calculated to 1600 liter-torr/mole. This measured value is about twice as high as the value of 700 liter-torr/mole calculated from the ratio of measured values of the saturated vapor pressure and the aqueous solubility of P_4. This is another indication that our measured vapor pressure is too low. If the literature value of the vapor pressure is used with our measured value of the aqueous solubility, then the calculated value of H is very close to the value of H measured directly. The assumption that H = 1600 torr M^{-1} suggests that P_4 is a moderately volatile chemical and that the volatilization rate will be controlled by mass transport resistance in both the gas and liquid phases. The first-order rate constant for volatilization is conveniently expressed as Equation 4

$$K_v = \frac{1}{L} [r_\ell + rg/H]^{-1} \quad , (4)$$

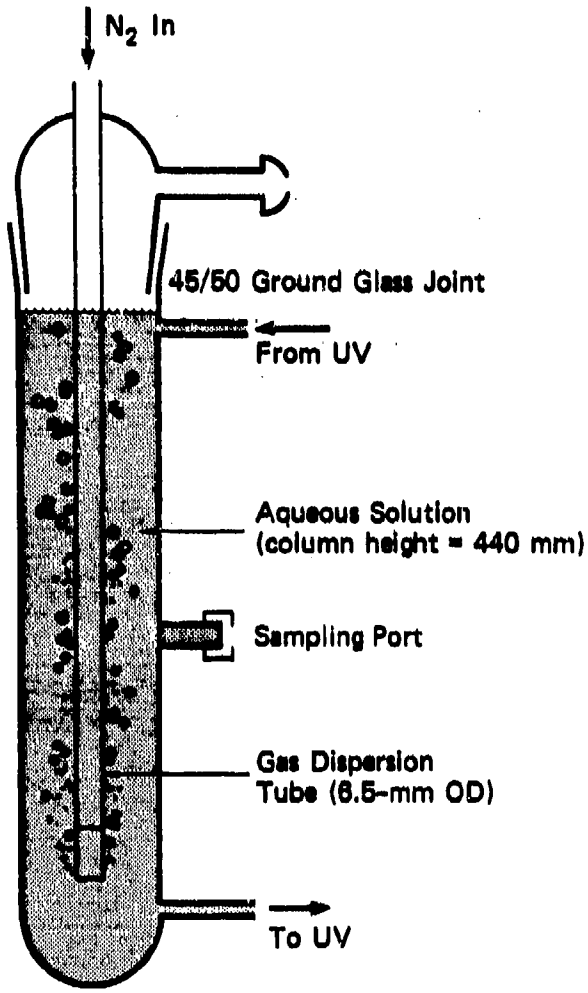

FIGURE 14 SAMPLING SYSTEM FOR DETERMINATION OF HENRY'S LAW CONSTANTS

where L = depth of the water body

r_l = liquid phase resistance

r_g = gas phase resistance

H = Henry's constant in dimensionless units.

Assuming that $r_l \sim 200$ sec cm^{-1}, $r_g \sim 5$ sec cm^{-1} (moderately turbulent conditions in both the liquid and air phases) and L (water depth) = 1 m, we can estimate the volatilization half-life of P_4 in a water body such as a pond. Assuming that H = 1600 torr M^{-1} (0.088 in dimensionless form), K_v can be calculated from Equation 4 and the volatilization half-life ($t_{1/2}$) is given by

$$t_{1/2} = \frac{0.693}{K_v} = 5.6 \text{ hours.}$$

Henry's constant, together with an appropriate value of the soil partitioning coefficient, can also be used to estimate the partitioning of P_4 in a soil column.

If equilibrium partitioning between the soil air (A), soil water (w), and soil solids (s) phase is assumed, then Bomberger et al. (1982) have derived simple expressions for the fraction of chemical λ in these phases, as shown in Equations 5-7.

$$\lambda_A = \text{fraction compound in air phase} = \frac{\theta_A}{\theta_A + \frac{\theta_w}{H} + (1 - \theta_A - \theta_w)\frac{K_{oc}F_{oc}\,d}{H}} \quad (5)$$

$$\lambda_w = \text{fraction compound in water phase} = \frac{\frac{\theta_w}{H}}{\theta_A + \frac{\theta_w}{H} + (1 - \theta_A - \theta_w)\frac{K_{oc}F_{oc}\,d}{H}} \quad (6)$$

$$\lambda_s = \text{fraction compound in solid phase} = \frac{(1 - \theta_A - \theta_A)\frac{K_{oc}F_{oc}\,d}{}}{\theta_A + \frac{\theta_w}{H} + (1 - \theta_A - \theta_w)\frac{K_{oc}F_{oc}\,d}{H}} \quad (7)$$

If we assume for simplicity that the soil volume fractions are equal ($\theta_A = \theta_w = \theta_s = 0.33$), the soil specific gravity d = 2.65 g cm^{-3}, the fraction organic content $F_{oc} = 0.001$, and K = 400 cm^3 g^{-1} (see Section IV.B), then

$$\lambda_A \sim 0.01$$

$$\lambda_w \sim 0.09$$

$$\lambda_s \sim 0.90$$

This estimate indicates that dissolved P_4 will partition primarily between the soil solids and water phases of a wet soil. The fraction of P_4 that partitions into the soil water (λ_w) is sufficiently high that appreciable leaching of dissolved P_4 should be expected. Moreover λ_A is sufficiently high that modest volatilization losses of P_4 may also be expected.

This model of course assumes that P_4 is dissolved in soil water and achieves an equilibrium distribution between the three soil phases. The P_4 in each phase will therefore be subject to oxidative or hydrolytic transformation, dependent on available oxygen and water contents associated with each phase.

F. Dissolution Rate of P_4

A flow system (Figure 15) was used to study the dissolution rate of solid phosphorus at 25°C. Oxygen-saturated water or oxygenated water was passed through a cell containing a piece of P_4 with an exposed surface area of 1.25 cm^2. The eluent was collected in volumetric flasks. In the first experiments, aliquots of the aqueous eluent were reacted with excess molybdate reagent to form the heteropoly blue complex. The total phosphorus concentration was determined by monitoring the UV absorbance at 830 nm. In subsequent experiments, the aqueous eluent was discharged into hexane. The hexane was then analyzed for P_4 by GC analysis. Water-soluble phosphorus compounds (presumably orthophosphate was the principal compound) were again reacted with

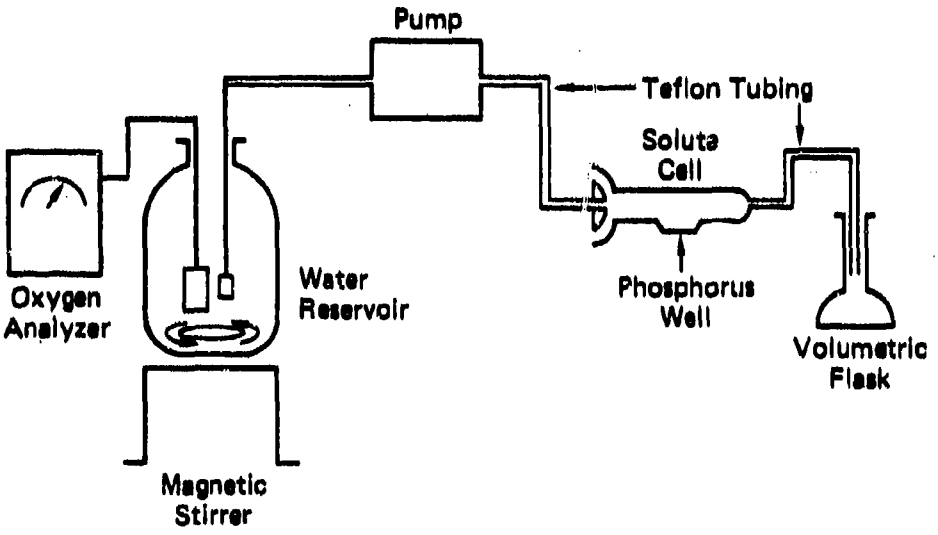

FIGURE 15 DISSOLUTION APPARATUS

molybdate reagent and total phosphorus in the aqueous extract was determined.

The initial measurements were done using a Van Roy pump with a flow rate of about 3 ml min^{-1}. The steady-state total phosphorus concentration was 0.03 ± 0.004 ppm, which corresponds to a dissolution rate of 6.6 μg hr^{-1}. Subsequent runs were performed at lower volumetric flow rates using both the Van Roy pump and a Gilson Mini 2 pump for the lower flow rates. All of these experiments were performed using oxygen-saturated water. The results, (Table 7) indicate that, in general, the average dissolution rate decreases with decreasing flow rate. This is expected because at lower rates the hydrodynamic boundary layer next to the phosphorus becomes thicker, which retards the diffusion of oxygen and oxidized species to and from the phosphorus surface, respectively.

Table 7

SUMMARY OF DISSOLUTION EXPERIMENTS IN O_2-SATURATED WATER

Flow Rate (ml/min)	Avg Aqueous Conc P (ppm)	Average Dissolution Rate (μg/hr)
3.00	0.03	6.7
0.54	0.05	2.0
0.42	0.15	3.5
0.34	0.13	2.6
0.14	0.32	1.5
N_2-purged water		
0.33	0.12	2.4
0.29	0.13	2.5

Rate studies done with nitrogen-purged water, fresh P_4 water, and aged P_4 water gave the same dissolution rates at steady state as those with oxygen-saturated water (compare the dissolution rates for the three experiments with a flow rate of approximately 0.3 ml min^{-1}). As shown in Figure 16, the rate of orthophosphate (and other water-soluble oxidation products) dissolution decreased rapidly as the oxidized species formed during the loading of the cell were dissolved and swept away in the fresh P_4 water. The aged P_4 water, which had been conditioned for 10 days with oxygen-saturated water, initially eluted more oxidized species, but the rate of dissolution decreased rapidly. The total amount of phosphorus eluted with the oxide species was about 25 μg for the aged water. If the oxidized species were orthophosphate, the thickness of this oxide layer for the exposed area (1.25 cm^2) can be calculated to be:

$$\left(\frac{25\ \mu g}{1.25\ cm^2}\right)\left(\frac{cm^3}{1.9\ g}\right)\left(\frac{g}{10^6\ \mu g}\right)\left(\frac{97\ g\ H_2PO_4}{31\ g\ P}\right) = 3 \times 10^{-5}\ cm$$

or about 3000 Å.

Thus, at long times, when the oxide species are dissolved, the steady-state dissolution rates are dominated by the dissolution of P_4, and therefore the fresh and aged waters gave the same dissolution rate (Figure 17). Moreover, at the relatively high flow rates used in these experiments, the dissolved P_4 did not oxidize appreciably before being collected in the hexane and therefore the concentration of oxide species in the aqueous eluent became negligible at long times.

At lower flow rates, the rate of dissolution of P_4 is expected to diminish further. Unfortunately, 0.14 ml min^{-1} was the lower limit of volumetric flow that we could obtain with our flow pumps. However, the dissolution rate of 1.5 μg/hr per 1.25-cm^2 exposed surface that we

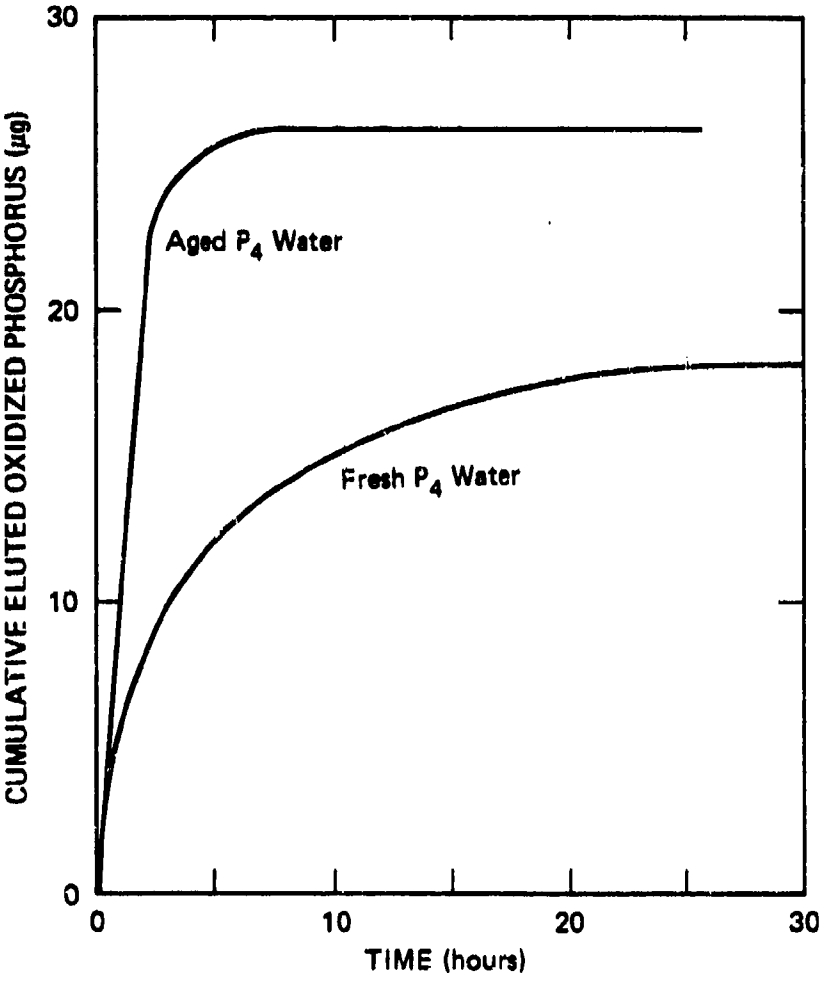

FIGURE 16 CUMULATIVE MASS OF PHOSPHORUS ELUTED IN AQUEOUS FRACTION OF ELUENT

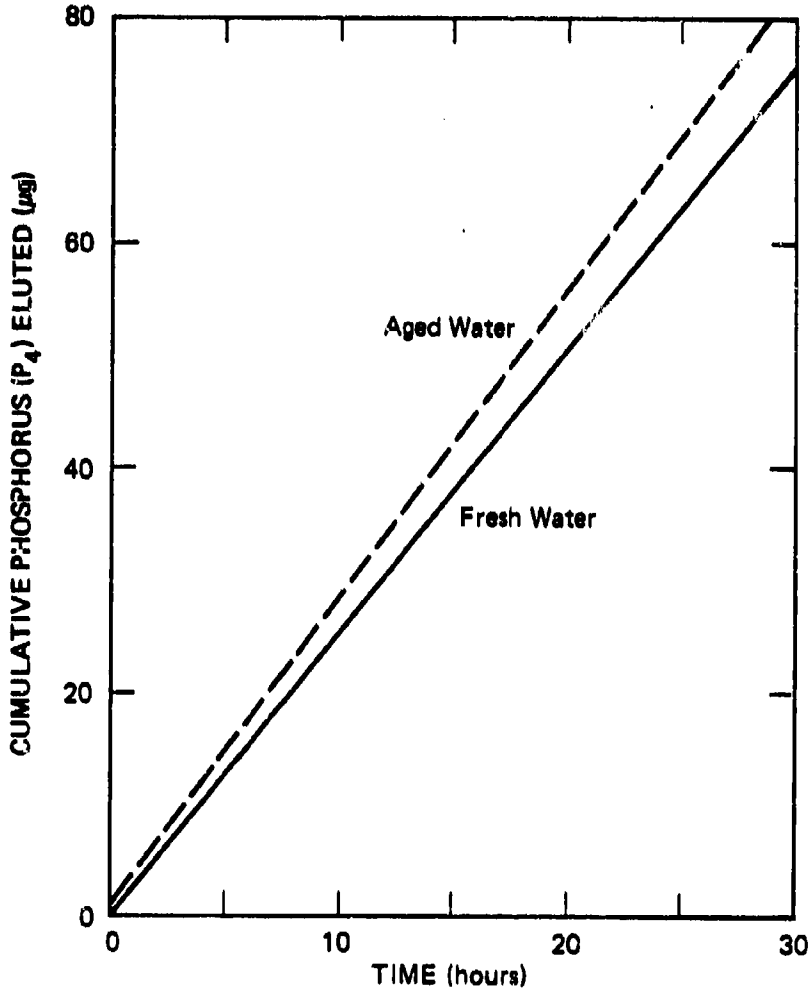

FIGURE 17 CUMULATIVE MASS OF PHOSPHORUS ELUTED AS P_4

measured at this flow rate can be used to estimate an upper limit to be expected for dissolution of P_4.

For example, a 1 cm^3 spherical particle of P_4 in soil would have an exposed surface area of 4.8 cm^2. Thus, the amount of P_4 dissolved in one hour would be

$$(1.5\ \mu g/hr)\ \frac{4.8\ cm^2}{1.25\ cm^2} = 5.8\ \mu g/hr.$$

The amount dissolved in one year would be 51 mg or about 2.8% of the total mass of the 1 cm^3 P_4 particle. Thus, we would expect that this P_4 particle would persist in the environment for many years. The persistence of this particle would, of course, be orders of magnitude greater than the persistence of P_4 dissolved in soil water.

G. PH_3 Properties--Solubility in Water and Henry's Constants

PH_3 (1010 ppm in He) was bubbled through 300 ml of Milli-Q water contained in the Henry's apparatus (Figure 14) submerged in a constant-temperature bath. Water samples were withdrawn for analysis of PH_3 content from a sample port ~ 8" from the tube bottom and ~ 4" beneath the Milli-Q water surface. Solubility measurement were conducted at three temperatures (9.6, 29.7, and 49.7°C). Samples were taken until the PH_3 analyses gave consistent results, usually in about 60 min. Bubbling was stopped just before sampling to prevent the presence of bubbles in the sample. The results, shown in Figure 18, fit a good straight line. From Equation 2, the slope of the line times 2.3 R equals the heat of solution of PH_3 in water. The result, -5.65 kcal $mole^{-1}$, suggests that PH_3 interacts with water, but, to a lesser degree than does ammonia (ΔH_s = -8.28 for NH_3).

The measurement also permits calculation of Henry's constant (H_c) because at saturation, the partial pressure of PH_3 above the solution equals the concentration of PH_3 in the flow stream. The result at 25°C is a value of 6.8×10^4 L-torr $mole^{-1}$.

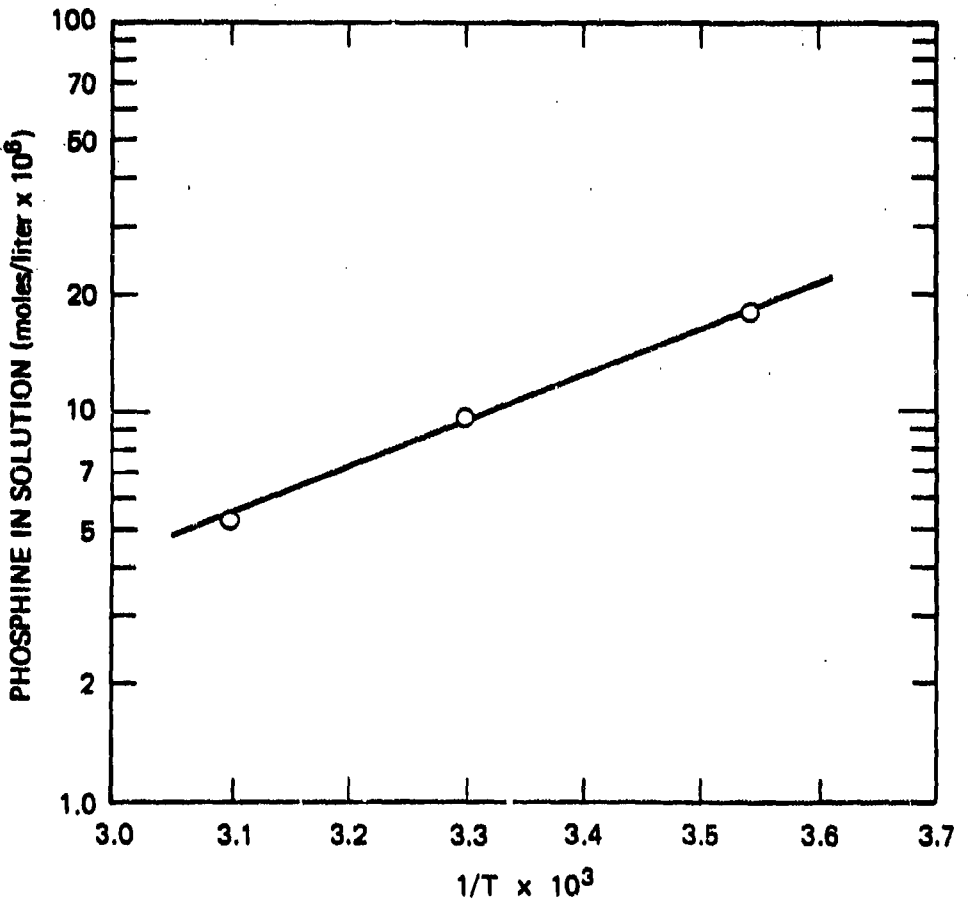

FIGURE 18 SOLUBILITY OF PHOSPHINE IN WATER AS A FUNCTION OF TEMPERATURE

The solubility of PH_3 in water has been previously measured by A. Stock et al. (1909) and R. E. Weston (1954). Weston reports solubility data in terms of the Ostwald coefficient β (conc. of PH_3 is solution/conc. PH_3 is the gas phase). Values for β are unitless because the same concentration units are used. Weston's data summary is poor because he reports only PH_3 pressures and not concentration. However, the concentration of dissolved PH_3 (moles/L) can be calculated by:

$$[PH_3]_{sol} = \frac{[PH_3]_g}{\beta}$$

where $[PH_3]_g = P/RT$.

Henry's constant at 25°C from Weston's results is 3619 l-torr $mole^{-1}$, a value significantly lower than ours. Furthermore, from the effect of temperature on solubility, Weston calculates $\Delta H_{sol} = -2.95$ kcal $mole^{-1}$, which is lower than our value by a factor of about two. The major problem with Weston's results is the uncertainty of the indirect method that he used to measure dissolved PH_3. Phosphine was extracted from the solution by repeated cycles of freezing, thawing, and stirring, and the amount of extracted gas was measured in a gas burette.

Weston concludes that Henry's law for PH_3 is obeyed from 100 to 700 mm and that PH_3 does not show acidic or basic character when dissolved in water. Van Wazer 1958 reports that PH_3 in water undergoes gradual decomposition into P_4, H_2, and a hydride of the approximate formula P_2H. A solid hydrate of PH_3 has been reported (Skinner 1887) with the probable formula $PH_3 \cdot 5.9\ H_2O$ (Claussen, 1951).

The results, summarized in Tables 8 and 9, suggest that PH_3 is more soluble in water and has a higher heat of solution than O_2.

Table 8

HENRY'S CONSTANT AND SOLUBILITY
FOR PHOSPHINE, OXYGEN, AND NITROGEN

Gas	K_h (torr-L mole^{-1}) SRI	Weston[a]	Battino[b]	Solubility in H_2O at 1 atm (moles/L)
PH_3	6.80×10^4	3.62×10^3	-	1.12×10^{-2} (SRI)
O_2	-	-	5.99×10^5	1.27×10^{-3}
N_2	-	-	1.17×10^6	6.47×10^{-4}

[a]Weston (1954).
[b]Battino (1966).

Table 9

HEATS OF SOLUTION OF GASES
IN WATER

Gas	ΔH_{sol} (Kcal mole^{-1}) NBS[a]	Battino[b]	SRI
HCl	-17.9		
NH_3	-8.28		
O_2		-3.44	
PH_3			-5.65

[a]NBS Circular 500.
[b]R. Battino (1966).

H. Physical Properties and Transport Studies Summary

The aqueous solubilities for P_4 were reasonably consistent with reported values. The vapor pressure was about half that reported in the

literature. The Henry's constant that we measured for P_4 using a gas-purge method was about twice what we calculated from the ratio of measured pressure and solubility. This discrepancy is probably due to an error in our measured value of the vapor pressure. The Henry's constant value of 1600 torr M^{-1} indicates that P_4 is fairly volatile in water. The actual volatilization rate of P_4 from water depends on the turbulence of the water body and the air. For P_4 dissolved in a shallow pond, we estimate that the volatilization half-life is on the order of several hours to several days.

The sorption of P_4 to soil is complicated by solution-phase chemistry. P_4 oxidizes rapidly in water, but the process appears to be retarded by the presence of water-soluble soil organic matter. P_4 is not strongly sorbed to soil and is moderately volatile. Therefore, in the absence of chemical transformation we would expect P_4 to be reasonably mobile (leachability and volatility). However, because the oxidation of P_4 is very rapid relative to the estimated time scale for leaching or volatilization, detailed estimation of P_4 mobility is not warranted.

The persistence of particulate P_4 was also estimated by measuring the dissolution rate of P_4 wafers in water at 25°C. The rate was found to be very low, therefore, we estimate that particulate P_4 will persist in a terrestrial environment for many years.

The solubility of red phosphorus in water was too low for us to measure. Because of this very low solubility, we expect that the rate of dissolution of red phosphorus in water is considerably lower than that of white phosphorus. The rate-determining step for dissolution of red phosphorus under aerobic conditions is very likely to be oxidation of the outer layer of red phosphorus particles.

V CHEMICAL TRANSFORMATIONS

The chemical transformation studies centered primarily on the oxidative transformations of the parent compounds, RP/BR and WP/F, the hydrolysis of polyphosphates, and the reactions of phosphine with hydroxyl radical and ozone. These processes in soil, water, or air environments are discussed below.

A. Oxidation of Solid RP/BR in Water

The potential exists for RP/BR to be deposited in aquatic environments from its accidental or intentional deployment into water bodies. Because RP/BR has essentially zero solubility in water, any oxidative transformations would occur at the solid-water interface, eventually producing orthophosphoric acid by hydrolysis of phosphorus oxides.

To study this biphasic reaction as a function of particle size, 2.0-g samples of RP/BR pellets and powder were weighed into 100-cc volumetric flasks and covered with deionized water. Synthetic air was bubbled into the flasks to provide a continuous oxygen-saturated suspension at 8 ppm. Aqueous samples were withdrawn periodically and analyzed by titrimetry for total phosphorus content (i.e., RP was calculated from H_3PO_4). The percentages of RP/BR oxidized as a function of time are shown in Figure 19. Orthophosphoric acid was produced in a linear fashion corresponding to zero-order kinetics over the first 600 hr at 1 or 8% conversions. The projected lifetime for RP/BR powder (<0.01 cm^2) and pellet (0.4 cm^2) were calculated to be 1.0 and 8.0 years, respectively. Consequently, we project that smoke devices deployed into aquatic environments will persist, with half-lives greater than 4 years.

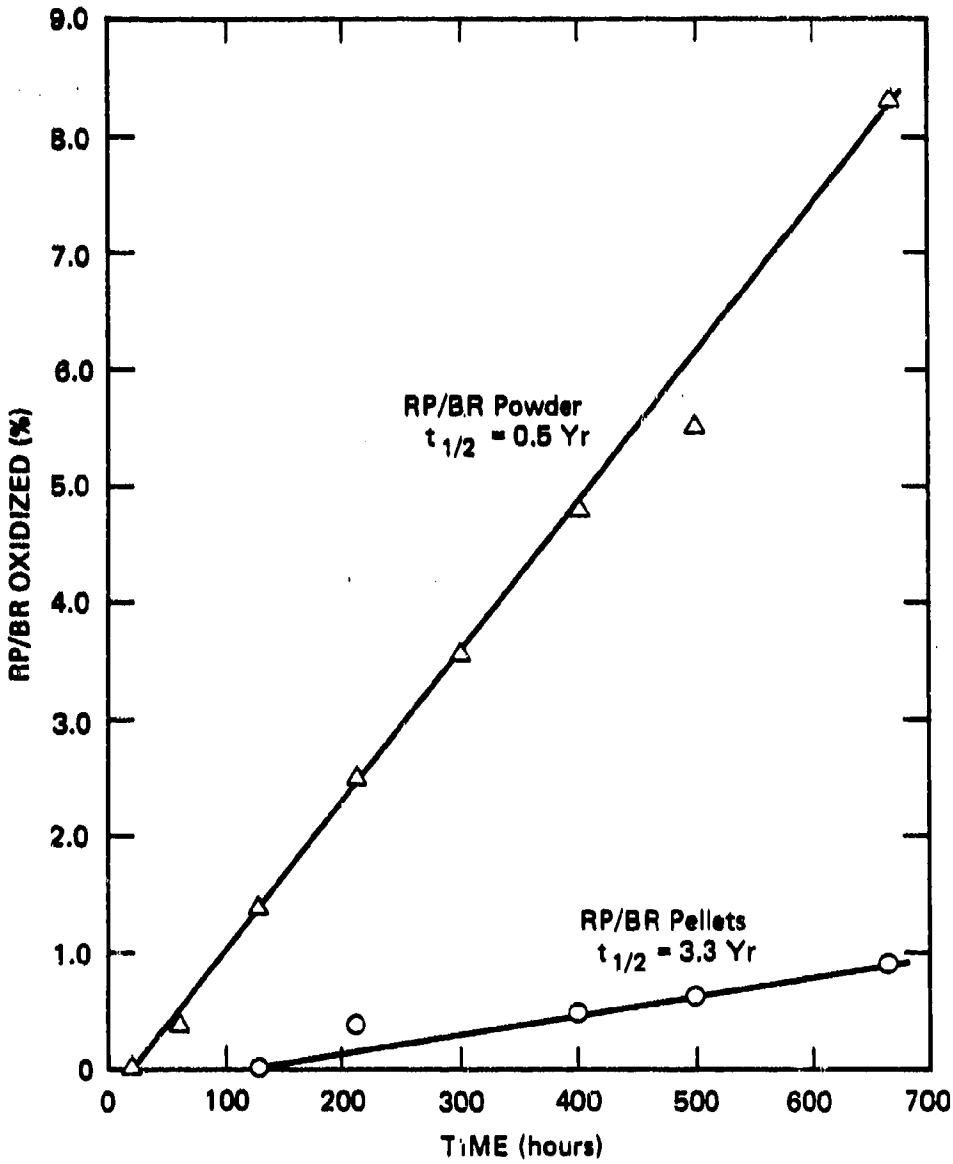

FIGURE 19 OXIDATION OF RP/BR PELLETS AND POWER IN AIR-SATURATED WATER

B. Oxidation of Solid RP/BR in Air as a Function of Relative Humidity and Oxygen Partial Pressure

RP/BR can also be dispersed on the ground due to spillage, ignition malfunction, or incomplete combustion. In these cases, air oxidation will be a primary process for transformation.

To study this process, 2.0-g samples of RP/BR were held in a desiccator at 25°C at different relative humidities (87% and 31%). Periodically, samples were removed, weighed, and heated in boiling water, and the aqueous phase was analyzed by titrimetry.

The pellets were found to be very hydroscopic, with weight gain rates of 0.23 mg g^{-1} hr^{-1} at 87% relative humidity and 0.20 mg g^{-1} hr^{-1} at 37% relative humidity. This is not unusual due to the known desiccating properties of P_2O_5 (P_4O_{10}), an expected oxidative tranformation product (hydrolysis yields orthophosphoric acid).

Oxidation of RP/BR as a function of time appears to be independent of relative humidity (Figure 20) and follows zero-order kinetics over the first 600 hr. From these data, a lifetime of 3.5 years was calculated. At some point we might expect the oxidation to deviate from linearity and become limited by oxygen diffusion through the surface oxide layers. However, from the length of the projected lifetime, we would expect that RP/BR surfaces would be renewed by natural precipitation.

The effect of oxygen pressure was examined to evaluate the persistence of RP/BR in environments where oxygen was limiting, such as in soils of various depths where reaction is limited by diffusion of oxygen to the RP/BR surface. For these experiments, 2.0- g samples of RP/BR pellets were exposed to 1 atmosphere of N_2/O_2 mixtures containing 20, 10, 5, and 0% oxygen. Samples were withdrawn after 300 to 500 hr of exposure and analyzed for oxidation products by the standard titration technique. The results are plotted in Figure 21 in terms of the rate of RP oxidation versus oxygen partial pressure. If we assume that the oxidation is linear with time (at least up to the point where oxygen diffusion becomes rate-limiting), an initial half-life for each data

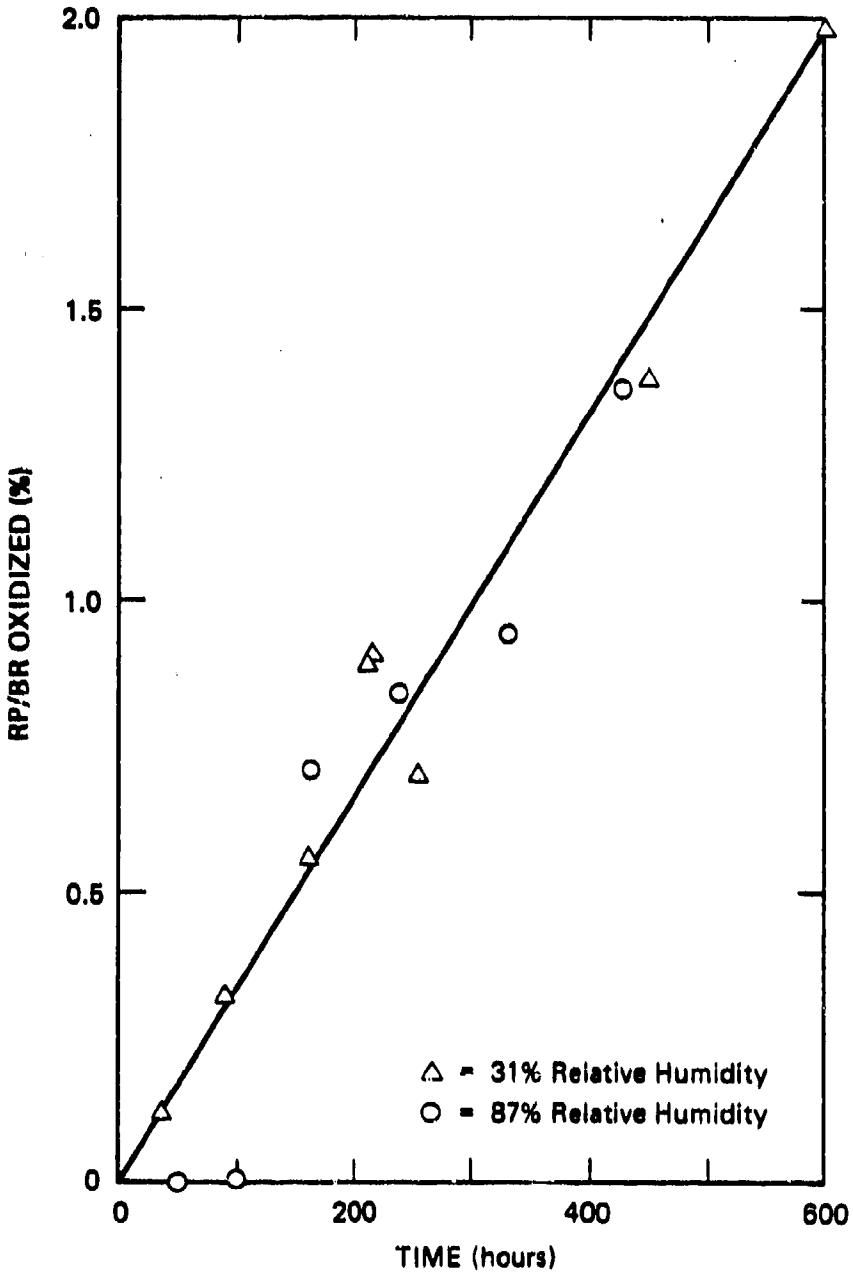

FIGURE 20 EFFECT OF RELATIVE HUMIDITY ON THE OXIDATION OF RP/BR PELLETS

point can be calculated as shown in Figure 21. The RP/BR half-life versus oxygen partial pressure is plotted in Figure 22. This curve allows us to predict RP/BR stability under partially anaerobic conditions such as in soils and sediments. It is apparent from the curve that RP/BR will be persistent in low-oxygen environments.

C. Oxidation of Solid WP/F in Water

The oxidation of solid WP/F in water was performed in a similar manner to that described for RP/BR in water and was monitored by the release of orthophosphoric acid to the air-saturated water. A plot of the percent P_4 oxidized versus time is shown in Figure 23. By fitting the data points to a straight line and assuming zero-order kinetics, a half-life of 2.43 years (2.35×10^3% hr^{-1}) was calculated for a 1 cm^3 chunk of white phosphorus. During the course of this and subsequent experiments, the P_4 surface whitened with time due to oxidative and/or hydrolytic changes. This may limit oxidation by establishing a barrier at which the tranformation becomes limited by oxygen diffusion through the barrier. This surface skin was difficult to characterize due to its poor solubility in water and organic solvents. These findings suggest that the barrier is polymeric in nature. Thus, we project that the half-life of 2.43 years is minimum for a 1 cm^3 piece of white phosphorus and that longer half-lives could result when diffusion of oxygen becomes the rate-limiting process.

D. Oxidation of Solid WP/F in Air and Soil

WP/F reacts rapidly in air, beginning with wisps of white smoke followed by inflammation in less than 5 min. Dainton and Bevington (1945) have studied this reaction as a function of temperature and air partial pressure. Their data suggest that phosphorus will inflame under most environmental temperatures (>5°C) and pressures. Therefore, no further studies were conducted to evaluate this process because environmental persistence is expected to be extremely short for WP/F on terrestrial surfaces.

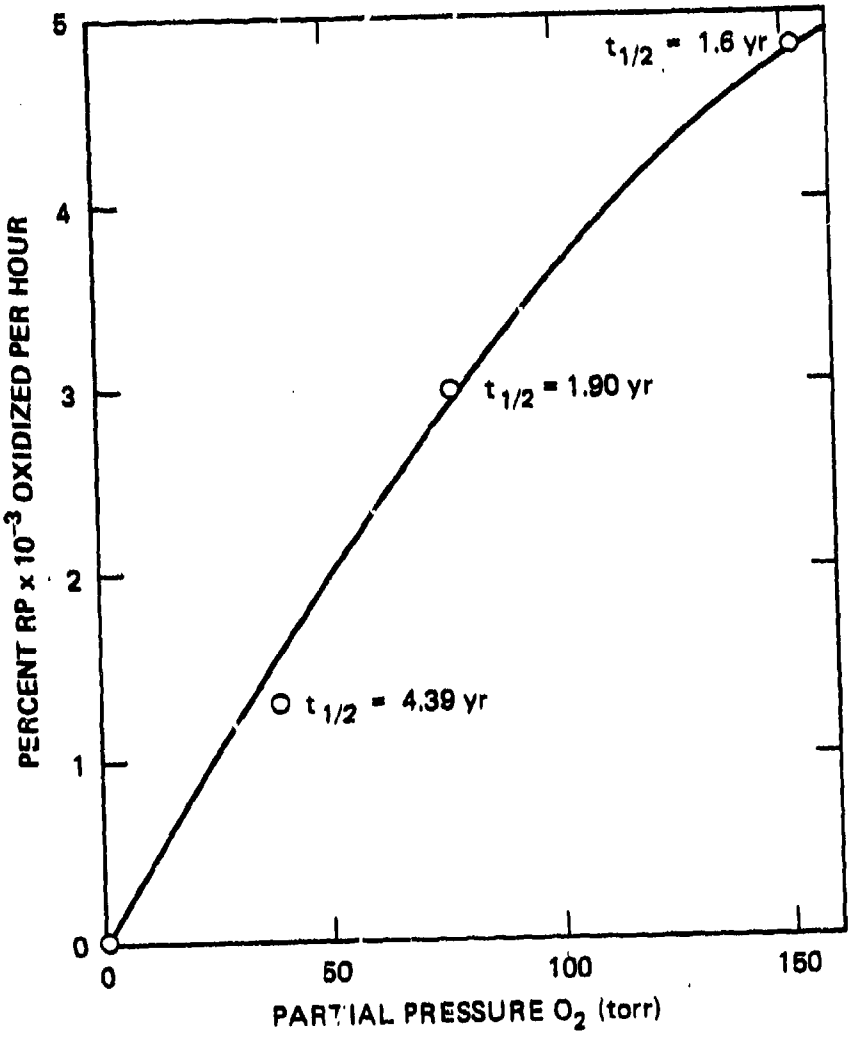

FIGURE 21 OXIDATION OF RP/BR PELLETS AT 1 ATMOSPHERE AND 100% RELATIVE HUMIDITY AS A FUNCTION OF O_2 PARTIAL PRESSURE

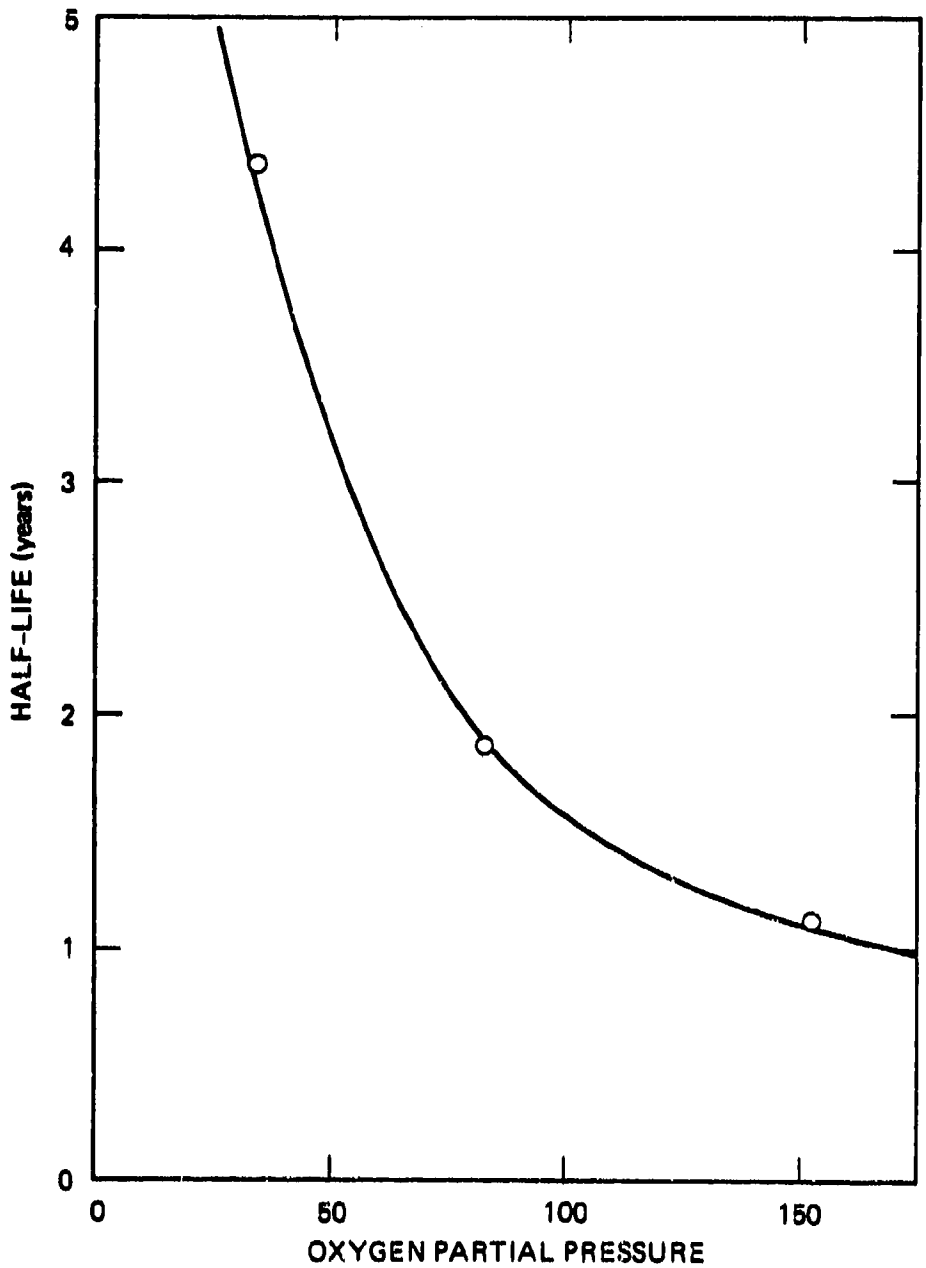

FIGURE 22 OXIDATION HALF-LIFE OF RP/BR PELLETS AT 1 ATMOSPHERE AND 100% RELATIVE HUMIDITY AS A FUNCTION OF OXYGEN PARTIAL PRESSURE

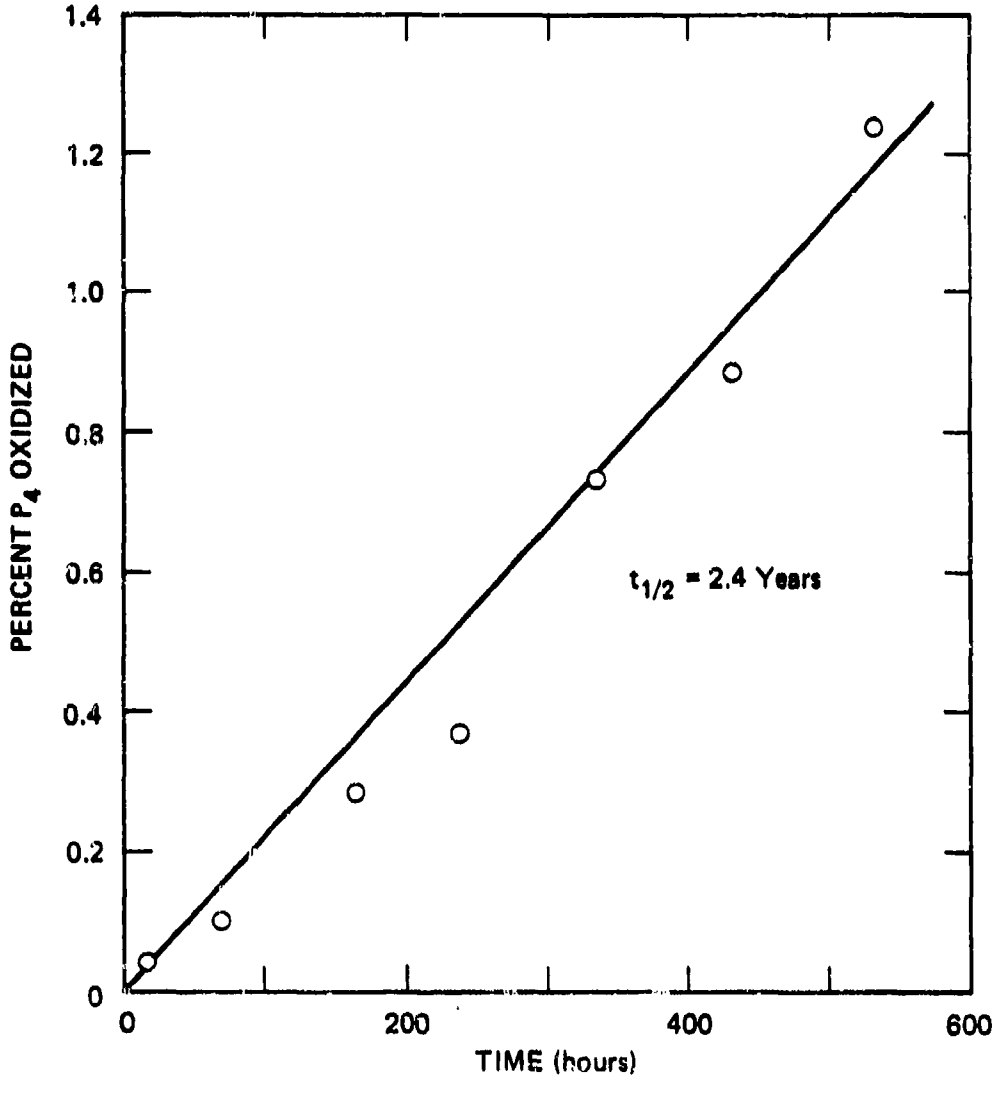

FIGURE 23 OXIDATION OF WP/F IN AIR-SATURATED WATER

From the two examples of WP/F oxidation in air (20% O_2, spontaneous) and water (8×10^{-4}% O_2, $t_{1/2}$ = 2.46 years), the dependence on oxygen concentration is obvious. Thus, for WP/F buried in soil, oxygen-diffusion rates through the soil column and depth will be critical factors in the estimation of persistence. Because most soils become anaerobic short distances below the soil surface, we project that the half-life of WP/F buried in soil will be extremely long.

E. Hydrolysis of WP/F and RP/BR Burn Residues

The residues of WP/F and RP/BR burns contain the same profile of linear condensed polyphosphates as observed in the aerosol burns with the addition of small amounts of higher homologs up to P_{22}-polyphosphates. The pH of the residue is low (2.1) and results in a self-catalyzed acid hydrolysis of the polyphosphates. This is readily observed in the chromatographic profiles of WP burn residues at 0, 4, 24, and 96 hr (Figure 24). If the rate of formation of orthophosphoric acid is used as a measure of the rate of hydrolysis of the mixed linear polyphosphates, then a first-order rate constant of 0.014 hr^{-1} can be calculated from the 0- and 96-hr data. This corresponds to a residue half-life of 49 hr for conversion to orthophosphoric acid. In this time frame, the concentrations of P_2 and P_3 homologs increase due to the hydrolysis of higher homologs, but their hydrolysis will essentially be complete in 96 hr. Thus, the persistence of burn residues is expected to be short as long as low pH conditions are maintained.

F. Generation of Phosphine from WP/F and RP/BR

The initial analysis of the vapor phase from WP/F and RP/BR burns showed the presence of small amounts of phosphine (PH_3). The finding of a reduced product (oxidation state -3) in an oxidizing environment probably results from the disproportionation of lower phosphorus oxides in the presence of water, as shown below.

$$P_4O_6 + 6H_2O \longrightarrow PH_3 + 3H_3PO_4 \qquad (1)$$

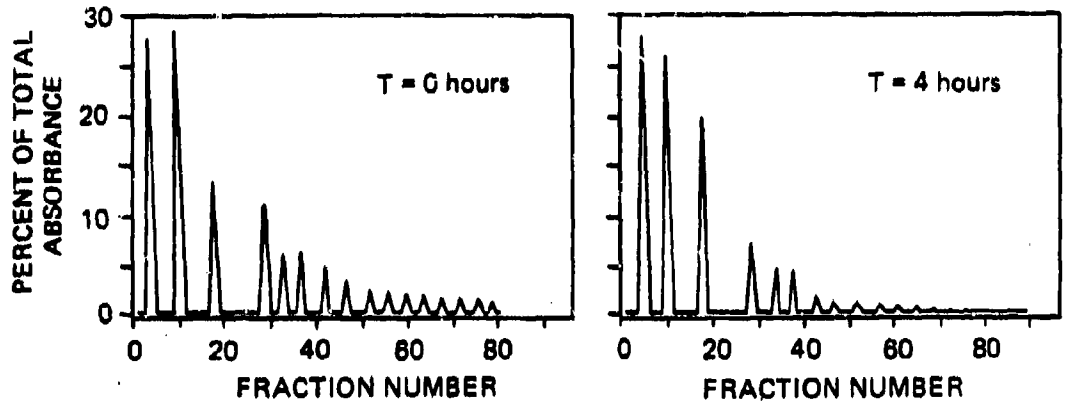

APPROXIMATE AREA PERCENT

Linear Phosphate	Area Percent
P1	24.77
P2	24.82
P3	11.14
P4	9.49
P5	5.22
P6	5.15
P7	4.05
P8	2.83
P9	2.89
P10	1.87
P11	1.65
P12	1.50
P13	1.46
P14	1.27
P15	1.19
P16	0.00

APPROXIMATE AREA PERCENT

Linear Phosphate	Area Percent
P1	27.83
P2	25.94
P3	19.44
P4	7.01
P5	4.42
P6	4.23
P7	1.78
P8	1.29
P9	0.92
P10	0.76
P11	0.55
P12	0.43
P13	0.33
P14	0.29
P15	0.24

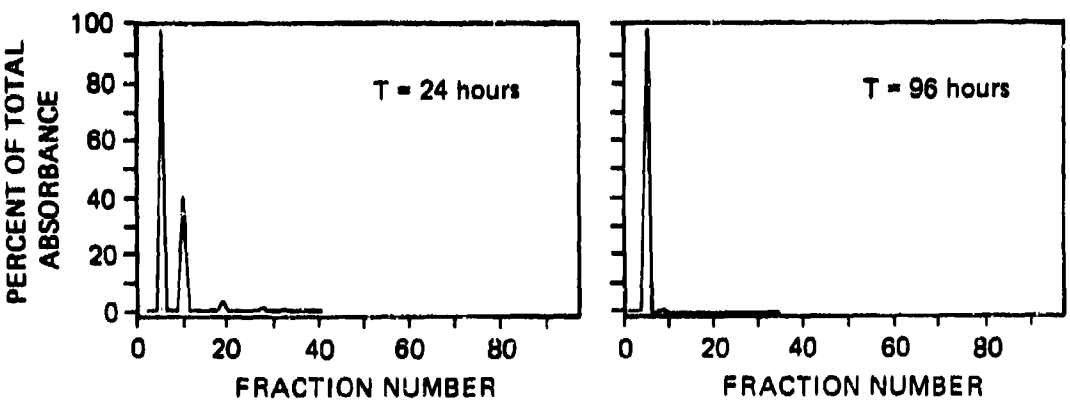

APPROXIMATE AREA PERCENT

Linear Phosphate	Area Percent
P1	68.52
P2	28.00
P3	2.61
P4	0.64
P5	0.23

APPROXIMATE AREA PERCENT

Linear Phosphate	Area Percent
P1	99.54
P2	0.46
P3	

FIGURE 24 CHROMATOGRAPHIC PROFILES OF WP BURN RESIDUES AS A FUNCTION OF TIME

To study this effect, a 1.67-g sample of WP/F was allowed to react with 1 atm of air at 100% relative humidity in a 492-cc Monel reactor. After the initial reaction, the pressure in the reactor was readjusted to 1 atm with air. Vapor samples were removed periodically and analyzed for phosphine by GC the following conditions:

Instrument: Hewlett-Packard 5730A Gas Chromatograph

Column: 4 mm x 2.5 m glass column packed with 80/100 mesh Porapak P

Column Temp: 75°C isothermal

Flow rate: 35 cc min^{-1} N_2

Detector: Nitrogen-phosphorus (NP)

Instrument calibration was performed using 10- and 1000-ppm standards in helium obtained from Matheson Gas Products.

The formation of phosphine as a function of time is shown in Figure 25. Nearly 500 ppm of phosphine (0.1% of initial P_4) was generated after 300 hr. Although the rate of oxidation was not determined, the oxidation of WP/F was 91% complete, as measured by titrimetry, at the end of the experiment.

The effect of oxygen on the generation of phosphine was investigated by weighing 1-g samples of WP/F into the Monel reactor and condensing various oxygen concentrations into the reactor at -196°C. The reactor was allowed to warm to room temperature, at which a vigorous reaction occurred. Vapor samples were removed approximately 1 hour after combustion and analyzed for phosphine. The concentration of phosphine versus oxygen concentration is shown in Figure 26. The results demonstrate that in the presence of water, phosphine is formed in a logarithmic fashion that is inversely related to the oxygen concentration. This is a reasonable expectation for the decomposition of reactive intermediate (X) by competitive pathways (Equation 8).

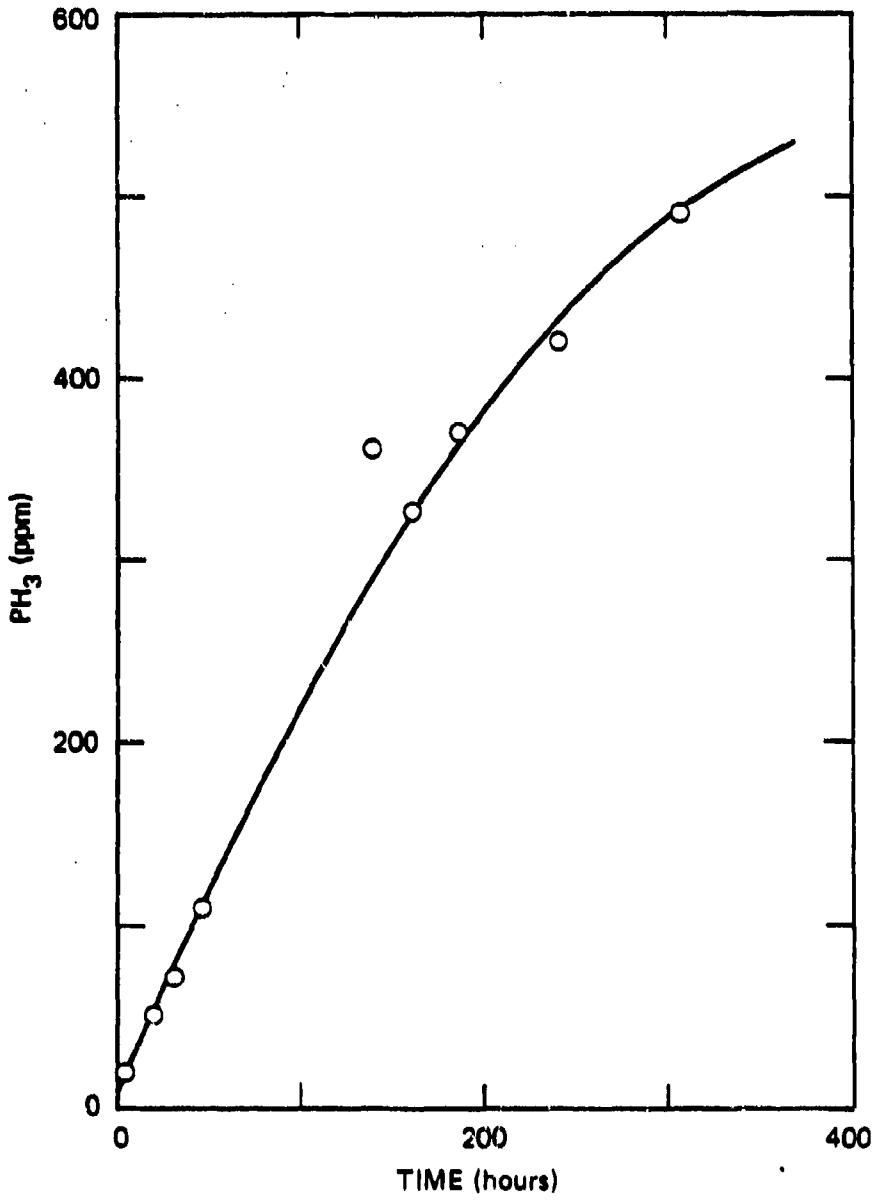

FIGURE 25 GENERATION OF PHOSPHINE FROM THE COMBUSTION OF 1.67-g OF WP/F IN AIR AT 100% RELATIVE HUMIDITY

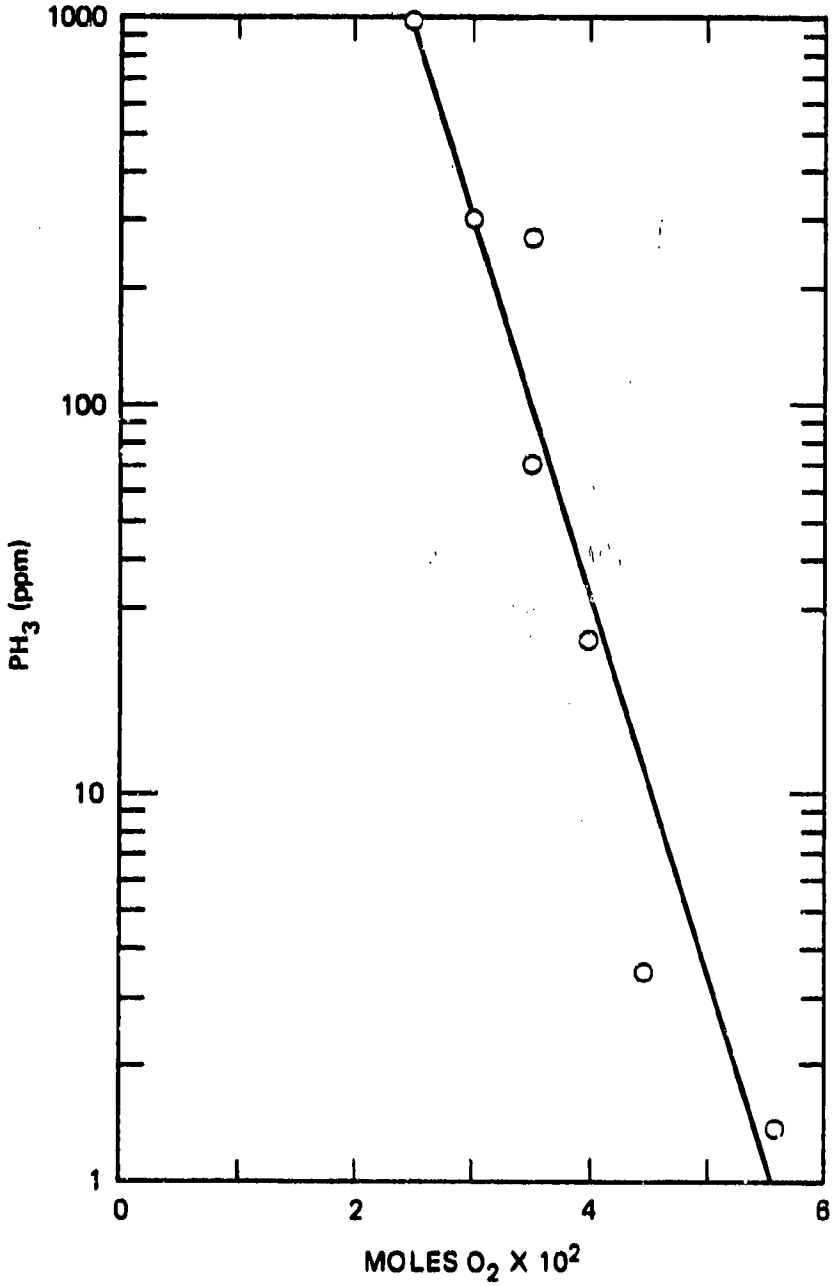

FIGURE 26 GENERATION OF PHOSPHINE FROM 1.0-g OF WP/F AS A FUNCTION OF OXYGEN CONCENTRATION

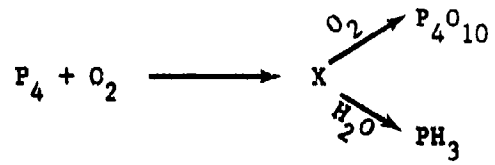

Thus, phosphine formation is favored at low oxygen pressures such as might be found in soils or storage tanks when moisture is present.

The generation of phosphine from RP/BR burns was also investigated. Analogous to the WP/F study, 2-g samples of RP/BR pellets were ignited with a Nichrom fuse wire in 3 atm of oxygen at 100% relative humidity in the 492-cc Monel reactor. Following combustion, the reactor was adjusted to 1 atm with air. Vapor aliquots were periodically removed and analyzed for phosphine by GC. After time periods up to 200 hrs, no phosphine was detected at 30, 50, or 60% conversions of RP/BR. Although we had difficulty in maintaining the burn of RP/BR in the reactor, we conclude that the partial oxidation of RP/BR yields a lower fraction of lower phosphorus oxides than was observed with WP/F. This result, however, is inconsistent with the similarity in aerosol products between the two smoke agents.

In studies designed to determine products arising from uncombusted RP/BR (such as materials that might be discarded or partially combusted) we were able to detect the generation of phosphine. In this study, RP/BR pellets were maintained in the reactor in atmospheres containing 5, 10, and 100% oxygen at 1 atm and 100% relative humidity. The formation of phosphine at each oxygen concentration versus time is shown in Figure 27. In this case, phosphine concentration increases with time and oxygen concentration (note Y-axis). This is opposite to what was observed for WP/F and is a result of the nonspontaneity of RP/BR reactions in air (i.e., higher energy of activation for polymeric P_4 vs monomeric P_4). The expected initial rate of phosphine formation (up to 200 hr) vs oxygen concentration is shown in Figure 28. For normal environmental conditions under high humidity, we project a rate of approximately 0.3 ppm hr^{-1}.

If the generation of phosphine is dependent on water as a reactant, its rate of formation should be a function of relative humidity. To

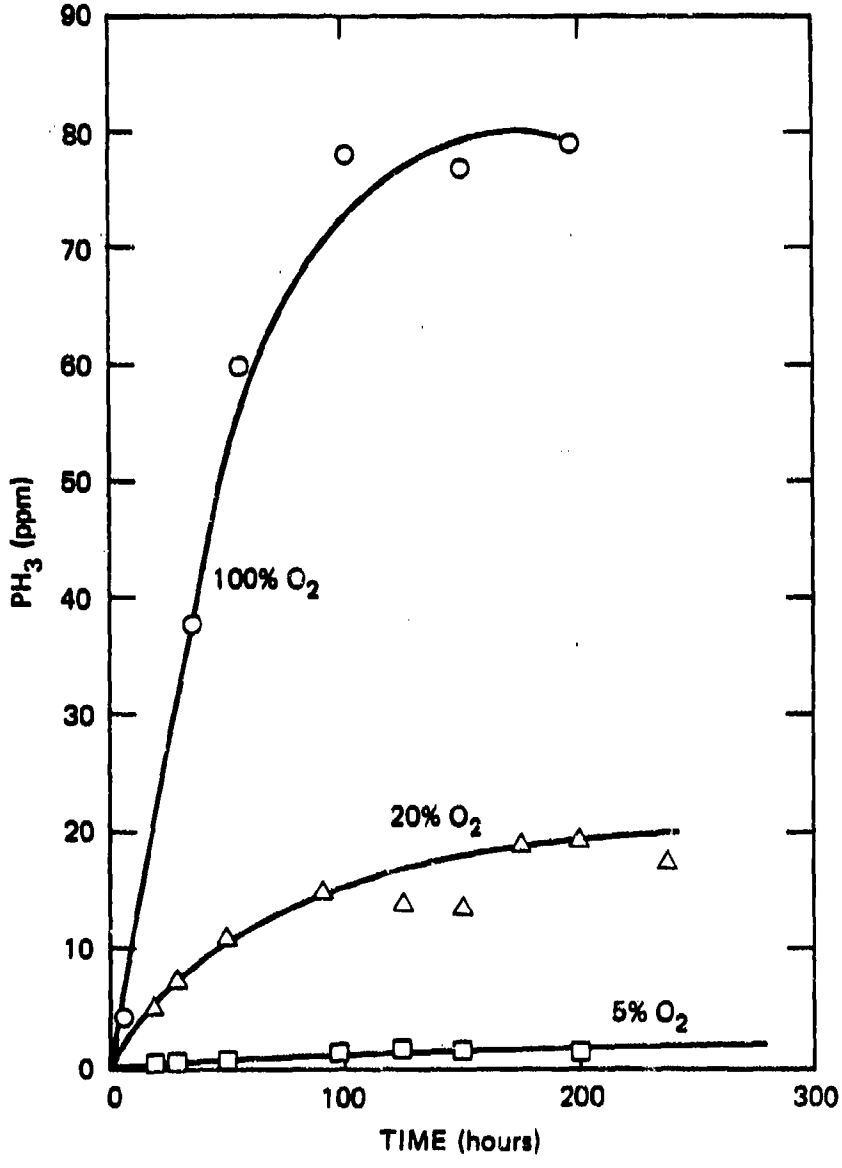

FIGURE 27 GENERATICN OF PHOSPHINE FROM RP/BR PELLETS AT 100% RELATIVE HUMIDITY AS A FUNCTION OF TIME AND PERCENT ATMOSPHERIC OXYGEN

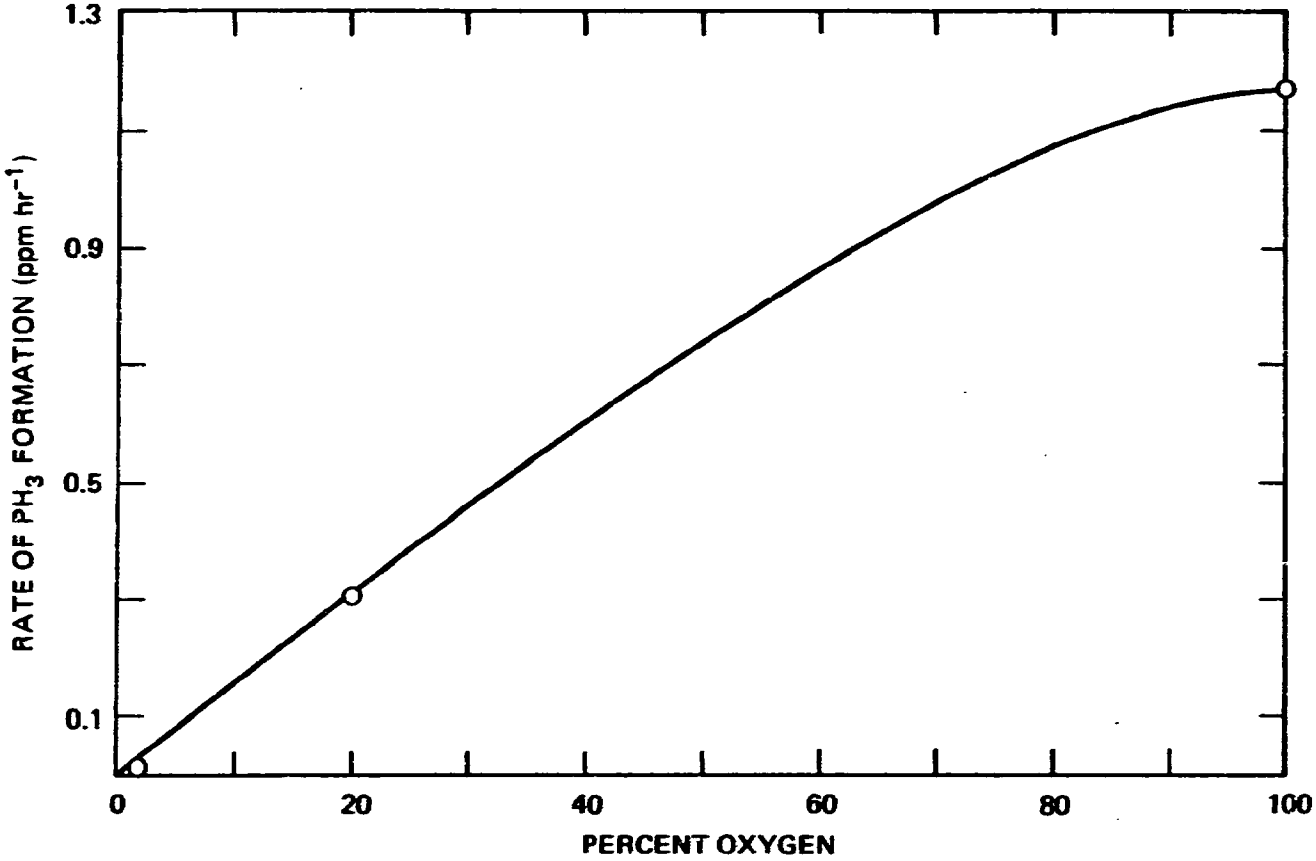

FIGURE 28 RATE OF PHOSPHINE FORMATION AS A FUNCTION OF PERCENT OXYGEN

study this effect, 2-g samples of RP/BR were placed in a glass beaker in the Monel reactor at 1 atm air above constant humidity solutions (saturated $CaCl_2 \cdot 6H_2O$ = 32% RH; saturated $Ca(NO_3)_2 \cdot 4H_2O$ = 52% RH; H_2O = 100% RH). Vapor aliquots were removed periodically and analyzed for phosphine by GC.

Phosphine concentration vs time for each relative humidity are plotted in Figure 29. These data indeed show a phosphine dependence on relative humidity for the initial formation rates. The leveling-off effect is probably due to surface coatings that limit the diffusion of oxygen to the RP/BR surface. A semilog plot of initial rate vs relative humidity is shown in Figure 30 and, except for one data point, gives a nearly linear fit over humidities ranging from 32 to 100%.

The fraction of mass of RP/BR converted to phosphine is small. However, because of the toxic nature of the latter component, the conditions that favor its formation should be noted, especially in environments where RP/BR may be concentrated.

G. Tranformations of WP in Water--Oxidation and Hydrolysis

The stability of WP in water has been reviewed by Sullivan (1979); variable half-lives ranging from 0.85 to 700 hr were reported. Our review of these studies revealed that the experimental design was inadequate in many cases because losses due to volatilization were not considered. We therefore performed experiments to identify the transformation processes responsible for the loss of WP in water and to estimate the rate of each loss process. Losses due to volatilization were discussed in Section III.E.

The loss of P_4 in water was determined in sealed glass reaction flasks with high-purity, metal-free, deoxygenated water prepared using vacuum-line techniques. This precaution was taken because of the reported catalytic effects of metal ions on WP transformations (Sullivan, 1979). The prepared water was saturated with either air or argon for 2 hr and filled the flask to 90% of its volume. WP in ethanol was then introduced into the aerated or argonated reaction flasks by

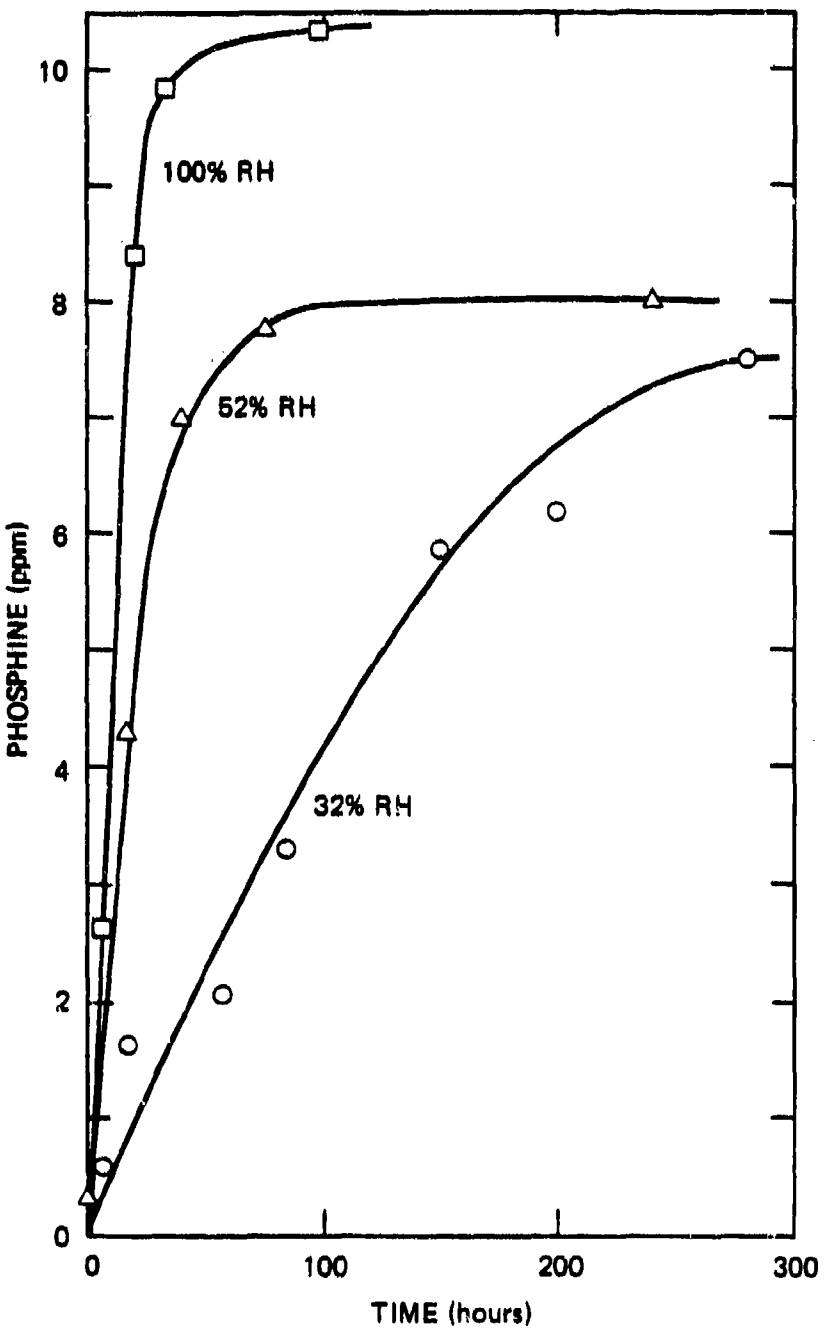

FIGURE 29 EFFECT OF RELATIVE HUMIDITY ON THE GENERATION OF PHOSPHINE FROM RP/BR PELLETS AT 1 ATMOSPHERE AIR

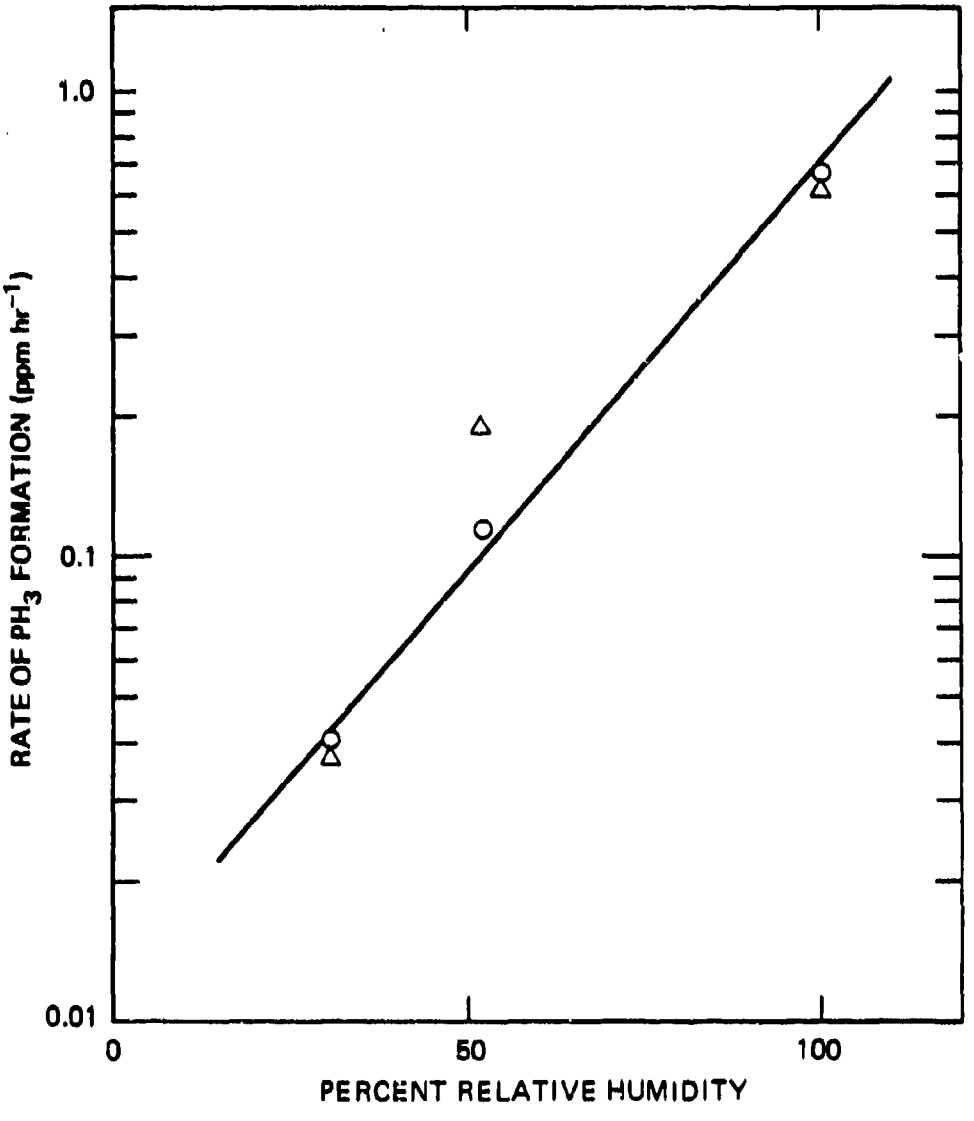

FIGURE 30 GENERATION OF PHOSPHINE FROM RP/BR PELLETS IN AIR AS A FUNCTION OF RELATIVE HUMIDITY

syringe through a Teflon-rubber septum to yield final WP concentrations of 0.5 to 1.0 ppm. Upon the introduction of WP/ethanol, white vapor was observed above the solution. The vapor dissipated slowly--more rapidly with air than with argon. An analysis of the vapor by GC showed P_4 present in the headspace.

Aliquots of the aqueous solutions were removed at selected time intervals, extracted with hexane, and analyzed for WP by GC. A first-order plot of the loss of P_4 in argon- and air-saturated water is shown in Figure 31. The data show good correlation for a first-order kinetic plot and suggest that both hydrolysis and oxidation occur in water. The apparent first-order rate constant for hydrolysis is k_{H_2O} = 8.27 ($\pm$ 1.21) x 10^{-3} hr^{-1} ($t_{1/2}$ = 84 hr) and for oxidation plus hydrolysis is $k_{H_2O + O_2}$ = 1.66 ($\pm$ 0.47) x 10^{-2} hr^{-1} ($t_{1/2}$ = 42 hr). By difference,[2] the oxidation rate constant is k_{OX} = 8.33 x 10^{-3} hr^{-1}, nearly identical to the hydrolysis rate constant.

If hydrolysis occurs, reduced P_4 species must be produced along with phosphorus oxides (H_3PO_2, H_3PO_3, or H_3PO_4). The only reduced species that result from phosphorus hydrolysis are hydrogen and phosphine. To test for the production of hydrogen gas, P_4 was placed in water in an N_2 atmosphere, and headspace gases were analyzed for hydrogen by GC and a thermal conductivity detector. After 94 hr, no hydrogen gas could be detected. A similar experiment was performed to detect phosphine. The results of these experiments are detailed in Tables 10 (absence of oxygen) and 11 (presence of oxygen). The rate constants for loss of P_4 calculated from these data are 8.27 ($\pm$ 0.15) x 10^{-3} hr^{-1} for hydrolysis ($t_{1/2}$ = 84 hr) and 1.23 ($\pm$ 0.05) x 10^{-2} hr^{-1} for oxidation plus hydrolysis ($t_{1/2}$ = 56 hr). The data show that a small percentage of P_4 lost is converted to phosphine, which appears in the headspace. Analyses of phosphate (PO_4^{-3}), phosphite (PO_3^{-2}), and hypophosphite by indirect photometric chromatography and spectrophotometry (molybdate complex) show erratic results during the P_4 transformation, as shown in Table 12. This may be a result of unknown interfering ions in the profile or poor peak integration of small peaks

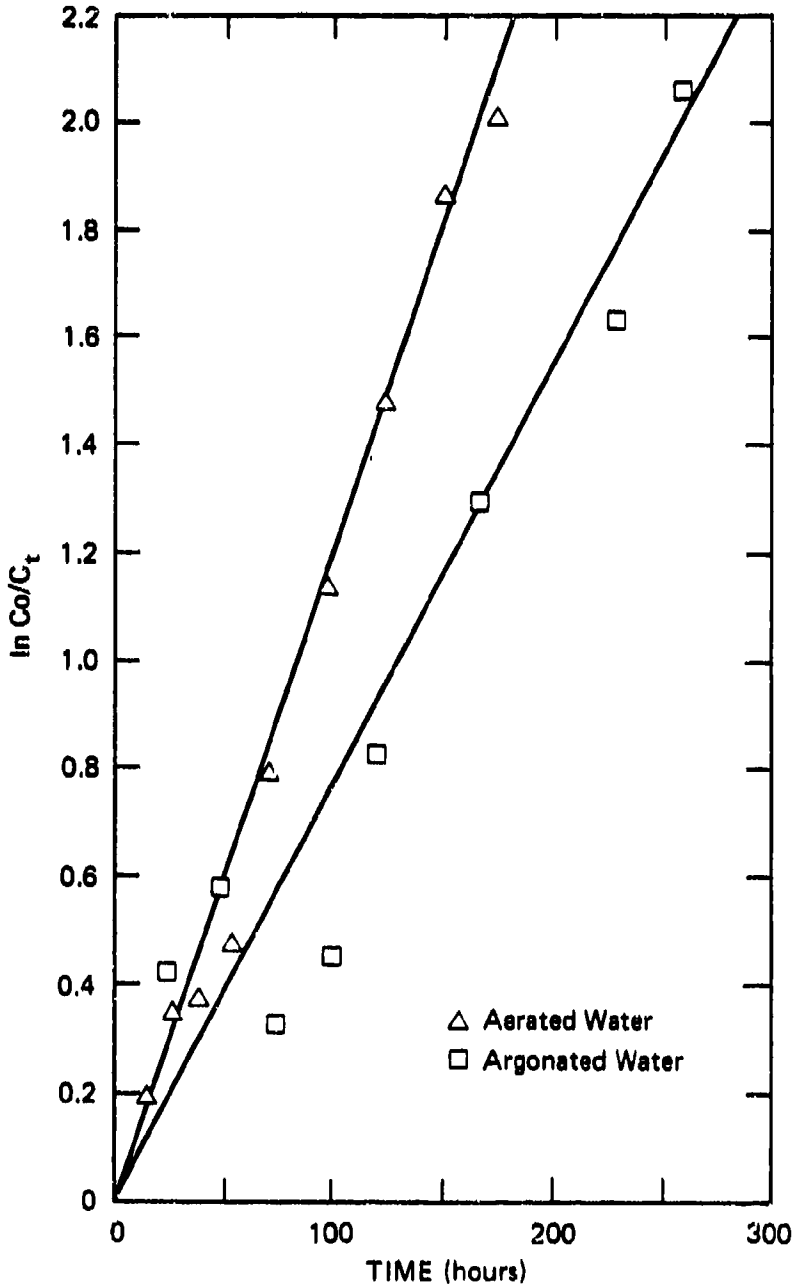

FIGURE 31 HYDROLYSIS AND OXIDATION OF P_4 IN WATER

Table 10

LOSS OF P_4 IN WATER IN THE ABSENCE OF OXYGEN[a]

(hr)	Vol Sol[b] (ml)	P_4 (ppm)	Vol Headspace	PH_3[c] (ppm)	10^3 mmol P_4	10^5 mmol P_4 Lost in Sampling	10^4 mmol P_4 Consumed	10^6 mmol PH_3	% Yield of PH_3[d]
0	500	1.62	17.5	NM	6.53	—	—	—	—
1	497	1.56	21.0	0.84	6.25	3.92	2.38	0.71	0.30
2	494	1.49	24.5	NM	5.94	7.69	5.17	—	—
19	491	1.39	29	3.44	5.50	11.3	9.17	3.99	0.44
22	488	1.28	35.5	3.51	5.04	14.7	13.5	4.98	0.37
26	485	1.23	41.5	5.98	4.81	17.8	15.4	9.93	0.64
43.5	482	1.11	46.5	8.80	4.31	20.8	20.1	16.4	0.82
46	479	1.12	51.5	8.72	4.33	23.5	19.7	18.0	0.91
50	476	NM[e]	55	7.64	—	—	—	—	—
67	476	0.97	58.5	8.56	3.72	26.2	25.5	20.5	0.78
95	473	0.72	65.5	15.6	2.75	28.5	30.5	40.9	1.34
192	470	0.32	70.5	1120	1.21	30.2	50.2	316	6.29

[a] Millipore water (500 ml) was argonated to remove oxygen prior to introduction of an ethanol solution of P_4.

[b] The solution volume and the headspace volume change with time due to sampling. Phosphine samples taken before and after P_4 samples are averaged; reported headspace volumnes are also averaged.

[c] Phosphine concentration in the headspace.

[d] % Yield calculated from $(PH_3/\Delta P_4) \times 100$.

[e] Not measured.

Table 11

LOSS OF P_4 IN AERATED WATER[a]

Time (hr)	Vol Sol[b] (ml)	P_4 (ppm)	Vol Head-space	PH_3[c] (ppm)	10^3 mmol P_4	10^5 mmol P_4 Lost in Sampling	10^4 mmol P_4 Consumed	10^6 mmol PH_3	% Yield[d] of PH_3
0	450	0.93	67	4.52	3.38	—	—	12.1	—
1	447	0.83	78	1.96	2.99	2.25	3.65	6.12	1.68
2	444	0.98	84.5	0.82	3.51	4.06	(-1.70)	2.77	—
4	441	0.84	89.5	3.42	2.99	6.43	3.28	12.2	3.72
5	438	NM[e]	92.5	4.74	—	—	—	17.5	—
6	438	0.83	95.5	3.40	2.93	8.46	3.64	13.0	3.57
23	435	0.60	101	4.91	2.10	10.5	11.7	19.8	1.69
30	432	0.60	106	15.0	2.09	14.5	11.4	63.6	5.58
49	429	0.45	112	39.5	1.56	16.0	16.6	177	10.7
147.5	426	0.15	119	100	0.52	17.1	26.9	476	17.7

[a] Millipore water (450 ml) was aerated with synthetic air prior to introduction of an ethanol solution of P_4.
[b] The solution volume and the headspace volume change with time due to sampling. Phosphine samples taken before and after P_4 samples are averaged; reported headspace volumes are also averaged.
[c] Phosphine concentration in the headspace.
[d] % Yield calculated from $(PH_3/\Delta P_4) \times 100$.
[e] Not measured.

eluting close to each other. However, the production of phosphine does suggest that internal P_4 oxidation-reduction reactions are occurring and that they may be hydrolytic in nature or may involve oxygen after the generation of a hydrolytic intermediate.

A possible hydrolytic mechanism that could generate phosphine is shown in Scheme 1.

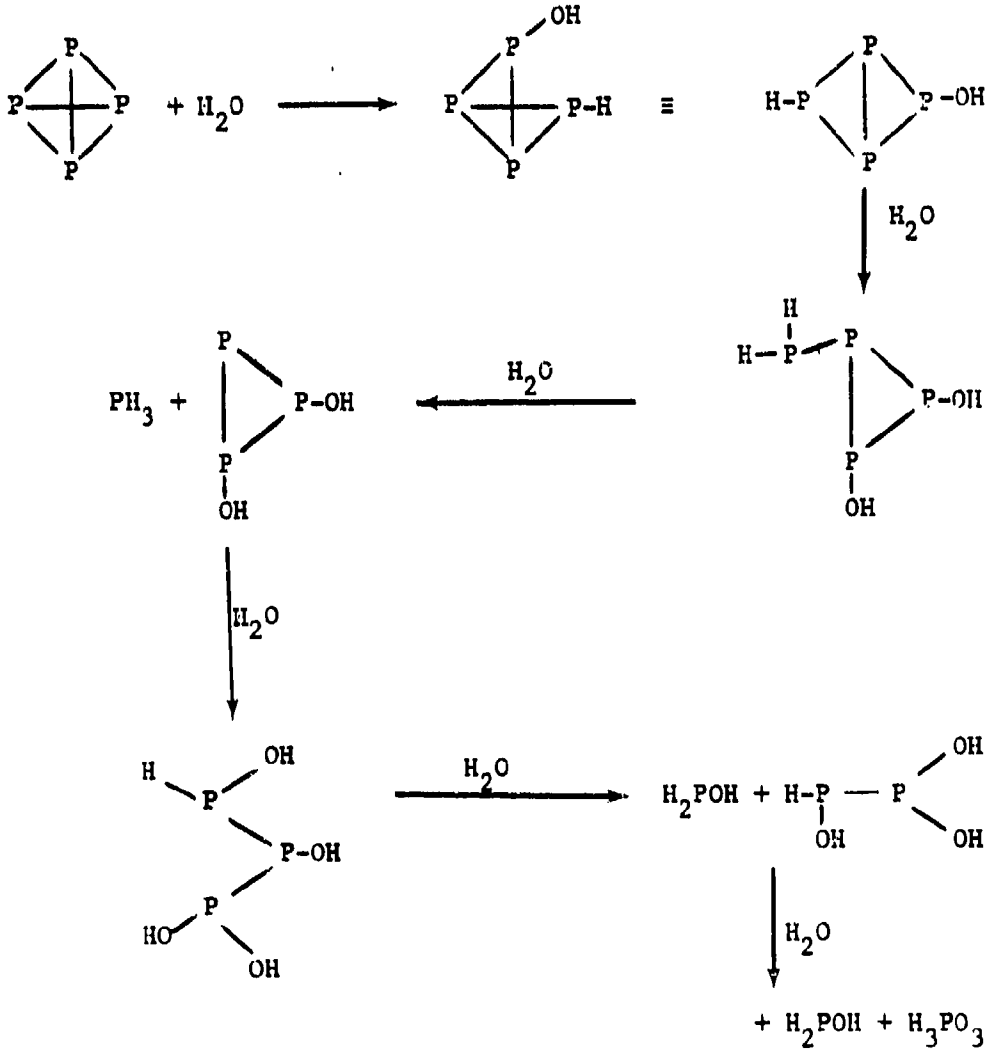

SCHEME 1

The overall reaction is shown in Equation 9.

$$P_4 + 5H_2O \longrightarrow PH_3 + 2H_2POH + H_3PO_3 \qquad (9)$$

Table 12

THE FORMATION OF PHOSPHATE, PHOSPHITE, AND HYPOPHOSPHITE IN P_4 TRANSFORMATION STUDIES (ppm)

Time (hr)	$P_4 \times 10^2$ mmoles		$H_3PO_2 \times 10^2$ mmoles		$H_3PO_3 \times 10^2$ mmoles		$H_3PO_4 \times 10^2$ mmoles	
	Oxid	Hyd	Oxid	Hyd	Oxid	Hyd	Oxid	Hyd
0	2.2	2.0	0.9	0.2	0.4	1.0	1.1	1.4
17	2.1	1.6	2.6	3.1	0.8	1.8	0.3	3.0
40	1.4	1.3	1.0	0.4	1.2	1.3	3.6	1.3
161	0.3	0.1	1.8	6.0	1.2	5.6	2.4	14.4

Although these data are inconclusive as to the exact mechanism of P_4 loss in water, they do indicate that the loss does not depend, to any large degree, on oxygen and that half-lives are generally less than 100 hr.

Contrary to the above transformation results, we found that P_4 was stable in water for up to 21 days in the presence of cysteine and sodium thioglycollate, which were used as oxygen scavengers (see Biotransformation, Section VI.A). We reported that P_4 solutions were

also stabilized in natural waters in the absence of oxygen (see Physical Transport, Section IV.B). In an attempt to understand the stabilization afforded by these solutions, we repeated the cysteine/sodium thioglycollate experiment under conditions identical to those in the hydrolysis studies, using 0.25 g each of cysteine and sodium thioglycollate dissolved in 500 ml of argonated Millipore water. The results of three trials are shown in Table 13.

Table 13

P_4 HYDROLYSIS STUDIES IN THE PRESENCE OF CYSTEINE AND SODIUM THIOGLYCOLLATE

Trial 1		Trial 2		Trial 3	
Time (hr)	P_4 (ppm)	Time (hr)	P_4 (ppm)	Time (hr)	P_4 (ppm)
0	0.42	0	1.00	0	0.29
16.5	0.39	16.5	0.89	16.5	0.30
89	0.25	89	0.57	89	0.14

The rate constants for the loss of P_4 are Trial 1 = 5.69 (± 0.1) x 10^{-3} hr^{-1} ($t_{1/2}$ = 121 hr); Trial 2 = 1.12 (± 0.17) x 10^{-3} hr^{-1} ($t_{1/2}$ = 100 hr), and Trial 3 = 4.99 ± (1.3) x 10^{-3} hr^{-1} ($t_{1/2}$ = 139 hr). The average for these trials is 3.93 (± 0.52) x 10^{-3} hr^{-1} ($t_{1/2}$ = 120 hr). These results indicate some degree of stability relative to the absence of cysteine and sodium thioglycollate; however, the stability is not as great as that observed in the biotransformation studies.

The interaction of WP with other solutes was further investigated by UV absorption spectroscopy and by nuclear magnetic resonance (NMR-^{31}P) spectroscopy. We measured the UV-VIS spectra in 10-cm cells using 3 x 10^{-5} M phosphorus solutions in water and in benzene. The λ_{max} and molar absorptivities appear in Table 14.

Table 14

MOLAR ABSORPTIVITIES AND ABSORPTION MAXIMA
FOR WHITE PHOSPHORUS IN WATER AND BENZENE

	λ_{max} (nm)	ε (mol^{-1} cm^{-1})
P_4 in water	320	480
	335	455
P_4 in benzene	325	4.88×10^3
	340	3.89×10^3

The shift in λ_{max} is not unusual for different solvents, but the increase in the molar absorptivities by a factor of 10 suggests a solvent-solute interaction. This type of association may mimic the charge-transfer complexation observed with iodine and benzene.

The interaction of WP with benzene was further studied by ^{31}P-NMR. WP was dissolved in deuterated cyclohexane containing 100 ppm of tributylphosphate (as an internal standard). The WP resonance was observed at -526 ppm. The chemical shift reported in the literature for WP is -460 ppm in carbon disulfide and is stated to be concentration-dependent (Crutchfield et al., 1967). Benzene was then added to the WP solution and the spectrum was rerun. Chemical shifts of up to 1 ppm were observed. From a plot of chemical shift differences vs added benzene, the energy of interaction was calculated by the method of Lynden-Bell (1969) to be 1 Kcal/mole for the WP-benzene interaction in cyclohexane. Although this observed interaction appears to be very weak, it does indicate that such interactions exist and could possibly offer some degree of stabilization of WP in natural water.

Previous to these studies, the kinetics and mechanism of oxidation of WP in water were believed to parallel vapor-phase reaction pathways where the oxidation proceeds via a radical chain mechanism. The results

of this study demonstrate that the chemistry is not straightforward because the WP loss in water was approximately the same with or without oxygen. For environmental-fate analysis, a rate constant of 1×10^{-2} hr^{-1} will adequately describe the chemical transformation processes (oxidation plus hydrolysis); however, it should be remembered that stabilization of P_4 under selected conditions was observed. Although the loss of WP followed good pseudo-first-order behavior, the lack of a complete material balance between WP and its products indicates that the loss processes are not completely understood.

H. Hydrolysis and Photolysis of Selected Polyphosphates

Osterheld (1972) reviewed the literature on hydrolysis of polyphosphates (discussed in the Phase I report), and extensive literature exists indicating that the hydrolysis is highly pH-dependent, showing both acid and base catalysis. At neutral pH, the hydrolysis of any linear long-chain polyphosphate to shorter chains has a half-life around 20 days. The cyclic polyphosphates decompose at a much slower rate; at neutral pH, their half-life is around 3 years.

Because these hydrolysis reactions have been so well studied, we performed studies to confirm these numbers and to determine whether photolysis could enhance these hydrolysis rate constants.

In the initial studies, we measured the UV-VIS spectra and NMR spectra for orthophosphate, phosphorus acid, hypophosphorus acid, pyrophosphate, tripolyphosphate, hexametaphosphate, and the hydrolytic products of phosphorus pentoxide in water.

The UV-VIS spectra were measured over a concentration range of 10^{-4} to 10^{-1} M in water in 1-cm cells. Over the concentration ranges studied, no systematic deviations from Beer's Law were observed. The pH of each solution and ^{31}P-NMR of selected samples were measured to confirm the species present. For $(NaPO_3)_6$, the pH decreased from 8.1 to 7.1 with increasing concentration, indicating the development of an acidic species. Only one species was detected for $(NaPO_3)_6$ in water by ^{31}P-NMR. Phosphorus (V) oxide in water has three species detectable by ^{31}P-NMR; the mixture contains 10% phosphate, 50% $P_3O_{10}^{5-}$, and 40% $P_4O_{13}^{6-}$. All other compounds were as expected.

All the spectra contain a strong UV absorption with a tail extending toward the visible and in most cases, a shoulder superimposed on the tail. The results are tabulated for all compounds in Table 15. Halmann and Platzer (1965) previously studied the UV-VIS spectra of Na_2HPO_4, and our results are in good agreement with theirs.

We concluded that photolysis screening studies for P_4O_{10}, $(NaPO_3)_6$, and $Na_5P_3O_{10}$ were necessary. The extinction coefficient values for Na_2HPO_4 and $Na_4P_2O_7$ are smaller, but photolysis may also be important for these compounds if the quantum yield is very high. Therefore, photolysis screening studies were conducted for all five compounds.

We performed both the photochemical screening study and the preliminary hydrolysis screening study by ^{31}P-NMR. The chemical shift of selected compounds as measured on our Jeol FX90Q or reported in Crutchfield et al. (1967) are given in Table 16. The hydrolysis of these chemicals was followed by comparing the integrated intensity due to phosphoric acid to all other resonances.

Each compound was dissolved in a 1:1 mixture of H_2O and D_2O to yield 5×10^{-3} M solution. The pH of the solution was adjusted to 7 with phosphoric acid. Each solution was transferred to two NMR tubes, sealed, and analyzed by ^{31}P-NMR. One tube of each compound was placed in a rack and exposed to sunlight; the second tube, to be used as a control, was covered with aluminum foil and also placed in the rack. The tubes were removed from the rack and analyzed by ^{31}P-NMR every 7 days up to a total of 28 days. No differences between the blanks and photolyzed solutions were observed, suggesting that photolysis will not be an important fate process for these compounds. No change in the NMR spectra of orthophosphate or hexametaphosphate was observed. Small changes were observed for pyrophosphate and tripolyphosphate, but the reaction had not reached the first half-life after 28 days.

To further qualify the hydrolysis rate of pyrophosphate and tripolyphosphate, we ran the reaction at pH 3, 7, and 12 and analyzed the reaction by HPLC. Solutions of 1×10^{-4} M polyphosphate were made

Table 15

MOLAR ABSORPTIVITIES ε (L mol^{-1} cm^{-1}) OF PHOSPHORUS OXYCOMPOUNDS FROM 270 TO 360 nm

Wavelength λ (nm)	Ortho-Phosphate Na_2HPO_4	Phosphorus Acid H_3PO_3	Hypophosphorus Acid H_3PO_2	Pyrophosphate $Na_4P_2O_7$	Tripoly-phosphate $Na_5P_3O_{10}$	Hexameta-phosphate $(NaPO_3)_6$	Phosphorus Pentoxide P_4O_{10}
270	0.94	0.24	0.05	---	1.73	---	3.45
280	---	---	---	0.85	---	---	3.12
290	0.89	0.14	0.04	0.74	1.53	2.70	2.49
300	0.79	0.12	0.02	0.58	1.34	2.42	2.24
310	0.65	0.11	0.01	0.41	1.13	2.03	2.14
320	0.05	0.10	0.01	0.26	0.93	1.54	1.91
330	0.39	0.09	>0.01	0.15	0.72	1.08	1.68
340	0.32	0.08	>0.01	0.10	0.70	0.71	1.50
360	0.25	0.08	>0.01	0.08	0.63	0.36	1.26

Table 16

CHEMICAL SHIFTS OF SOME PHOSPHORUS CONTAINING COMPOUNDS[a]

Compound	ppm
H_3PO_4	0
P_4O_6	-112
P_4[b]	-460
H_3PO_3	4.5, J_{H-P} = 700 Hz
PH_3	238, J_{H-P} = 180 Hz
H_3PO_2	12, J_{H-P} = 535 Hz
$(NaPO_3)_6$[c]	-22.5
$(NaPO_3)_4$[c]	-23
$(NaPO_3)_3$[c]	-21
$P_2O_7^{-4}$	-11
$P_3O_{10}^{-5}$	α = -11.5, β = -23.9, $J_{\alpha\beta}$ = 16.7 Hz
$P_4O_{13}^{-6}$	α = -11.5, β = -23.9, $J_{\alpha\beta}$ = 16.7 Hz, $J_{\beta\beta}$ = 15.9 Hz

[a]Reported in Crutchfield et. al. (1967).
[b]Measured in CS_2. In hexane we measured the chemical shift to be -526 ppm.
[c]These resonances are broad and virtually indistinguishable on our NMR.

71

in pH 3, 7, and 12 buffers. These solutions were loaded into sealed glass ampoules such that there were ~ 10 ampoules for each chemical at each pH. The ampoules were then submerged in an oil bath regulated at 25°C; at regular intervals they were removed and analyzed by HPLC. At pH 3, a pseudo-first-order rate constant of 1.39×10^{-3} hr^{-1} was measured, yielding a calculated half-life of 20 days for either phosphate.

We were unable to obtain rate data for the pH 7 and 12 solutions because of very slow transformation rates. We suspect that at the higher pHs, the high negative charge associated with the ionized polyphosphate limits a base hydrolysis.

Although these findings may be true for pyro- and tripolyphosphates, Griffith and Buxton (1967) showed hydrolysis rates to approach a maximum at pH 7, with increasing chain length. The first-order rate constants ranged from 4.6×10^{-6} min^{-1} ($t_{1/2}$ = 105 days) for tetrapolyphosphate to 7.5×10^{-5} min^{-1} ($t_{1/2}$ = 6.4 days) for heptapolyphosphate at pH 7 and 30°C. These investigations suggested a trend toward a maximum hydrolysis rate constant of 8.0×10^{-5} min^{-1} with increasing chain length. However, Gill and Riaz (1969) did not find this to be true; they measured a first-order rate constant for a 54 phosphorous atom polyphosphate of 3.0×10^{-6} min^{-1} ($t_{1/2}$ = 160 days) at pH 7 and 40°C.

The above rate constants are the result of two competitive processes, one being an end-group clipping of orthophosphoric acid and the other being the splitting of a trimetaphosphate (cyclic tripolyphosphate) from the chain. The latter process is probably influenced by a coiled structure of the polyphosphate in solution. The data of Gill and Riaz show that end-group clipping is three times more rapid than trimetaphosphate production at pH 7, whereas the data of Griffith and Buxton show the same ratio of rate constant to vary from 3 to 5 to 7 for penta-, hexa-, and heptapolyphosphates. Although there is no obvious rationale for the discrepancy in these data, it should be pointed out that both processes do occur and are environmentally relevant.

Associated with the biotransformation studies of polyphosphate smoke aerosols (P_1-P_{16}), we observed complete stability of all components in pure water at pH 7 over a 16-day period. However, in sterilized natural water, substantial losses of the P_{10}-P_{16} polyphosphates were observed within six days, with concomitant increases in tripolyphosphate and trimetaphosphate, the cyclic analog of tripolyphosphate (Figure 32). Thus, catalysis by natural water components (probably metal ions, i.e., Mg^{+2}) appears to promote a tripolyphosphate chain cleavage that assists the hydrolysis of long-chained polyphosphates in the environment at neutral pHs.

I. Transformations of Phosphine (PH_3)

Because of the toxic nature of PH_3, studies were performed to evaluate its persistence in the environment. PH_3 is a minor component of the reactions of P_4 in water and soil. Owing to its higher vapor pressure, (1×10^4 torr), almost all PH_3 formed will volatize to the atmosphere, where oxidation and photolysis are the important loss processes.

The UV spectrum of PH_3 shows no absorption beyond 240 nm (Calvert and Pitts, 1966), indicating that no photolysis will occur in sunlight. The other reactions of possible importance are direct reaction with O_2 and oxidation by ozone and OH radical.

We examined the stability of PH_3 in the dark in the presence of air and found no significant loss over a period of several days. The stability of mixtures of PH_3 and NO in air also was studied; at 40 ppm of NO in air, we found that the rate constant for loss of PH_3 was 4.44×10^{-21} cc/molec-s, which corresponds to half-life in the troposphere of about 5000 yr. Therefore, we initiated both literature and laboratory studies to develop reliable values for rate constants for oxidation by ozone and OH radical.

We found no literature values for oxidation of PH_3 by ozone, but did find one report, by Lorenz and Zellner (1982), of the flash photolysis oxidation of PH_3 with OH. They reported a value of

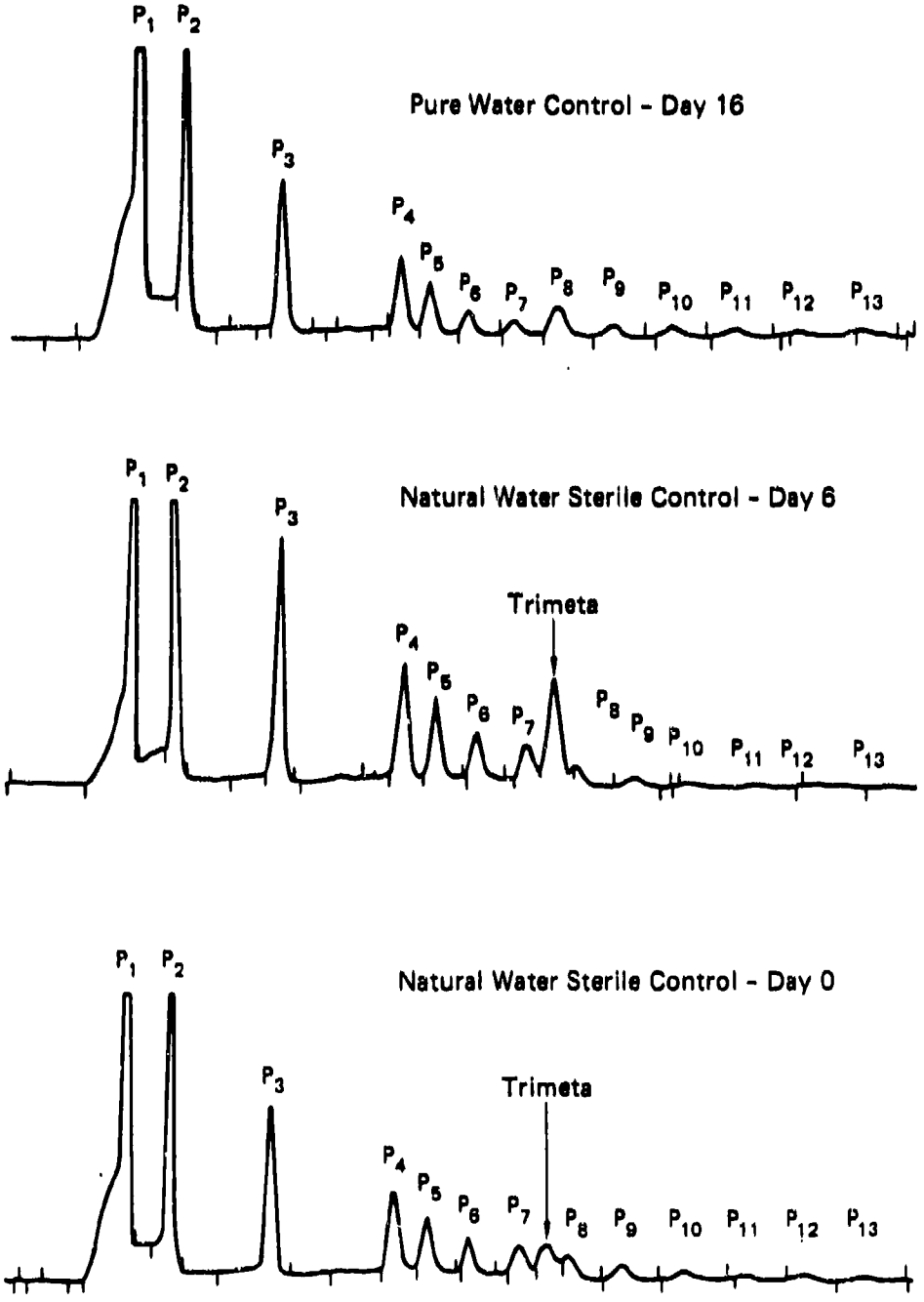

FIGURE 32 HPLC PROFILES OF CONTROL WATER FOR THE BIOTRANSFORMATION OF POLYPHOSPHATES

$k(OH) = 1.6 \times 10^{-11}$ cc/molec-s, which corresponds to a half-life in the troposphere of 5 hr, based on an averaged OH concentration of 2×10^6 molec/cc. For comparison, toluene has a value of k(OH) of 6.1×10^{-12} cc/molec-s (Atkinson, 1975).

Although k(OH) values for organics often are correlated with bond strengths within families of compounds with reported bond strengths, no such data are available for the phosphine family and we found only one reference to the P-H bond strength in PH_3, reported by Sanderson (1971) as between 70 and 80 kcal/mol. This low value implies that PH_3 should react readily with a variety of oxidants in the atmosphere, including OH, NO_3, and O_3.

1. Oxidation with Ozone

Several experiments were performed with mixtures of ozone and PH_3 in air in the dark at 25°C, using 1 to 2 ppm PH_3 and 11 to 4000 ppm O_3 to measure the rate constant. These experiments, summarized in Table 17, show that the rate constant is about $0.5\text{-}1.0 \times 10^{-17}$ cc/molec-s. Experiment 4 showed good linearity over three orders of magnitude in concentration, an usually wide range for a kinetic experiment. Ozone typically is about 1×10^6 times more abundant than OH radical in the troposphere and, when concentration differences are taken into account, $k(O_3)$ would be comparable to a k(OH) value of 1×10^{-11} cc/molec-s, very close to the reported value.

Table 17

OXIDATION OF PH_3 BY OZONE

Run #	Phosphine (ppm)	O_3 (ppm)	Results
1	2.0	0	No measurable reaction after 86 min
2	1.92	4120	100% PH_3 reacted in less than 2 min
3	1.68	368	100% PH_3 reacted in less than 2 min
4	1.32	21.6	$k_{O_3} = 1.0 \times 10^{-17}$ cm^3 molec^{-1} sec^{-1}
5	1.34	11.5	$k_{O_3} = 0.56 \times 10^{-17}$ cm^3 molec^{-1} sec^{-1}

2. Oxidation of PH_3 with OH

We initiated some experiments to measure k(OH) for PH_3 to compare with the one literature value, which was measured at lower pressure. Before doing any experiments with OH- generating system (Atkinson et al., 1981), we performed a few control experiments with mixtures of PH_3 in air with and without NO, MeONO, and CCl_4--all constituents of the OH-generating system. Dark controls showed no loss of PH_3 in any of the mixtures. However, we found rapid loss of PH_3 (1 to 10%/min) in several mixtures when they were exposed to afternoon sunlight. Results were quite reproducible from one day to the next in a given mixture, but showed wide variation (tenfold) from one mixture to another. Thus, removal of NO from mixtures in air markedly slowed the loss of PH_3, but photolysis of PH_3 in ultrapure N_2 gave a rate ten times larger than that in air. In helium the results are opposite to those in nitrogen. These results are summarized in Tables 18 and 19.

Because none of the components of these PH_3 mixtures should absorb any significant solar photons, we have to seek an explanation for these rapid reactions in some other directions or at least exclude other reasonable possibilities.

Table 18

PHOTOLYSIS OF PH_3 IN AIR OR NITROGEN[a,b]

PH_3 (ppm)	N_2 (ppm)	O_2 (ppm)	% PH_3 Reacted	% ΔPH_3/min[a]
1.45	1×10^6	--	83[c,d]	11
1.45	9.7×10^5	2.2×10^5	11[c,d]	1.4

[a]Photolyzed from 3:09 to 3:19 pm in cloudy weather.

[b]PH_3 derived from 1100 ppm PH_3 in N_2; all concentrations in ppm.

[c]Data corrected to clear-sky conditions using a power meter.

[d]Dark controls gave no change in PH_3.

Table 19

PHOTOLYSIS OF PH_3[a]

PH_3 (ppm)	He (ppm)	O_2 (ppm)	N_2 (ppm)	% ΔPH_3	% ΔPH_3/min
11	10%	--	--	3.4[b]	0.34
1.08	9.8×10^4	7.0×10^5	1.98×10^5	19.8[c]	1.46

[a]PH_3 derived from 11 ppm PH_3 in He.

[b]Photolyzed 10 min in sunlight from 11:01 to 11:11 am; dark control stable.

[c]Photolyzed 13 min in sunlight from 5:03 to 5:17 pm; dark control stable.

We have no clear explanation for the photoreactivity of these mixtures; however, some possibilities are discussed below.

Surface-promoted photolysis might occur if PH_3 or some other species were sorbed to the glass, thus creating a surface-sorbed species that absorbs light of > 300 nm. To test for this possibility, and using carefully clean bulbs (5% HF, distilled water, baking at 550°C), we measured rates of loss of PH_3 in air where the light source, a filtered Hg light, either was collimated to a narrow spot on the bulb or remained uncollimated to expose the entire bulb surface. No significant differences in rates were noted, indicating that photolysis is a homogeneous process.

Trace photocatalysts in the PH_3 are likely sources of the phenomenon. Fluck (1973) describes diphosphine (P_2H_4) as a common contaminant in PH_3 that causes the PH_3-air mixture to become spontaneously flammable. Possibly P_2H_4 also is a photocatalyst to initiate chain oxidation of PH_3. However, P_2H_4 cannot explain the very fast loss of PH_3 in pure N_2. Only the presence of another trace oxidant--such as NO_2 or O_3 can--lead to loss of PH_3. However, ozone will lead to rapid dark oxidation and NO_2 needs to be present at stoichiometric levels to effect significant conversions of PH_3. We cannot rule out residual light absorption by PH_3 itself as the cause of the slower rates in helium and air.

A practical approach to estimating the lifetime of PH_3 in the troposphere is to expose PH_3 to sunlight in outdoor air and use the measured rate constant to estimate the half-life or lifetime. One experiment with outdoor air with 1.8 ppm PH_3 and a 15-min exposure to sunlight gave a rate of loss of 1.6% min^{-1} at 23% conversion, essentially the same as reported in Tables 18 and 19. If we take 0.5% min^{-1} as the diurnally average rate of loss of PH_3, this is equivalent to a half-life in the troposphere of 2.3 hr. We can compare this value of $t_{1/2}$, with the value of $t_{1/2}$ calculated at 5 hr for OH radical and at 8 hr for ozone. Thus, ozone and OH radical have nearly the same

reactivity and both are somewhat slower than photolysis. We conclude, therefore, that the persistence of PH_3 in the environment will be short even though the roles of sunlight and other tropospheric agents in PH_3 transformation are not completely understood.

J. Chemical Transformation Summary

The chemical fate of RP/BR released into the environment will be controlled by oxidative transformation. The expected half-life of RP/BR suspended in aerated aquatic or soil environment is expected to range from 1.7 to 3.0 years. In environments where transformation is limited by oxygen diffusion (such as in soil) or the buildup of surface oxide layers, the half-life is expected to be significantly longer.

The chemical fate of WP/F is strongly dependent upon the environment in which it is released. WP/F will oxidize rapidly in air at temperatures above 5°C. However, the rate of oxidation is dependent on oxygen concentrations. Under anaerobic conditions, such as buried in soil, the half-life is projected to be greater than 2 years.

There is evidence to suggest that WP/F is lost by other mechanisms other than oxidation. Hydrolytic processes appear to occur to soluble WP in water at equivalent rates to that of oxidation. The half-life of soluble WP in water is estimated at 42 hours.

The products of the chemical transformation of RP/BR or WP/F are orthophosphoric acid, polyphosphoric acids, meta-phosphoric acids, and phosphine. The linear polyphosphates are rapidly converted to orthophosphoric acid at pH 3 and below. At environmental pHs, their stability is enhanced and half lives of greater than 100 days can be expected.

Phosphine is expected to partition to the atmosphere rapidly where reactions with ozone and hydroxyl radical will limit it's half-life to several hours. Laboratory measurements of the rate constants for oxidation of PH_3 with ozone and HO radical use much higher concentrations of reactants than are found in the atmosphere. However

the calculated half-lives for PH_3 in the troposphere are based on space and time-averaged concentrations of ozone and HO in the lower troposphere and are independent of the method used for measuring the rate constant.

VI BIOTRANSFORMATION

The chemical transformation studies indicated that phosphorus compounds would be stable in environments low in oxygen and at neutral pH. Under these conditions, microbial populations offer an alternative pathway to chemical transformation. Therefore, the biotransformation of several phosphorous species was investigated.

A. WP/F - Water

Because of the rapid volatility of WP and its reactions with oxygen in water solutions, the biotransformation studies were conducted in sealed containers under anaerobic conditions to enhance stability.

In the initial studies we evaluated the toxic effect of WP on anaerobic microorganisms.

We collected soil at SRI and inoculated the supernatant from a soil-water mixture into Difco fluid-thioglycolate medium or into a medium containing glucose (500 ppm), yeast extract (100 ppm), and basal salts.* The flasks were flushed with N_2 gas, stoppered with a Bunsen stopper, and incubated at 25°C.

The grown anaerobic microorganisms were inoculated into flasks containing medium and white phosphorus that had been added to benzene to give a final concentration of 1-3 ppm (near saturation). A control flask was inoculated with solvent only. The turbidity of the media was measured after 24 hr; no growth inhibition was noted in the white

---

*The phosphate-buffer basal-salts medium contained, per liter: 1.8 g of K_2HPO_4, 0.2 g of KH_2PO_4, 0.5 g of $(NH_4)_2SO_4$, 0.05 g of NaCl, 0.05 of $MgSO_4.7H_2O$, 0.1 g of $CaCl_2.2H_2O$, 0.003 g of $FeSO_4.7H_2O$, and 1 ml of trace elements solution. The trace elements solution contained, per liter: 0.1 g of H_3BO_3 and 0.05 g each of $CuSO_4.5H_2O$, $MnSO_4.H_2O$, $ZnSO_4.7H_2O$, Na_2MoO_4, and $CoCl_2.6H_2O$.

phosphorus-containing solutions compared with the controls, indicating that white phosphorus will not be toxic to anaerobic microorganism populations at aqueous saturation levels.

The biodegradability of WP was screened in soils and sediments collected from PBA. For the anaerobic biotransformation test, 500-ml screw-capped erlenmeyer flasks were filled with PBA creek water (WP Creek leading to Yellow Lake) and 0.05 M tris buffer was added. The flasks were placed in an anaerobic chamber, purged with N_2 gas for 2 hr, and preincubated for 4 days. To one flask was added 50 ppm of yeast extract and enough WP from a 600-ppm benzene-ethanol stock solution to yield a final WP concentration of 3 ppm. Autoclaved creek creek containing solvent only was used as a sterile control. Our original attempts to maintain sterility of autoclaved creek water with mercuric chloride solutions failed when WP was observed to transform in less than one day, probably due to a catalytic effect of mercuric ion. Also, significant losses of WP occurred if rubber-stoppered flasks were used, probably due to sorption from the headspace.

All flasks were capped with Teflon liners and incubated in the anaerobic chamber in the dark. Aliquots were removed periodically, extracted with hexane in the anaerobic chamber, and analyzed for WP by GC. Under the above conditions, WP was not biologically or chemically tranformed after 63 days of incubation with or without 50 ppm of added yeast extract. WP added to a local pond water was found to be stable after 14 days of incubation under anaerobic conditions.

That WP was stable in water for 63 days and in pond water for 14 days in the anaerobic chamber was at variance to the chemical transformation studies on WP, which showed both hydrolytic and oxidative transformations to occur, with half-lives of 80 and 42 hr respectively. When the study was conducted in PBA well water, WP decreased from 3.9 to 0.6 ppm in 53 days. A sterile control decreased from 3.6 to 2.6 ppm during the same period. However, when the PBA well water was inoculated into media containing TBSM (0.05 M tris buffer based salts medium lacking phosphate), thioglycolate, cysteine, glucose,

and casamino acids, no transformation occurred after 32 days. This difference in stability is puzzling but may be related to WP interactions with media components, which are not well understood. We also noted enhanced WP-soil extract stability over spiked blank controls. Regardless of what these interactions are, we conclude that biotransformation of WP will not occur rapidly in the environment.

B. WP/F-Soil

A series set of experiments similar to those described above was performed using soil and creek-bottom sediments collected from PBA.

The creek-bottom sediment was sieved through a 2-mm screen and 26.7 g of the wet sediment (20 g dry weight) was put into each of several screw-capped test tubes (25 x 200 mm). Nitrogen-purged water was added to give a total water content of 10 ml in each tube. The tubes were placed in a Forma Scientific Anaerobic System Chamber. After 5 days of preincubation, white phosphorus in benzene/ethanol (1/4 600 ppm stock solution) was added to yield 6 ppm in dry soil, and the samples were capped and incubated in the anaerobic chamber.

Sterile controls were prepared by autoclaving the sediment twice in successive days followed by the addition of white phosphorus. Previous attempts to maintain the sterility of soil by autoclaving followed by mercuric chloride addition resulted in a 90% loss of white phosphorus after one day of incubation. Therefore, mercuric chloride was not added in the control.

Periodically, duplicate tubes were removed from the anaerobic incubator, extracted with hexane anaerobically, and analyzed the WP. The concentration of white phosphorus in PBA creek sediment gradually decreased from 6.1 to 3.1 ppm during 44 days of incubation. However, the concentration in the sterile control also decreased--from 5.4 to 3.7 ppm during 39 days. These data indicate that there is no significant evidence for biotransformation in this sediment.

We had also initiated a biotransformation screening test in PBA soil obtained from a white phosphorus dump site. During 35 days of incubation, the white phosphorus concentration decreased from 5.2 to 0.2 ppm. The concentration in the sterile control decreased at a slower rate--from 5.2 to 1.7 ppm over the same period.

We observed the same phenomenon in SRI soil; the white phosphorus concentration decreased from 5.0 to 0.02 ppm in 4 days but the concentration in the sterile control decreased from 5.0 to 3.2 ppm.

These results show that (1) white phosphorus transformed in flooded, autoclaved soils under anaerobic conditions and that the rate varied, depending on the soil, and (2) white phosphorus transformed faster in some nonsterile soils than in autoclaved, sterile controls. Although this transformation could be biological, some change in the chemical properties of the soil due to autoclaving could be responsible for the differences in transformation rates.

To determine whether these WP transformations in nonsterile soil are biological, small amounts of these WP-transformed soil-water mixtures were inoculated into TBSM with thioglycolate and cysteine, 100 ppm glucose, 100 ppm casamino acids, and 3 ppm WP, contained in Teflon-lined, screw-capped flasks. After 32 days of incubation no WP biotransformation was observed.

Because the pH of the dump-site soil was 3.2, we also prepared citric acid buffer (pH 3.6) to replace the above tris-buffered medium, and the microorganism from the test tube containing WP-tranformed dump-site soil were inoculated. No biotransformation was observed during 12 days of incubation.

From this result it appears that the difference in WP-transformation rate that we observed in PBA and SRI soils between autoclaved and nonautoclaved soil is due to chemical changes in soil, and hence the transformation was nonbiological, or that biotransformation microorganisms are difficult to grow under our test conditions.

C. RP/BR

Because of the extremely low solubility of RP in water and the lack of evidence for the biotransformation of WP in water and soil, no screening studies for the biotransformation of RP/BR were conducted.

D. Condensed Linear Polyphosphates

Because linear condensed phosphates are present in the smoke product, screening tests for biotransformation were conducted with local water and soil. Tripolyphosphate (TPP) was used as a representative of this chemical group.

For aqueous aerobic biotransformation screening, test water from a pond near Searsville Lake was collected and 4 or 20 ppm of TPP (1 and 5 ppm-P, respectively) was added to 2 liters of pond water with and without 100 ppm glucose and 20 ppm yeast extract as supplemental organic nutrients. The amount of condensed phosphate was analyzed by the difference in orthophosphosphate content before and after heat-acid hydrolysis of the water sample.

In the presence of organic nutrients, both the 4- and 20-ppm TPP solutions were completely transformed (>95%) to phosphate in 5 days. In the absence of organic nutrients, 30% of the TPP was transformed (0.3 ppm-P consumed) at 4 ppm TTP and only 10% (0.5 ppm-P consumed) at 20 ppm TPP. No transformation of TPP was observed in autoclaved lake water at 4 or 20 ppm. These results indicate that TPP can be transformed rapidly (compared with chemical hydrolysis) in nonsterile waters under aerobic conditions. It is apparent that organic nutrients accelerate the transformation, and, they may be the limiting factor in the above pure natural water experiment.

To confirm that the transformation is biological, the pond microorganisms were inoculated into tris buffer-basal salt medium containing various amounts of glucose and yeast extract and 20 ppm of TPP. The percent transformation of TPP after 5 and 7 days of incubation is shown in Table 20.

Table 20

AEROBIC CONVERSION OF TPP TO PO_4^{-3} AS A FUNCTION OF EXTRA ORGANIC NUTRIENTS

Nutrients Added (ppm)		Percent Conversion to PO_4^{-3}	
Glucose	Yeast Extract	5 days	7 days
100	20	95	95
50	10	85	100
25	5	60	80
50	10 (noninoculated medium	0	0

The biotransformation of TPP was also studied in anaerobic water. Searsville Pond water was placed in the anaerobic chamber, purged with nitrogen gas, and incubated overnight. Tris buffer was added to maintain the pH at 7. TPP (20 ppm) was added to the water with an without the addition of glucose and yeast extract. After 6 and 10 days of incubation, TPP was transformed in all cases, as shown in Table 21.

Table 21

ANAEROBIC TRANSFORMATION OF TPP AS A FUNCTION OF ORGANIC NUTRIENT CONCENTRATION

Nutrients Added (ppm)		Percent TPP Transformed	
Glucose	Yeast Extract	6 days	10 days
100	20	72	81
50	10	48	62
0	0	20	38
Sterile Control	--	16	16

These results show that TPP can be biotransformed anaerobically. This transformation is slightly slower than that observed under aerobic conditions, and the transformation rate is dependent on the level of organic nutrients present. The losses observed in the sterile control are probably artificial.

The aerobic biotransformation of TPP also occurred in soil. TPP (500 ppm) was added to 10 g of soil (dry weight) in test tubes and moistened with 3 ml of water; 500 ppm of TPP (125 ppm-P) was used because the soil contained a large amount (~ 350 ppm-P) of extractable phosphate. Soil autoclaved twice in 2 days was used as a sterile control. Periodically, test tubes were removed from the incubator and the soil was extracted with 50 ml of 0.1N H_2SO_4 and filtered. The residue was washed with 150 ml of 1N H_2SO_4. The filtrates were combined and analyzed for orthophosphate before and after heat-acid hydrolysis of the sample.

TPP in nonsterile soil was hydrolyzed rapidly, with a half-life of 2 days. In sterile soil, the rate of hydrolysis was much slower, with a projected half-life of more than 8 days. Thus, it appears that the biotransformation of TPP will occur readily in soil under aerobic conditions.

The biotransformation of TPP was also studied in anaerobic soil in the following manner. Anaerobic soil was prepared by placing 10 g of soil in test tubes, flooding the soil with water in an anaerobic chamber, and incubating overnight. Soil autoclaved twice on successive days and placed in the anaerobic chamber was used as a sterile control. To the nonsterile soil was added 1000 ppm of TPP (250 ppm-P) and the soil was incubated. Test tubes were removed from the chamber periodically and analyzed for increase in phosphate production. After 13 days of incubation, 90% of TPP was biotranformed, whereas 65% was transformed in sterile soil.

Under aerobic and anaerobic conditions in waters and soils, TPP was evidently biologically hydrolyzed. Linear polyphosphates were found to

be synthesized and hydrolyzed in microbial cells. Polyphosphates serve as a phosphate reserve and storage center for phosphorus within cells, from which rapid biosynthesis of nucleic acid and phospholipids can take place. A number of enzymes that have been isolated from living tissues will hydrolyze pyrophosphate, tripolyphosphate, tetrapolyphosphate, and higher polyphosphates (Hooper, 1973)

Sutton and Larson (1964) and Sutton et l. (1966) found that half of pyrophosphate added to samples of over 200 soils hydrolyzed to orthophosphate in a few days to a few weeks. They found that the general level of biological activity in the soil was the factor exerting the most influence on the rate of hydrolysis. Gilliam and Sample (1968) found appreciable hydrolysis of pyrophosphate in soils that had been steam-sterilized. Hydrolysis in the same soils without sterilization was severalfold faster, presumably because of microbiological activity. Our findings for TPP parallel closely the reported fate of pyrophosphate.

The smoke aerosol and residue not only contain TPP and pyrophosphate, but also higher homologs up to P_{22} polyphosphates. The biotransformation of these components was investigated using a WP burn residue mixture of polyphosphates. These studies were complicated by chemical transformations, as described in Section V.H; however, transformation rates far exceeded those expected for chemical hydrolysis.

When the smoke residue concentrate (0.8 mM as phosphate) was added to pond water, the water became highly turbid, and HPLC analysis of the water showed that part of the polyphosphates had precipitated. The addition of 1 mM EDTA prevented precipitation, indicating that metals were involved in complexing the polyphosphates. The chemical transformations that occur in sterile water are shown in Figure 32. (pg. 92)

In nonsterile pond water with added glucose (50 ppm) and yeast extract (10 ppm), the linear polyphosphates with $n > 3$ undergo rapid transformation ($t_{1/2}$ = 2 days), with observable increases in TPP,

trimetaphosphate, and hexametaphosphate during the first week of incubation. The HPLC profiles of the smoke concentrate at Day 0 and Day 6 are shown in Figure 33. In the pond water without added nutrients, the results were similar to those for the sterile control, showing decreases in the concentration of higher polymers while the lower polymers concentrate after 2 weeks.

The above microorganisms were enriched and transferred into tris-buffered basal-salts medium with smoke concentrate, 50 ppm glucose, and 10 ppm yeast extract. In this medium, pyrophosphate was readily hydrolyzed ($t_{1/2}$ = 3 days), TPP concentration increased in the first week then decreased slowly, the P_4-P_{16} polymers decreased at variable rates ($t_{1/2}$ ~ 7 days), and trimetaphosphate did not increase but remained relatively persistent. When the glucose and yeast extract concentrations were increased to 200 ppm and 40 ppm, respectively, the hydrolytic processes were greatly accelerated and the TPP and trimetaphosphate concentrations were reduced 90% and 40% of their initial values, respectively, in three days. From these results, it appears that many processes are occurring in natural water that affect the persistence of polyphosphates:

(1) Metals can complex certain polymers and precipitate them from solution.

(2) Nonbiological hydrolytic processes occur, leading to the production of trimetaphosphate.

(3) The biotransformation of polyphosphates is nutrient-dependent, showing increasing rates with increasing nutrient concentrations.

(4) The biotransformation of pyrophosphate is relatively faster than that of the higher linear homologs.

(5) Biotransformation in the smoke condensate is slower for the cyclic metaphosphates than for the linear polyphosphates.

Polyphosphates can be a stored form of phosphorus nutrient in living cells and can even be synthesized by microorganisms (Hooper, 1983). Many microorganisms therefore possess specific enzymes to synthesize and hydrolyze polyphosphates. This specificity was

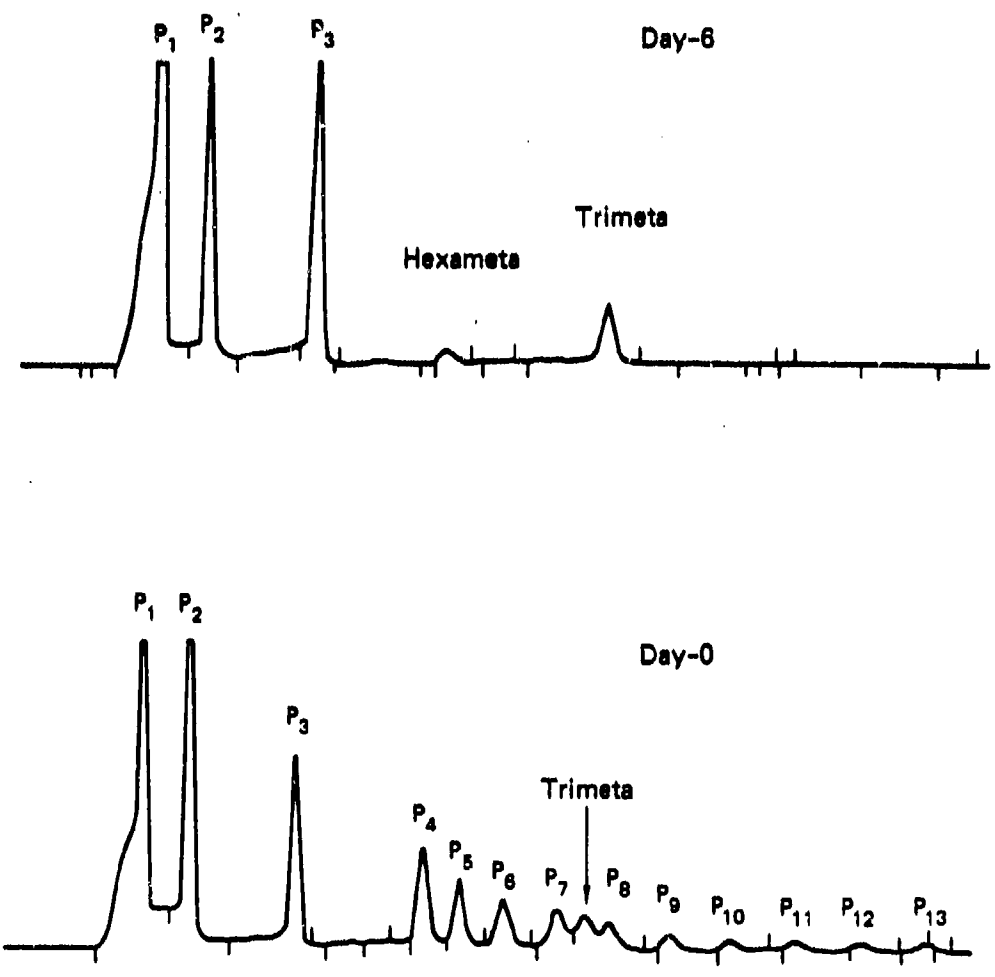

FIGURE 33 HPLC PROFILES SHOWING THE BIOTRANSFORMATION OF POLYPHOSPHATES AT DAY 0 AND DAY 6

demonstrated by Peck et al. (1973), who showed that bacteria that readily utilized TPP were poor utilizers of tetrapolyphosphate and those bacteria that readily utilized tetrapolyphosphate were poor utilizers of TPP. Thus, in the smoke condensate, it is not surprising to observe that the components hydrolyze at variable rates due to the concentration and availability of specific enzymes.

For a natural water body, we can assume under the worst case condition that the transformation of polyphosphates (P > 4) is limited by chemical hydrolysis if no polyphosphate-specific bacterial enzymes are present. The pseudo-first-order rate constants would range from 3 x 10^{-6} min^{-1} to 3 x 10^{-5} min^{-1} ($t_{1/2}$ = 160 to 16 days) (see Section V.G). Because most bacterial systems have some ability to hydrolyze polyphosphates (for example, TPP $t_{1/2}$ = 13 days, Table 21), we expect that most polyphosphates will have half-lives around 13 days (k_b = 3.7 x 10^{-5} min^{-1}), with faster rates predicted based on the level of organic nutrients.

E. Hexametaphosphate

Because metaphosphates resulting from the hydrolysis of the smoke condensate were observed by NMR and HPLC, we evaluated the ability of microorganisms to hydrolyze this class of cyclic polyphosphates.

Searsville Pond water was collected and buffered with tris buffer. To aliquots of the pond water we added 15 ppm of sodium hexametaphosphate (HMP) alone, or 15 ppm HMP (4.5 ppm-P) plus 50 ppm glucose (Glu) and 10 ppm yeast extract (YE), or 15 ppm HMP plus 100 ppm glucose and 20 ppm yeast extract. Autoclaved pond water plus 50 ppm glucose and 10 ppm yeast extract was used as a sterile control. The waters were incubated at 25°C in the dark. Periodically, samples were removed and HPM was analyzed by the orthophosphate colorimetric method before and after heat-acid hydrolysis of the polymer.

The amount of HMP transformed after 7 and 12 days of incubation is shown in Table 22.

Table 22

HMP HYDROLYZED AFTER AEROBIC INCUBATION
WITH SEARSVILLE POND WATER

Pond Water Sample	HMP Hydrolyzed (%) 7 days	12 days
Water alone	24	34
Water + 50 ppm Glu and 10 ppm YE	38	52
Water + 100 ppm Glu and 20 ppm YE	65	79
Sterile water + 50 ppm Glu and 10 ppm YE	0	0

The above results indicate that HMP is stable to chemical hydrolysis at neutral pH, but that biological transformation can occur [$k_h = 3.6 \times 10^{-7}$ min^{-1}, $t_{1/2} = 3.6$ years, Griffith and Buxton, 1965). The rate of biotransformation increased as a function of the amount of extra organic nutrients present in the solution. To confirm that microorganisms were responsible for the transformation, the pond water that showed HMP loss was inoculated into sterile media containing tris buffer basal salts (TBSM), 15 ppm HMP, and 50 ppm glucose-10 ppm YE or 100 ppm glucose-20 ppm YE. The amount of HMP hydrolyzed after 8 and 12 days of incubation is shown in Table 23.

Table 23

HMP HYDROLYZED IN TBSM AFTER INOCULATION
WITH POND WATER ORGANISMS

Nutrients Added	HMP Hydrolyzed (%) 8 Days	12 Days
50 ppm Glu-10 ppm YE	68	82
100 ppm Glu-20 ppm YE	81	92

The results show that the transferred microorganisms grew in the media and hydrolyzed HMP. As we have observed in the past, the

transformation rate was fastest in the medium that was highest in organic nutrients.

An experiment similar to that described above was performed under anaerobic conditions in which the buffered pond waters were purged with N_2 gas and placed in an anaerobic chamber overnight. Autoclaved pond water was used as a sterile control. The amount of HMP hydrolyzed after 5 and 9 days of incubation is shown in Table 24.

Table 24

HMP HYDROLYZED AFTER ANAEROBIC INCUBATION WITH SEARSVILLE POND WATER

Pond Water	HMP Hydrolyzed (%) 5 Days	9 Days
Pond water alone	22	68
Pond water + 50 ppm Glu and 10 ppm YE	79	100
Pond water (sterilized)	5	6

These results show that the HMP can be biotransformed under anaerobic conditions and that the transformation is accelerated by extra organic nutrients.

Like condensed linear phosphates, the metaphosphates are chemically stable at neutral pH. However, the latter appear to be biologically hydrolyzed in aerobic and anaerobic waters. The amount of organic nutrients affected the biological activity of the water, which in turn affected the rate of hydrolysis.

F. Phosphite

1. Screening Studies

A biotransformation screening test of phosphorus acid (H_3PO_3) was conducted because this compound was identified in the smoke condensate. Phosphite at 5 or 15 ppm-P (13 or 39 ppm H_3PO_3) was added

to natural water collected from Searsville Pond and Coyote Creek, California with and without 100 ppm glucose and 20 ppm yeast extract. The waters were incubated at 25°C in the dark. Samples were withdrawn periodically and analyzed for phosphite colorimetrically after an aliquot of sample was oxidized by bromine to form orthophosphate. The orthophosphate was analyzed by the vanadomolybdophosphoric acid colorimetric method before and after oxidation. Excess bromine was removed before color reaction by heating the sample in the autoclave or in boiling-water baths.

Phosphite remained stable for 15 days in Searsville Pond water; then the concentration decreased from 5 to 1 ppm at 22 days and was non-detectable (<0.1 ppm) at 29 days. In pond water with added glucose (50 or 100 ppm) and yeast extract (10 or 20 ppm), phosphite remained stable for 22 days, with the concentration decreasing to <0.1 ppm at 36 days. These results are shown in Figure 34.

A similar study was conducted in Coyote Creek water (Figure 35). Phosphite concentration decreased from 15 ppm to 1 ppm in 35 days after an acclimation period of 28 days. In this water, in the Searsville Pond water, the transformation was delayed as a function of the amount of extra organic nutrients added. In fact, when the above transforming organisms were inoculated into TBSM containing phosphite and various levels of glucose and yeast extract, no transformation of phosphite was observed after 23 days with either Searsville Pond or Coyote Creek organisms. Similar results were observed when neopeptone or nutrient broth was added to the TSBM-glucose-yeast extract medium and incubated for 30 days.

The Coyote Creek water that showed biotransformation of phosphite was centrifuged and the sediment was divided into three portions: one was resuspended in Coyote Creek water; the second was suspended in TBSM; and the third was suspended in TBSM plus 5 ppm of yeast extract. To all three suspensions was added 10 ppm-P of phosphite. The organisms in the resuspended Coyote Creek water transformed phosphite to < 1 ppm-P in 5

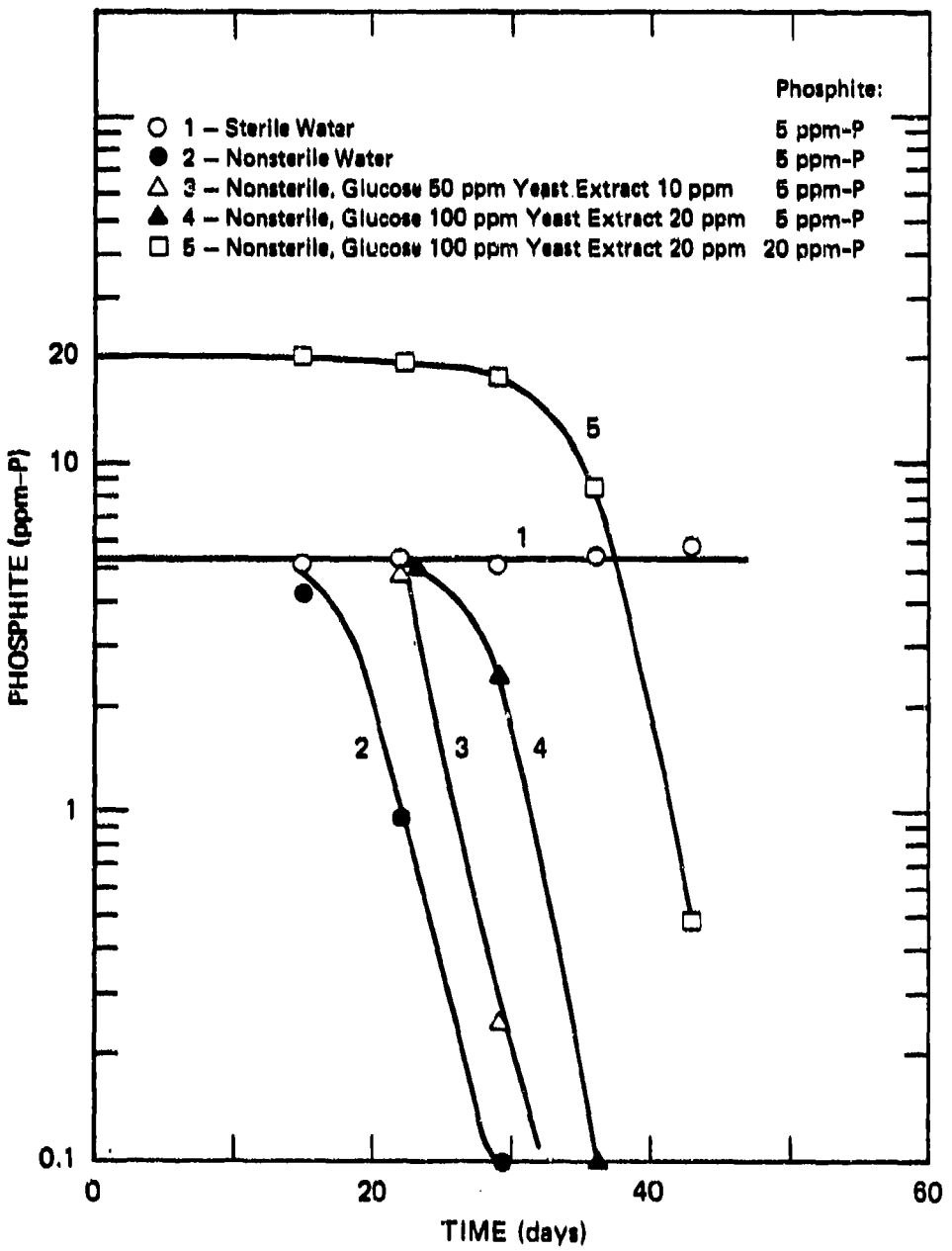

FIGURE 34 BIOTRANSFORMATION OF PHOSPHITE IN SEARSVILLE POND WATER

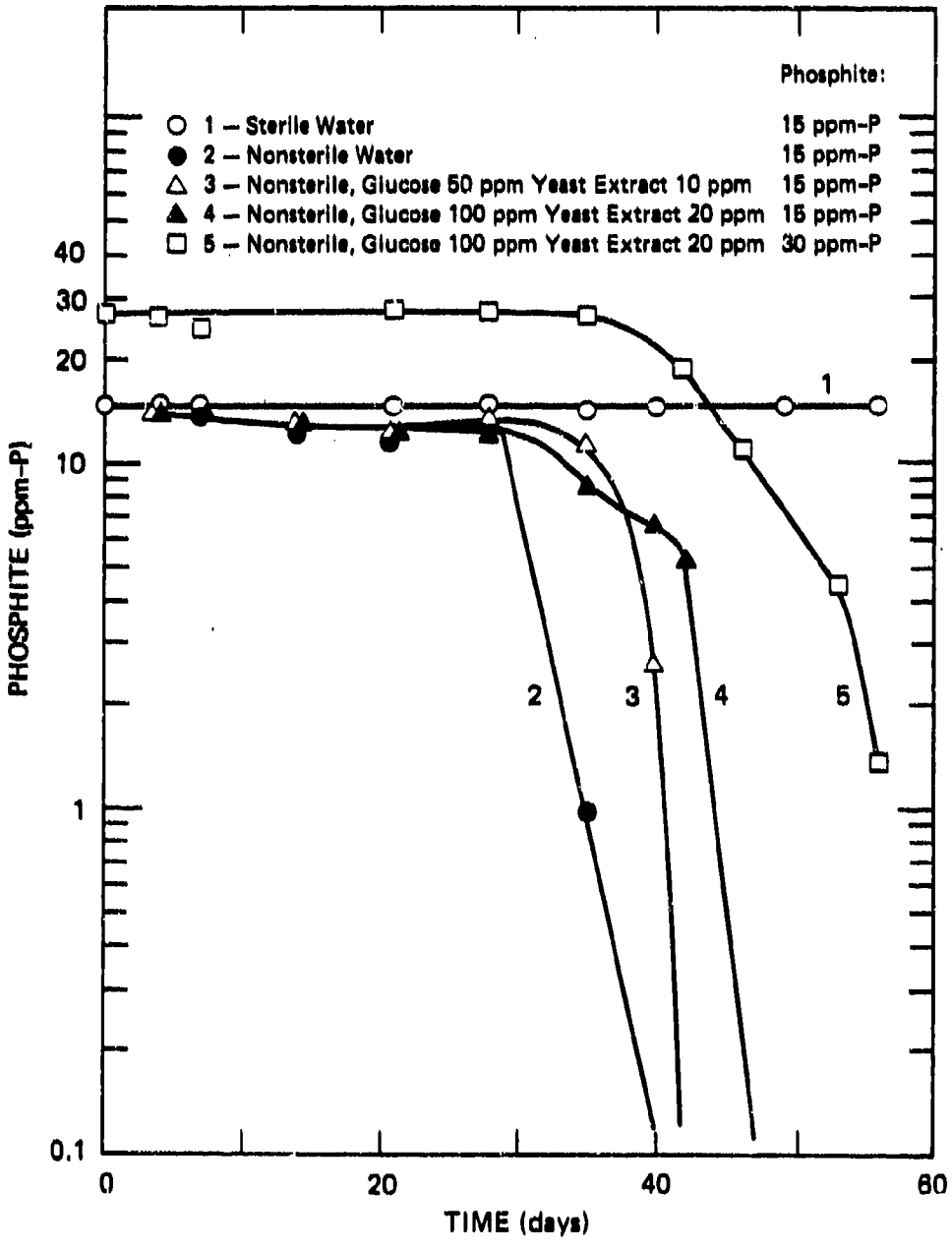

FIGURE 35 BIOTRANSFORMATION OF PHOSPHITE IN COYOTE CREEK WATER

days. No transformation was observed in the other two media after 12 days of incubation.

When the organisms from the first suspension were reinoculated into Coyote Creek or Searsville Pond water along with 10 ppm-P of phosphite, phosphite was transformed to < 1 ppm-P in 6 days.

From these results, it appears that phosphite can be biotransformed in natural water but not in TBSM. To further investigate this effect, phosphite-biotransforming organisms were inoculated into Coyote Creek water containing 10 ppm-P of phosphite. Up to 90% biotransformation occurred in 5 to 13 days. When basal salts were added to the Coyote Creek water, the biotransformation was slower. Therefore, it appears that instead of a lack of some specific natural water nutrient in the TBSM, some components of the TBSM may inhibit the phosphite biotransformation at the above concentration.

The biooxidation of phosphite to phosphate by microorganisms has been reported (Casida, 1959). However, the microorganisms required glucose as carbon source and oxidation ceased when the glucose was exhausted. The finding that two water-source microorganisms can biotransform phosphite without addition of glucose and that the addition of glucose and yeast extract extends the acclimation period is an interesting phenomenon in the metabolic disposition of phosphorus compounds by microorganisms.

Phosphite added to SRI soil at 200 ppm-P level did not oxidize during 42 days of incubation. Alexander (1977) reported that biological oxidation of reduced phosphorous compounds was evident when phosphite was added to soil. Accompanying the disappearance of the phosphite was an increase in the concentration of phosphate; the reaction was eliminated when toluene was added to inhibit a biological function.

2. Detailed Studies

We conducted a detailed kinetic study of the biotransformation of phosphite. Microorganisms from Coyote Creek water were grown in Coyote

Creek water containing 10 ppm-P of phosphite. The organisms were centrifuged, washed, and resuspended in one-fourth volume of Coyote Creek water containing 10 ppm-P of phosphite. Microbial mass was determined by plating properly diluted cell suspensions on Coyote Creek water-10 ppm-P of phosphite agar using the spread method. Grown colonies were counted and expressed as colony-forming units (CFU).

At 10 ppm-P of phosphite, the transformation rate appeared to be zero-order. The rate study was repeated using 9.0, 4.6, 1.5, and 0.7 ppm of phosphite, which yielding transformation rates of 0.117, 0.095, 0.048, and 0.037 ppm-P hr^{-1}, respectively. Lineweaver-Burk analysis of the data gives Equation 6:

$$\frac{C_o}{v} = \frac{K_s}{\bar{V}m} + \frac{C_o}{\bar{V}m} \quad , \quad (10)$$

where C_o = the initial phosphite concentration

v = the transformation rate

$\bar{V}m$ = the maximum transformation rate

K_s = the substrate concentration for half-maximum transformation rate

Hence, the calculated K_s is 2.7 ppm. Thus, first-order behavior will be observed only below 2.7 ppm. From the studies performed at 1.5 and 0.7 ppm-P of phosphite, we obtained pseudo-first-order rate constants of 0.108 hr^{-1} and 0.073 hr^{-1}, respectively, with an average colony count of 5.5×10^6 CFU/ml. From the average pseudo-first-order rate constant (0.091 hr^{-1}), the calculated second-order rate constant was 1.65×10^{-8} ml org^{-1} hr^{-1}.

For a natural water body such as Coyote Creek, in which the microbial population is 5×10^5 CFU ml^{-1}, the calculated pseudo-first-order rate constant is 8.3×10^{-3} hr^{-1} and the expected half-life for phosphite is 83 hr.

G. Biosorption

Biosorption of WP was conducted using four species of Gram-positive and Gram-negative cultures: Azotobacter beijerincki ATCC 19366, Bacillus cereus ATCC 11778, Escherichia coli ATCC 9637 and Serratia marcescens ATCC 13880. The organisms were grown in Tryptic Soy broth at 25°C overnight; at the late logarithmic growth phase they were harvested, washed, and resuspended in water. Equal optical densities of the organisms were mixed together and diluted to a desired concentration. The cells were dispensed in Teflon-lined, screen-capped test tubes and placed in an anaerobic chamber. The cell concentrations used were 4.0 and 2.0 mg/ml. WP in water was added from a stock solution to give a final concentration of 2.0 ppm. After a 1-hr exposure, the cells were centrifuged, and the supernatant and the cells were separated, extracted with hexane, and analyzed for P_4 by GC. From the analysis of triplicate tubes, the sorption coefficient for the cell suspension was calculated to be 156 ± 11 at 4.0 mg/ml and 185 ± 59 at 2.0 mg/ml. The overall average sorption coefficient was 176 ± 39; this value is considered to be low and not environmentally significant.

H. Biotransformation Summary

The results of the biotransformation studies showed that WP is not readily utilized by anaerobic aquatic bacteria. Polyphosphates, including the cyclic metaphosphates, can be hydrolyzed by both aquatic and soil microorganisms under aerobic and anaerobic conditions. This rate of hydrolysis is related to the amounts of organic nutrients present.

Phosphite is also readily transformed to orthophosphate under aerobic conditions; however, the transformation is inversely related to the amounts of extra organic nutrients. Half-lives of less than 100 hr are expected in most aquatic environments. This material is stable to chemical transformation; hence, microbes will be the primary route of transformation.

Biosorption of WP was found not to be significant for microorganisms. This result parallels the finding for the sorption of WP to soil; however, it would not be predicted from the K_{ow} value (1200). Although WP was found not to be toxic to aquatic bacteria at near aqueous saturation levels, it appears that this results from the material's poor partitioning to the cell wall.

Thus, all of the smoke-transformation products appear to be susceptible to microbial transformation in soil and water. (Phosphine was not studied because of its rapid partitioning to the atmosphere.) These studies indicate that microorganisms will play a major role in the transformation of smoke products to orthophosphoric acid.

VII PARTICLE CHARACTERIZATION AND DEPOSITION VELOCITY MEASUREMENTS FROM SCALE-MODEL DEPLOYMENT OF WP/F AND RP/BR MUNITIONS

Scale-model smoke-deployment studies were performed to characterize the smoke particles generated from RP/BR and WP/F and to determine the deposition velocity of particles from the aerosol phase. These data then become important in the overall environmental assessment of phosphorus smokes.

Smoke munitions were ignited in a 10' x 12' x 12'(H) chamber (Figure 36). With the RP/BR munitions, one 30-g batch of pellets was ignited every five minutes for a 30-min period. The WP/F munitions ignited on exposure to air and therefore were not as easy to control; one 67-g wedge was ignited at the start of the run and another 67-g wedge was ignited 10 min later. These methods of deployment led to a time variation in smoke concentration. This variation is less than ideal in terms of a laboratory study; unsteadiness, however, is probably characteristic of an actual field deployment.

Ambient air was drawn through the combustion chamber at a rate between 0.42 m^3/sec and 0.74 m^3/sec. These flow rates resulted in average smoke residence times in the chamber between 60 and 90 sec. Smoke generated in the chamber flowed out through a sampling duct (1' x 2' cross-section; Figure 36). Average flow velocities in the duct ranged from 5.1 mph to 9.0 mph. The duct contained a pool of water on which phosphorus smoke could deposit. The pool of water was in a trough (19" x 3'; area = 4413 cm^2); during the run, the trough was filled so that the water was level with the duct floor.

The size distributions of the smoke particles were measured with a piezoelectric (PZ) cascade impactor. The total mass concentration of the smoke was measured using the PZ impactor and a total filter

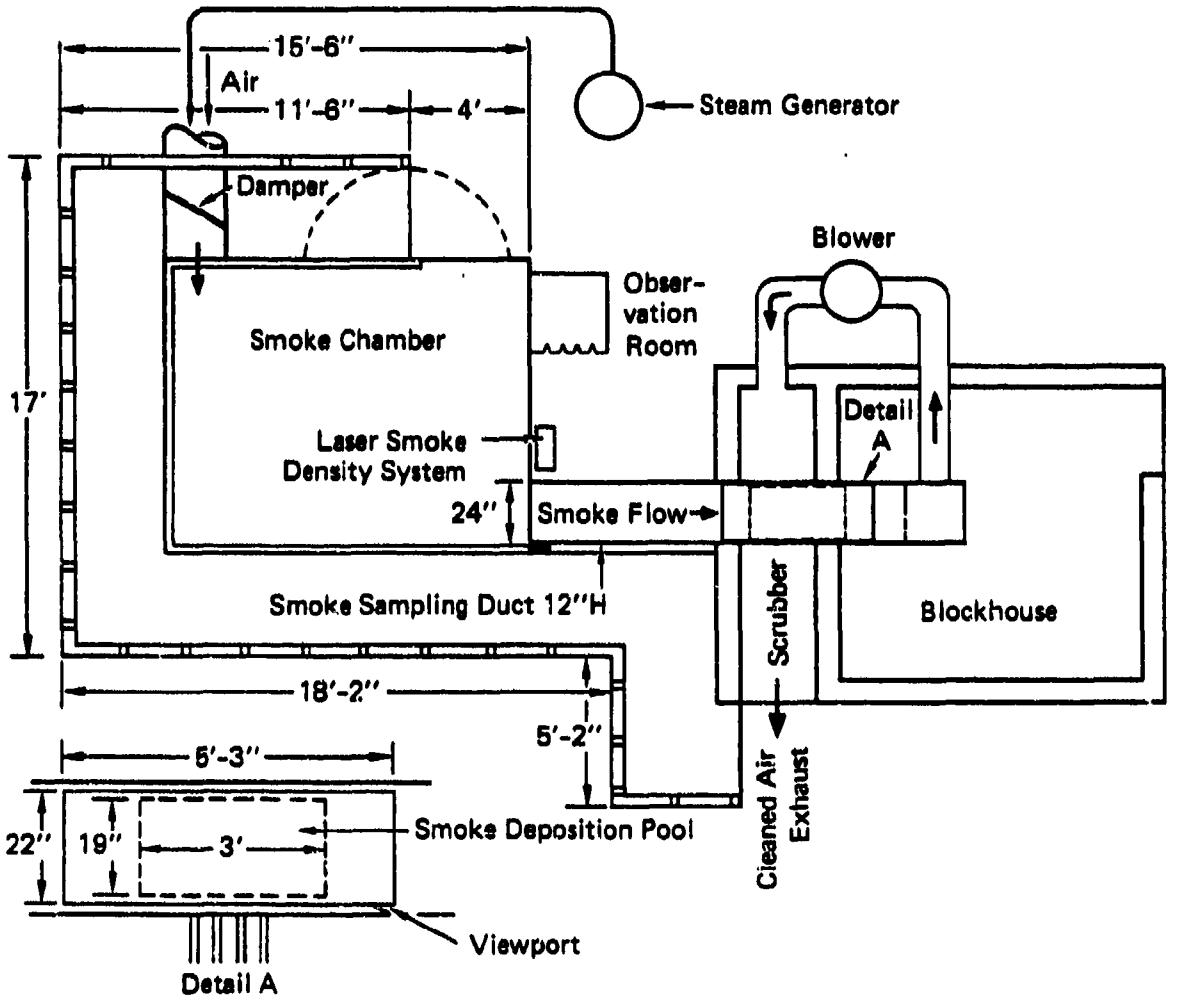

FIGURE 36 SCHEMATIC OF THE SRI SMOKE CHAMBER

Smoke drawn out of the smoke chamber by a blower passes through a sampling duct. This duct is equipped with laser smoke detectors, several sampling ports, and a water pool for particle deposition measurements. Smoke is exhausted through a scrubber.

sample. In addition, the mass of munitions used to make the smoke and the residue remaining after the run were measured. Hence, the time-averaged mass concentration of phosphorus in the smoke could be calculated.

The flux of phosphorus smoke to the pool of water was calculated by analyzing the water for phosphorus (ion chromatography). The flux of phosphorus (grams per unit area per unit time) could be calculated from the laboratory concentration measurement, the known run time, and the known area of the water pool. The time-averaged mass deposition velocity could then be calculated by dividing this flux by the concentration of phosphorus in the smoke.

Each munition was burned with a high and low flow velocity in the duct (approximately 10 and 5 mph) and with a low, medium, and high relative humidity (approximately 20, 50, and 80%). The mass median particle size varied from 0.95 to 1.23 μm for the RP/BR smoke and from 0.83 to 1.96 μm for the WP/F smoke (Table 25). There was a slight trend toward larger particles at the higher relative humidities, consistent with the ability of phosphorus smoke to absorb water.

Typical size distributions of these smokes are shown in Figures 37-42. These figures are in order from low to high humidity, with RP/BR first. The distributions tend to be bimodal, with the peak near 1 μm to 2 μm and one peak near 5 μm.

The mass concentration of smoke was highly variable (Table 26). This feature resulted from the fact that the PZ impactor takes point samples (approximately 1 sec sample time). However, even the filter samples were not very constant, indicating an actual unsteadiness in the smoke burn rate (filter sample time was 2 min). The phosphorus mass concentrations calculated from the difference between the final and initial weight of munition were generally lower than the concentrations measured by the PZ impactor and the filter samples. This feature is partially explained by the fact that the smoke is not all phosphorus (smoke had a phosphorus weight fraction of 34%).

Table 25

DEPLOYMENT CONDITIONS AND MASS MEDIAN SIZE
OF THE PHOSPHORUS SMOKE PARTICLES

Run No.	Fuel[a]	Run Time (sec)	Duct Velocity (cm/sec)	Duct Reynolds Number	Ambient Relative Humidity (%)	Mass Median Smoke Particle Size (μm)
10	R	2280	250	$6.78 \cdot 10^4$	22	0.984
11	R	2280	376	$1.02 \cdot 10^5$	22	1.13 ± 0.12
8	R	2400	273	$7.40 \cdot 10^4$	44	0.955 ± 0.05
4	R	1860	380	$1.03 \cdot 10^5$	54	1.04
6	R	2280	228	$6.18 \cdot 10^4$	86	1.49
7	R	2280	228	$6.18 \cdot 10^4$	78	1.17 ± 0.07
5	R	1800	380	$1.03 \cdot 10^5$	79	1.23 ± 0.06
14	W	1200	268	$7.26 \cdot 10^4$	26	1.33 ± 0.15
12	W	1620	402	$1.09 \cdot 10^5$	25	0.833
9	W	1620	246	$6.67 \cdot 10^4$	39	0.955
15	W	960	402	$1.09 \cdot 10^5$	52	1.32
16	W	1200	291	$7.89 \cdot 10^4$	75	1.30 ± 0.11
13	W	1260	393	$1.07 \cdot 10^5$	72	1.96

[a]Fuel is designated as R for RP/BR and W for WP/F.

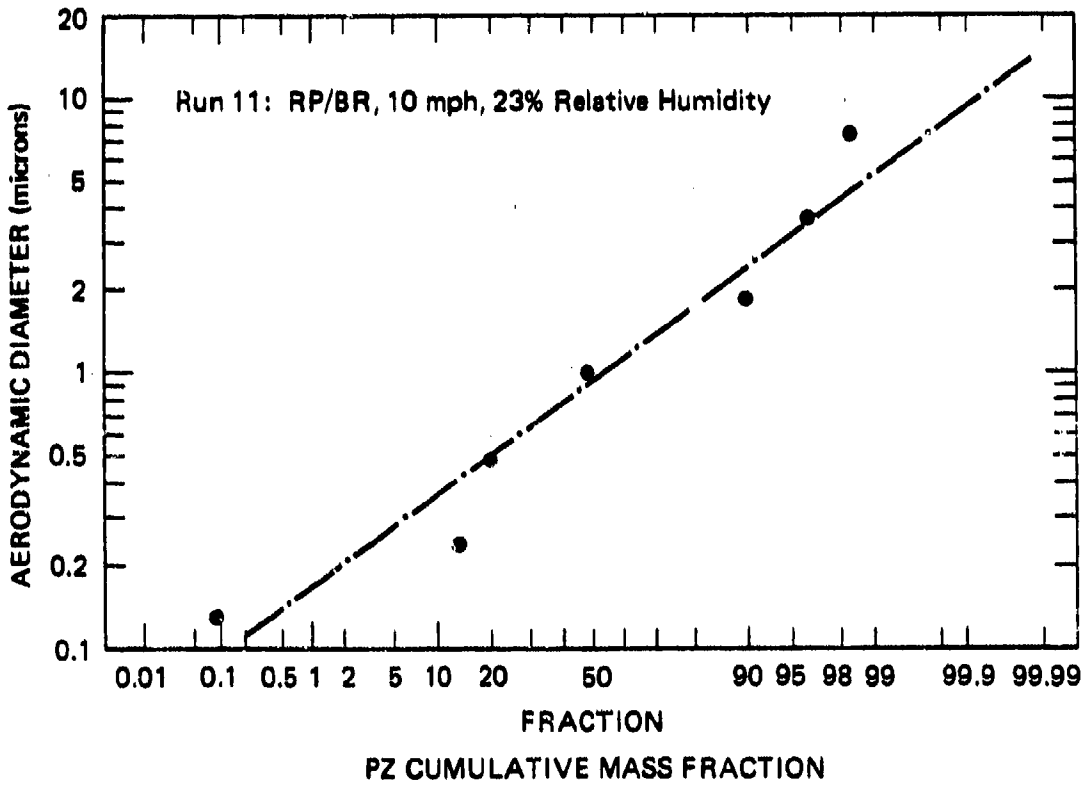

FIGURE 37 SIZE DISTRIBUTION FOR RP/BR SMOKE PARTICLES AT 10 mph WIND VELOCITY AND 23% RELATIVE HUMIDITY

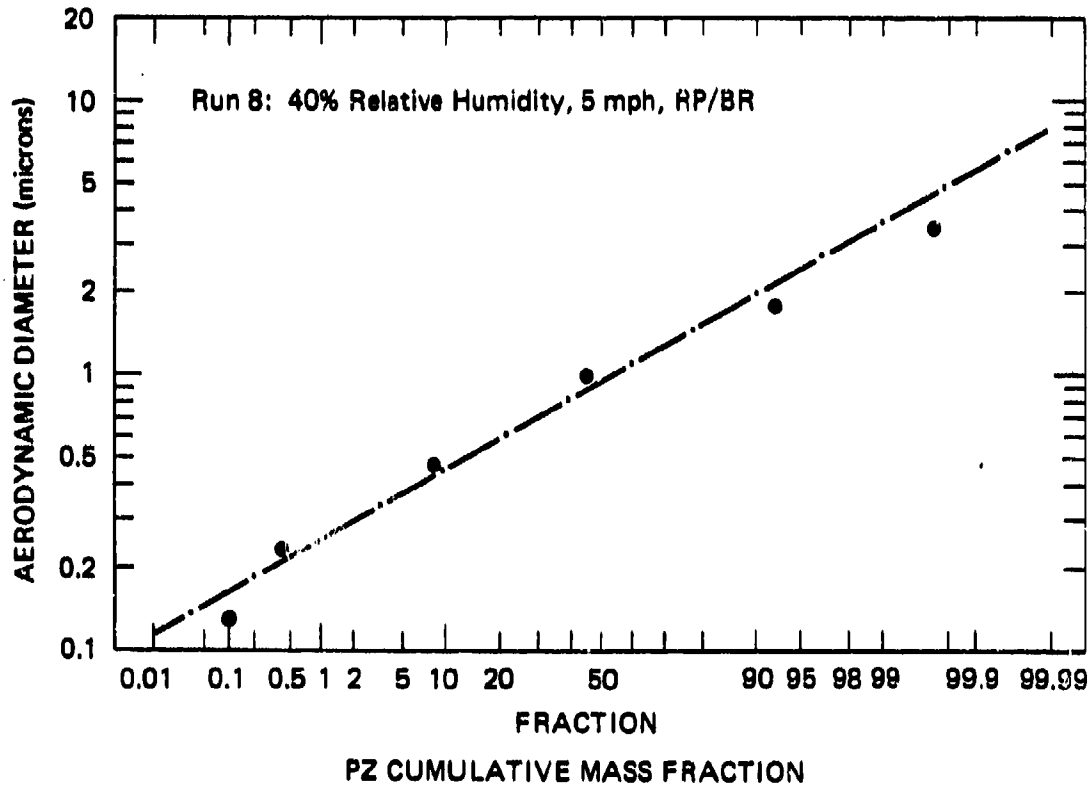

FIGURE 38 SIZE DISTRIBUTION FOR RP/BR SMOKE PARTICLES AT 5 mph WIND VELOCITY AND 40% RELATIVE HUMIDITY

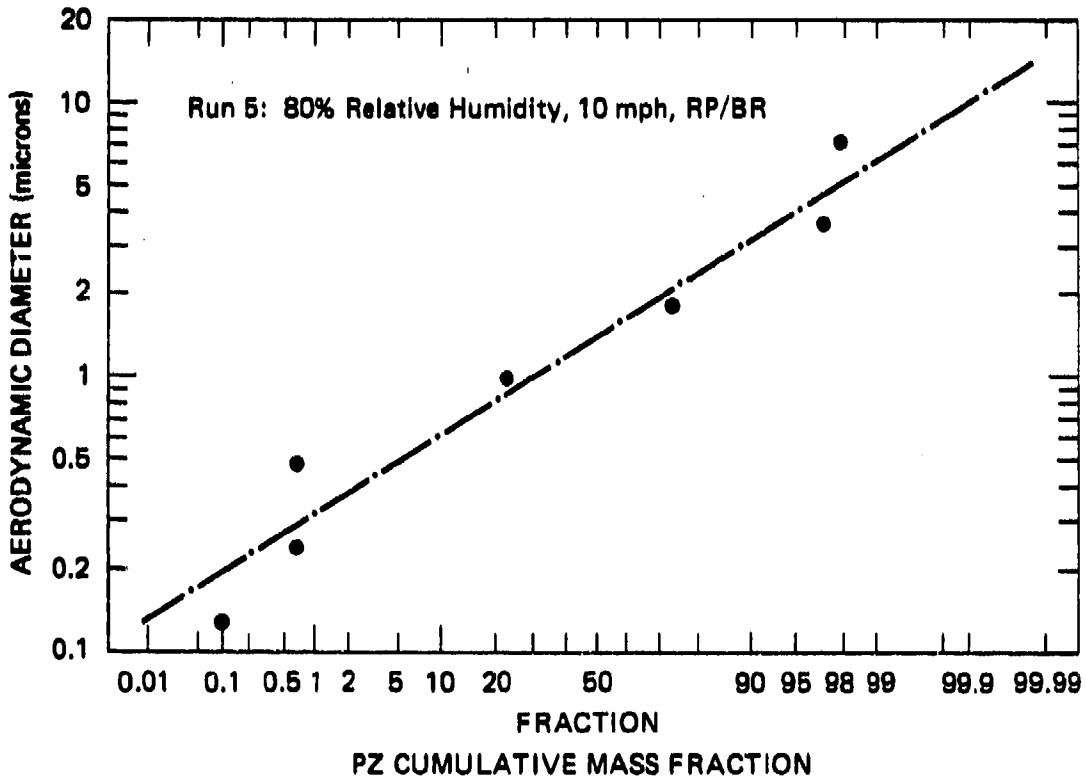

FIGURE 39 SIZE DISTRIBUTION OF RP/BR SMOKE PARTICLES AT 10 mph WIND VELOCITY AND 80% RELATIVE HUMIDITY

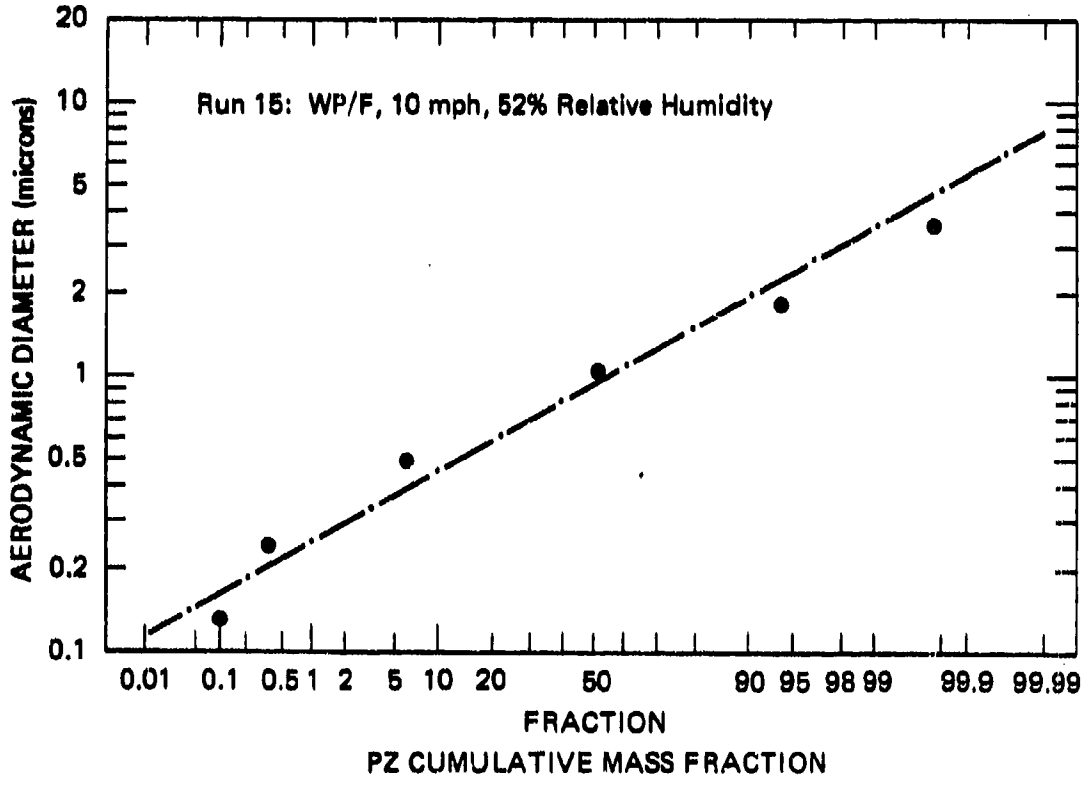

FIGURE 40 SIZE DISTRIBUTION OF WP/F SMOKE PARTICLES AT 10 mph WIND VELOCITY AND 52% RELATIVE HUMIDITY

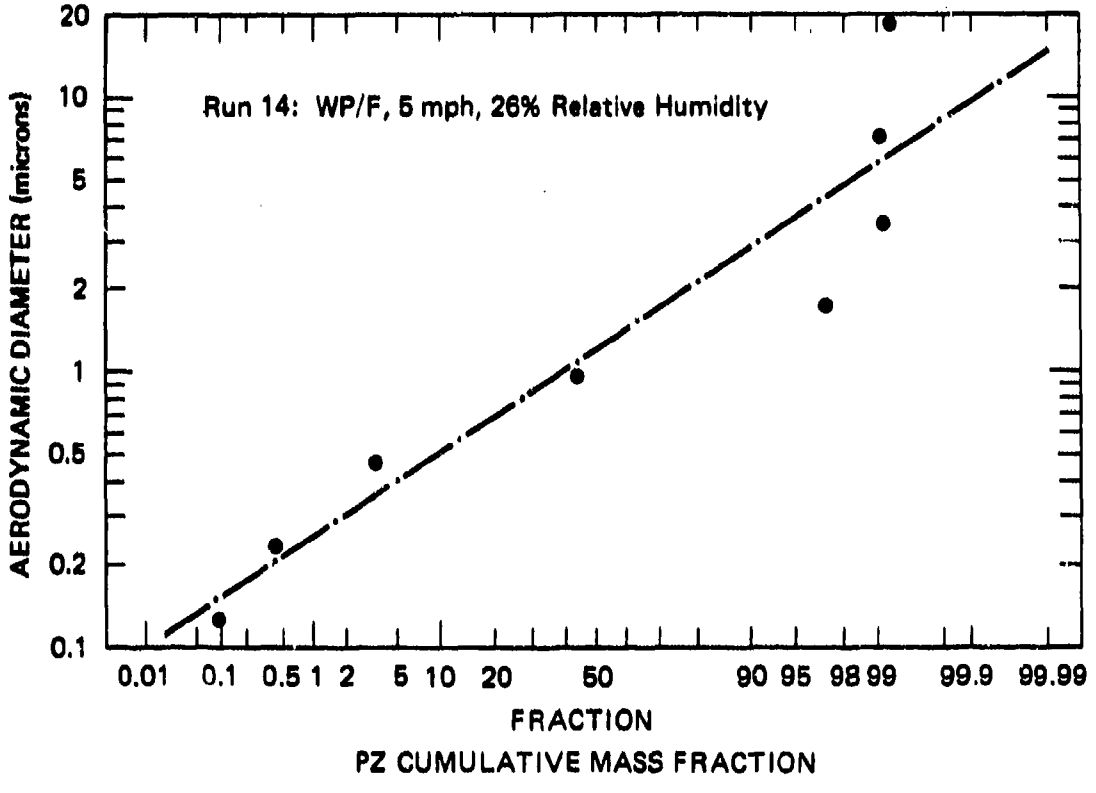

FIGURE 41 SIZE DISTRIBUTION OF WP/F SMOKE PARTICLES AT 5 mph WIND VELOCITY AND 26% RELATIVE HUMIDITY

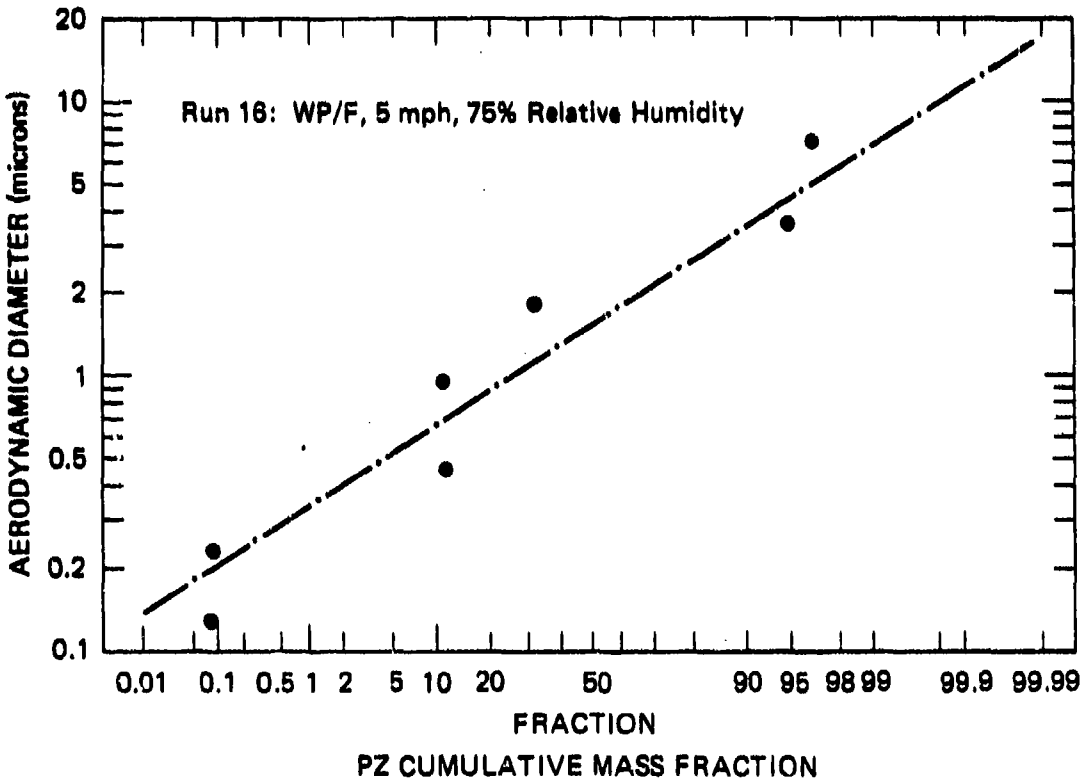

FIGURE 42 SIZE DISTRIBUTION OF WP/F SMOKE PARTICLES AT 5 mph WIND VELOCITY AND 75% RELATIVE HUMIDITY

Table 26

MEASURED TOTAL SMOKE CONCENTRATION
AND
CALCULATED PHOSPHORUS CONCENTRATION[a]

Run No.	Measured Smoke Concentration (PZ Impactor) (g/m^3)	Measured Smoke concentration (Filter) (g/m^3)	Calculated, Time-Averaged Phosphorus Concentration (g/m^3)
10	0.97	-	0.079
11	0.164 ± 0.066	-	0.052
8	3.52 ± 1.08	-	0.056
4	0.702	-	0.078
6	0.428	-	0.081
7	0.108 ± 0.017	-	0.076
5	0.404 ± 0.137	-	0.061
14	2.03 ± 0.87	0.792	0.119
12	2.37	0.391	0.063
9	0.904	-	0.092
15	1.42	0.920	0.102
16	0.154 ± 0.01	0.310	0.096
13	0.974	0.484	0.080

[a]Runs 10, 11, 8, 4, 6, 7, and 5 were performed with RP/BR and runs 14, 12, 9, 15, 16, and 13 were performed with WP/F.

Given the large fluctuations in instantaneous smoke concentrations, the deposition velocity should be calculated using the time-averaged phosphorus concentration. Table 27 shows the measured phosphorus fluxes to the water pool, the calculated mass-average settling velocity, and, for comparison, the settling velocity of a particle with a size equal to the mass median diameter for each run. The deposition velocities ranged from 0.015 to 0.05 cm/sec for RP/BR and from 0.07 to 0.019 cm/sec for WP/F; there is a trend toward higher deposition velocity with higher humidity, consistent with the trend toward larger particles with higher humidities.

The settling velocities of the mass median particle size are of the same order as the measured deposition velocities. This feature indicates that gravitational settling is dominating the deposition rate (as opposed to Browian or turbulent motion*). We expect, however, that the deposition velocity of phosphorus measured in our duct will exceed the settling velocity of the mass median particle size because our size distributions showed a substantial mass peak at a size (approximately 5 μm) significantly larger than the median size and because settling depends on the square of the particle size.

---

*Using a standard equation for turbulent deposition (Friedlander, 1977, p. 116), we find a deposition velocity on the order of 10^{-5} cm/sec.

Table 27

MEASURED PHOSPHORUS FLUXES
AND
CALCULATED DEPOSITION VELOCITIES

Run[a] No.	Phosphorus Flux to Water Pool ($g\ cm^{-2}\ sec^{-1}$)	Deposition Velocity[b] (cm/sec)	Settling Velocity of Mass Median Particle Size (cm/sec)
10	$6.79 \cdot 10^{-10}$	$8.64 \cdot 10^{-3}$	$3.26 \cdot 10^{-3}$
11	$8.56 \cdot 10^{-10}$	$1.66 \cdot 10^{-2}$	$4.63 \cdot 10^{-3}$
8	$1.15 \cdot 10^{-9}$	$2.04 \cdot 10^{-2}$	$3.31 \cdot 10^{-3}$
4	$1.31 \cdot 10^{-9}$	$1.68 \cdot 10^{-2}$	$3.93 \cdot 10^{-3}$
6	$1.34 \cdot 10^{-9}$	$1.65 \cdot 10^{-2}$	$8.06 \cdot 10^{-3}$
7	$1.13 \cdot 10^{-9}$	$1.49 \cdot 10^{-2}$	$4.97 \cdot 10^{-3}$
5	$3.03 \cdot 10^{-9}$	$5.0 \cdot 10^{-2}$	$5.49 \cdot 10^{-3}$
14	$1.02 \cdot 10^{-9}$	$8.58 \cdot 10^{-3}$	$6.42 \cdot 10^{-3}$
12	$4.34 \cdot 10^{-10}$	$6.94 \cdot 10^{-3}$	$2.52 \cdot 10^{-3}$
9	$6.54 \cdot 10^{-10}$	$7.10 \cdot 10^{-3}$	$3.31 \cdot 10^{-3}$
15	$1.21 \cdot 10^{-9}$	$1.19 \cdot 10^{-2}$	$6.32 \cdot 10^{-3}$
16	$1.84 \cdot 10^{-9}$	$1.90 \cdot 10^{-2}$	$6.13 \cdot 10^{-3}$
13	$1.14 \cdot 10^{-9}$	$1.42 \cdot 10^{-2}$	$1.39 \cdot 10^{-2}$

[a]Runs 10, 11, 8, 4, 6, 7, and 5 were performed with RP/BR and runs 14, 12, 9, 15, 16 and 13 were performed with WP/F.
[b]Flux divided by time-averaged phosphorus concentration (Table 26).

VIII ENVIRONMENTAL ASSESSMENT

A. Aquatic and Terrestrial Modeling

The laboratory studies showed that volatilization, oxidation, and hydrolysis processes would dominate the loss and movement of WP in the environment. These processes were modeled for some simplified conditions to determine whether more complex modeling was necessary. Reaction and transport phenomena associated with solid and dissolved P_4 were modeled for three simplified scenarios: solid P_4 placed in a turbulently flowing stream, solid P_4 placed in a stagnant water body, and solid P_4 buried in soil. A glossary of terms appears in Appendix 1 for identification of the mathematical symbols used in this section.

When solid P_4 is placed in a turbulently flowing stream, it will dissolve at a rate between 1 and 10 $\mu g/cm^2$-hr. The dissolved P_4 may then oxidize and hydrolyze in the water with a half-life of 42 hr (estimated shortest half-life) or may volatilize out of the water. The reported Henry's constant of 1600 torr-L/mole indicates that volatilization from a turbulent stream will be rapid. The equations, boundary conditions, and solutions to this problem are shown in Table 28. A calculation performed assuming a stream 4 feet deep and an eddy diffusivity of 1.0 cm^2/sec resulted in a volatilization half life, $t_{1/2}$, of 48.5 min. We believe that volatilization will therefore be the dominant removal mechanism of soluble P_4 from turbulent streams.

If solid P_4 is buried in soil, the rate of oxygen diffusion through soil will determine the rate of P_4 transformation. The equations, boundary conditions, and solutions for this problem are shown in Table 29. Assuming a soil porosity of 0.1 and a water fraction of 0.3, a simple calculation shows that 10 years would be required to completely oxidize a 1-cm-diameter piece of P_4 buried 12 cm beneath the surface. This calculation does not account for the possibility of an oxide layer accumulating on the surface of the P_4 chunk and restricting O_2 flux to

Table 28

SOLID P_4 IN A FLOWING STREAM

Equation	Boundary Conditions	Solution
Solid Chunk:		
$\frac{dM_c}{dt} = k_1 M_c^{2/3}$	$M_c = M_{co}$ at $t = 0$	$M_{co}^{1/3} - M_c^{1/3} = \frac{k_1}{3} \cdot t$
soluble P_4:		
$\frac{\partial C}{\partial t} = \epsilon \frac{\partial^2 C}{\partial y^2}$	$C = C_o$ at $t = 0$	$\frac{C}{C_o} = \frac{4}{\pi} \sum_{m=0}^{\infty} \frac{1}{2m+1} \exp\left[-\left(\frac{(2m+1)\pi}{2}\right)^2 \frac{\epsilon}{\delta^2} t\right] \sin\left(\frac{(2m+1)\pi}{2} \frac{y}{\delta}\right)$
	$C = 0$ at $y = 0$	
	$\frac{\partial C}{\partial y} = 0$ at $y = \delta$	
		$\frac{C_{avg}}{C_o} = \frac{8}{\pi^2} \sum_{0}^{\infty} \left(\frac{1}{2m+1}\right)^2 \exp\left[-\left(\frac{2m+1)\pi}{2}\right)^2 \frac{\epsilon}{\delta^2} t\right]$

ϵ = eddy diffusivity.
M_c = chunk mass.
C^c = concentration of P_4 in water; C_{avg} = average P_4 concentration in the stream.
δ = depth stream.
k_1 = dissolution and oxidation rate constant for solid P_4 in water; function of water velocity.

Table 29

SOLID P_4 BURIED IN LAND WITH NO SOLID LAYER FORMATION

Equation	Boundary Condition	Solution
$D_s \cdot \frac{d^2 P_{o2}}{dy^2} = 0$	$P_{o2} = 0.21$ Atm at $y = d$	$P_{o2} = 0.21 \text{ Atm} \cdot \frac{y}{d}$
$\frac{dM_c}{dt} = 1.5 \cdot 10^{-4} \frac{D_s}{d} \cdot M_c^{2/3}$	$M_c = M_{co}$ at $t = 0$	
$1.5 \cdot 10^{-4} = (0.21)(C_{air}) \cdot \pi \cdot (\frac{31gP_4}{64gO_2}) \cdot (\frac{3}{4\pi\rho_{P_4}})^{2/3}$		$M_{C_o}^{1/3} - M_C^{1/3} = \frac{0.21\ C_{air} \cdot \pi \cdot D_s}{3d} \cdot \frac{31}{64} \cdot (\frac{}{4\pi\rho_{P_4}})^{2/3} \cdot t$ (11)
$D_s = D_{air} \cdot (\frac{\theta_A 10/3_2}{\theta_A + \theta_W})$		

D_{air} = diffusivity of O_2 in air.

D_s = diffusivity of O_2 through soil

θ_A = volume fraction of soil that is air; i.e., the porosity.

θ_W = volume fraction of soil that is water.

P_{o2} = partial pressure of O_2.

d = depth to which the chunk is buried.

the unoxidized P_4. Therefore, the calculation represents the minimum lifetime of a buried mass of P_4.

If a solid layer forms, the problem can be described as shown in Figure 43. A rigorous analysis would require numerical computations to obtain the oxidation rate of phosphorus. However, a rough estimate may be obtained by simplifying the problem. If we assume that oxygen diffuses to the phosphorus only through the vertical soil column directly above the phosphorus, the equation describing oxygen transport through the soil is

$$D_s \frac{d^2 C_{O_2}}{dy^2} = 0 \qquad R < y < d \tag{12}$$

If the curvature of the phosphorus piece is neglected, the equation describing oxygen transport through the solid layer to the unreacted phosphorus is

$$D_{ox} \frac{d^2 C_{O_2}}{dy^2} = 0 \qquad r^* < y < R \tag{13}$$

We further assume that although r^* is a function of time, the rate of change of r^* may be neglected compared to the rate of change of the oxygen concentration. This type of quasi-steady-state assumption is explored further for the case of white phosphorus in water. The solution to Equations 12 and 13, with appropriate boundary conditions, is

$$\left(\frac{d-R}{D_s} + \frac{R}{D_{ox}}\right)(M_{C_c} - M_C) - \frac{0.75}{D_{ox}} \left(\frac{3}{4\pi\rho}\right)^{1/3} (M_{C_o}^{4/3} - M_C^{4/3})$$

$$= 0.21\, C_{air} \cdot \pi R^2 \cdot \frac{31}{64} \cdot t \tag{14}$$

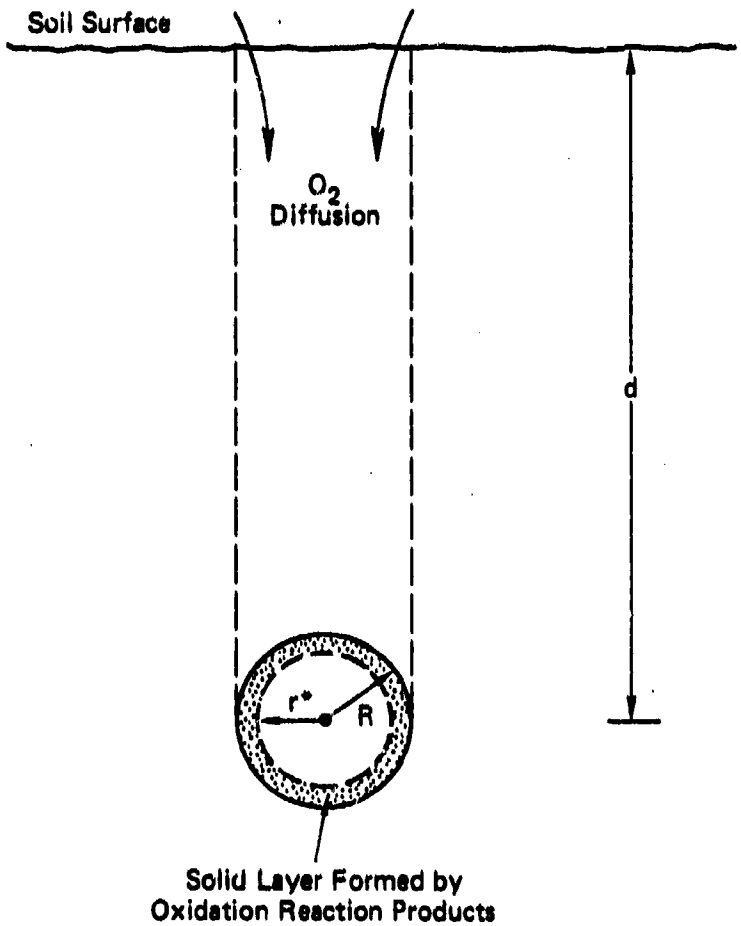

FIGURE 43 PHOSPHORUS OXIDATION IN SOIL, WITH FORMATION OF A SOLID LAYER

Figure 44 shows the time required to reach various stages of consumption of the piece of white phosphorus, with and without the formation of a solid layer. The y axis of Figure 44 gives the fraction of mass unreacted, and time is shown on the x axis. The curves in Figure 44 were generated from Equations 11 (Table 29) and 14. Table 30 shows the parameters used to generate the curves.

Table 30

PARAMETERS USED TO GENERATE CURVES IN FIGURE 44

Parameters	Value
d	15 cm
R	0.5 cm
D_s	$5.8 \cdot 10^{-4}$ cm^2/sec
D_{ox}	1.10^{-9} cm^2/sec
ρ	1.1 g/cm^3
C_{air}	$1.3 \cdot 10^{-3}$ g/cm^3

These results show that the extremely long oxidation time of the piece of phosphorus with solid-layer formation is due to the low value of D_{ox}. Although there are no data available on oxygen diffusion through solid layers of phosphorous oxidation products, the available data on diffusion through solids suggest that D_{ox} should be between 10^{-8} and 10^{-12} cm^2/sec. Therefore, if a solid layer forms on a piece of white phosphorus buried in the land, the lifetime will be extended from about 10 years to about 10,000 years.

In many cases, red phosphorus may be buried in the form of porous material, the same type used in experiments reported earlier. That material has a large internal surface area caused by the porous structure such that each gram of material has 1,500 cm^2 of surface.

$$A = \left(a\frac{cm^2}{g}\right) \cdot M_c \qquad (15)$$

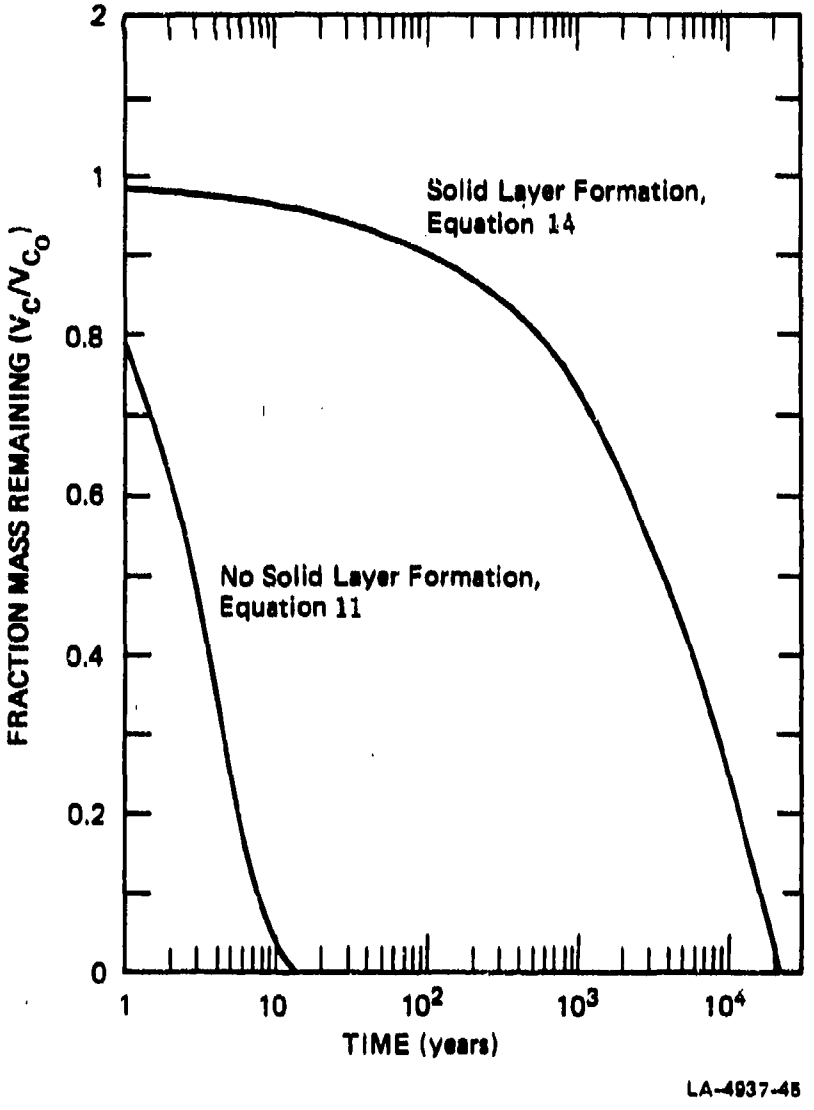

FIGURE 44 SIMULATED WHITE PHOSPHORUS OXIDATION IN SOIL

The proportionality factors a equals 1,500 cm^2/g for the material that SRI used for the experiments. A mass balance on a porous piece of red phosphorus gives the following:

$$\frac{dM_c}{dt} = -kaC_{O_2} \cdot M_c \tag{16}$$

Solving for Mc as a function of time gives

$$M_c = M_{co}\, e^{-kaC_{O_2} \cdot t} \tag{17}$$

The factor C_{O_2} is the concentration of oxygen at the phosphorus surface and, for buried material, may be less than the air concentration. C_{O_2} is found by equating oxygen flux through the soil to the rate of oxygen consumption by the phosphorus. An approximate relationship is

$$C_{O_2} = \frac{0.21\, C_{air} \cdot D_s}{\frac{kadR_o}{3} + D_s} \tag{18}$$

The experiments performed at SRI for red phosphorus oxidation were conducted over a relatively short period of time and essentially measured the initial degradation rate. From section IV,

$$\lim_{t \to 0} \left(\frac{dM_c}{dt}\right) = -1.7952 \cdot 10^{-8}\ g/sec = -kaC_{O_2} \cdot M_{C_o} \tag{19}$$

Since the red phosphorus was not buried in the experiments, d = 0, and $C_{O_2} = 0.21\, C_{air}$. The reaction rate constant can be calculated because the initial mass M_{C_o} was 2 g.

$$k = 2.397 \cdot 10^{-8} \text{ cm/sec} \qquad (20)$$

The time required for 95% of a 1-cm-diameter piece of red phosphorus to oxidize if it is buried 15 cm below the soil surface is approximately 11 years, assuming $D_s = 5.8 \cdot 10^{-4}$ cm^2/s. As with white phosphorus, if an oxide layer forms on the red phosphorus surface due to an accumulation of reaction products, the lifetime could be extended to thousands of years.

If nonporous red phosphorus is buried in soil, the lifetime will also extend into the thousands of years. A solid, spherical piece of phosphorus has a surface area of $4\pi R^2$ and will decay, without formation of a solid layer, according to equation 21:

$$M_{C_o}^{1/3} - M_C^{1/3} = \frac{0.21\ C_{air}}{3} \cdot 4\pi \cdot k \cdot \left(\frac{3}{4\rho\pi}\right)^{2/3} \cdot t \qquad (21)$$

A solid piece of red phosphorus initially 1 cm in diameter ($M_{C_o} = 0.524$ g) will require 2,600 years for complete oxidation without formation of a solid layer. The depth of burial does not appear in Equation 19 because the rate of oxygen consumption is very low for solid red phosphorus and the reaction rate controls the degradation process. An analysis performed for the presence of a solid layer predicted much longer oxidation times, as expected. That analysis was more complicated, requiring numerical solution, and it is not presented here.

If a piece of phosphorus is placed in a pool of still water, a solid layer may or may not form. The scenario of white phosphorus with no solid-layer formation results in a relatively short lifetime. In this case, a process of dissolution followed by simultaneous diffusion and reaction may proceed, leading to eventual consumption of the piece of white phosphorus. A quasi-steady-state analysis was performed for this case, in which the concentration profile of dissolved phosphorus is assumed to attain its steady-state value at all times as the piece of

phosphorus dissolves. Mass balances on dissolved and solid phosphorus yield two differential equations:

$$0 = \frac{D}{r^2} \frac{\partial}{\partial r} \left(r^2 \frac{\partial C}{\partial r}\right) - kC \tag{22}$$

where $C = P_4$ concentration in water, and

$$\frac{dR}{dt} = -\frac{D}{\rho} \cdot \frac{\partial C}{\partial r}\bigg|_{r = R} \tag{23}$$

where R = radius of piece of phosphorus in water

and

$C = C^*$ at $r = R$

$C \to 0$ as $r \to \infty$

$R = R_o$ at $t = 0$.

Equation 22 may be solved for the steady-state concentration profile, thus obtaining the concentration gradient at r = R for use in Equation 23. The result gives the radius R of the piece of solid phosphorus implicitly as a function of time:

$$\frac{C^*}{\rho} \cdot \frac{D}{R_o^2} \cdot t = -\left[\frac{R/R_o - 1}{\left[\frac{kR_o^2}{D}\right]^{1/2}} + \frac{1}{kR_o^2/D} \cdot \ln\left[\frac{1 + (kR_o^2/D)^{1/2}}{1 + \frac{R}{R_o}\left[\frac{kR_o^2}{D}\right]^{1/2}}\right]\right] \tag{24}$$

The steady-state concentration profile obtained from Equation 24 is

$$\frac{C}{C^*} = \frac{R}{r} \exp\left[-\sqrt{\frac{kR_o^2}{D}}\left(\frac{r}{R_o} - \frac{R}{R_o}\right)\right] \tag{25}$$

A sphere of influence around the piece of phosphorus may be defined as the distance at which the phosphorus concentration in the water drops to a predetermined fraction of the solubility value, C^*. That distance will shrink as the size of the piece of phosphorus decreases over time. Figure 45 shows the sphere of influence as a function of time. In this figure the sphere of influence is arbitrarily defined as the position where $C/C^* = 0.01$. Equation 24 was used to find the radius R of a piece of phosphorus at various times. At each of those times, R was used in Equation 25 to find the distance r at which $C/C^* = 0.01$. Figure 45 shows that the radius of the sphere of influence does not significantly decrease during the first half of the lifetime of a piece of white phosphorus. In fact, the sphere of influence is about 75% of its original value after 90% of the lifetime of phosphorus has elapsed. The value of the reaction rate constant and the diffusivity of phosphorus in water affect the size of the sphere of influence through the dimensionless parameter K.

The use of dimensionless variables often simplifies the solution procedure for differential equations. The dimensionless variables used in the analysis of the sphere of influence around a piece of white phosphorus allow a very general solution to be represented in a single plot, Figure 45. Figure 45 represents the solution for all values of the initial particle size, R_o, the diffusivity of phosphorus in water, D, the concentration of soluble P_4 at the particle surface, C^*, and the particle density, ρ. If a plot of the sphere of influence vs. time had been presented in dimensional units (simply r vs. t), values of R_o, D, C^*, and ρ would have been specified. Since R_o may change from case study to case study, and D and C^* are not known precisely, specifying those parameters to present a plot of the solution would reduce the utility of the plot.

Any case study can be conveniently evaluated with Figure 45 using the most up to date values of D, C^*, and ρ. For example, to analyze the case of particles initially 0.5 cm in radius, the quantities K, D, C^*, and ρ must be obtained. Data presented earlier indicate the half-life

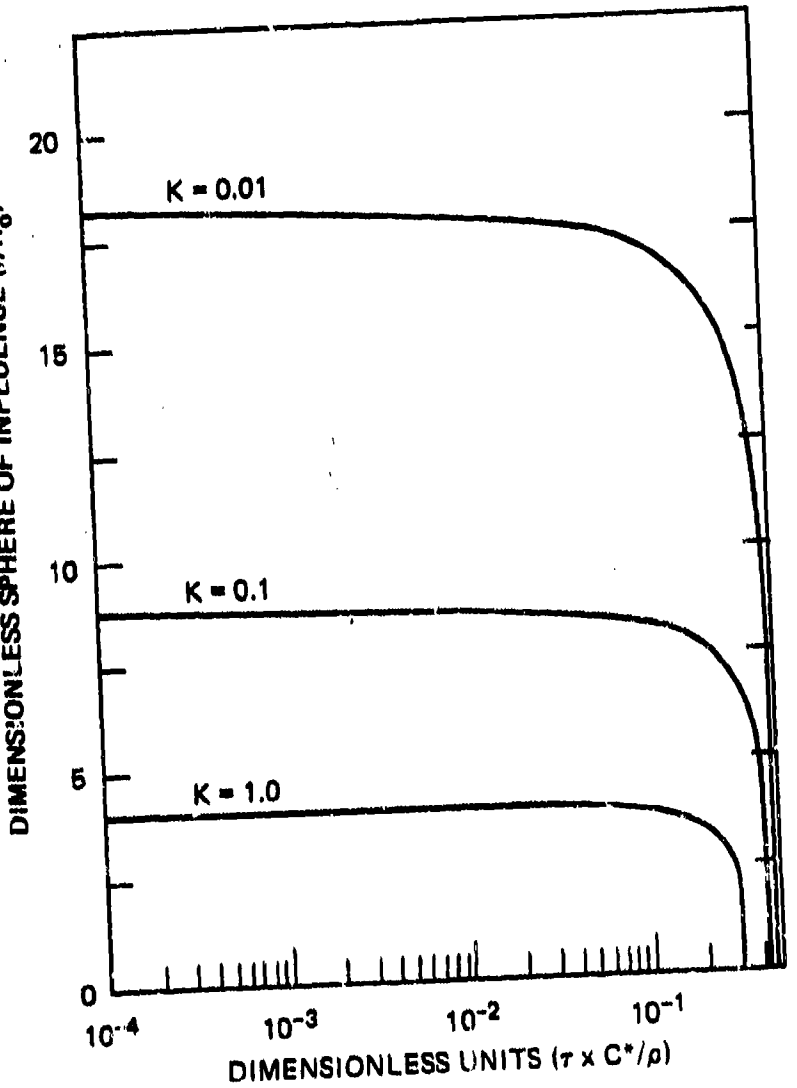

FIGURE 45 SPHERE OF INFLUENCE VERSUS TIME FOR WP WHERE C/C* = 0.01

of dissolved P_4 in water is approximately 42 hrs, giving a value of $K = 4.17 \cdot 10^{-6}\ s^{-1}$. The solubility of P_4 in water is approximately 4 ppm giving $C^* = 4.10^{-6}\ g/cm^3$. The density is about 2 g/cm^3. The diffusivity of solubile P_4 in water is not precisely known but assume $D = 10^{-4}\ cm^2/s$ for the purposes of this example. The dimensionless parameter K can be immediately computed,

$$K = \frac{kR_o^2}{D} = 1.04$$

A reasonable question to ask is, how large is the sphere of influence after 24 hrs. First, calculate the value on the abscissa of Figure 45 at T = 24 hrs (convert 24 hrs to seconds).

$$T\frac{C^*}{e} = \frac{TD}{R_o^2} \cdot \frac{C^*}{\rho} = 7.2 \cdot 10^{-5}$$

From Figure 45, the line labeled K = 1 approaches a value of about 4 on the ordinate for small values of $T\frac{C^*}{\rho}$, therefore, at T = 24 hrs, the size of the sphere of influence is 4 times the original particle radius, or 2 cm. After 2500 days, or 60,000 hrs, $T \cdot C^*/\rho = 0.18$ and $r/R_o \approx 3$, leading to a sphere of influence of 1.5 cm.

For this specific set of parameters, R_o, D, C^*, ρ, and K, a dimensional graph could have been constructed. The utility of the dimensionless graph, Figure 45, is illustrated with a second example. To analyze the case of particles initially 0.35 cm in radius the same procedure is used. In addition, postulate that diffusivity measurements made in the interval between the first analysis and this example reveal that $D = 5.10^{-4}\ cm^2/s$ rather $10^{-4}\ cm^2/s$ as originally assumed. Now,

$$K = \frac{kR_o^2}{D} \simeq 0.1$$

At T = 24 hrs,

$$T\frac{C^*}{\rho} \sim 7.2 \cdot 10^{-4}$$

Reading Figure 45 according to the line labeled K = 0.1 gives $r/R_o = 9$ so that the sphere of influence is 3.5 cm. At T = 2500 days,

$$T\frac{C^*}{\rho} = 1.8$$

In this case, $r/R_o = 0$ because the line for K = 0.1 decreased to zero at $TC^*/\rho \sim 0.4$.

These two examples are meant to show that a wide variety of case studies can be conveniently analyzed using Figure 45. As additional data become available on the behavior of P_4 in water, more precise values of parameters such as D and C^* can be incorporated easily.

A possible problem with the above analysis is the quasi-steady-state assumption that the concentration profile maintains its steady-state shape as the piece of phosphorus dissolves. For this assumption to be valid, the time required for the concentration profile to reach steady state must be very small relative to the lifetime of the piece of phosphorus. Figure 45 indicates a phosphorus lifetime of about 0.3 units on the x axis, which corresponds to $T = 1.5 \cdot 10^5$, assuming C^* = 4 ppm and ρ = 2 g/cc. The lifetime of a 1-cm-radius piece of phosphorus would then be about 48 years, assuming $D = 10^{-4}$ cm^2/sec.

An analysis of the transient behavior of the concentration profile was performed, and we determined that the time required to reach steady state is much less than the phosphorus lifetime (i.e., much less than

1.5×10^5 dimensionless time units). This analysis was performed by solving the transient diffusion and reaction equation,

$$\frac{\partial C}{\partial t} = \frac{D}{r^2} \frac{\partial}{\partial r} \left(r^2 \frac{\partial C}{\partial r}\right) - kC \qquad (26)$$

where

$$C = C^* \text{ at } r = R$$

$$C \to 0 \text{ as } r \to \infty$$

$$C = 0 \text{ at } t = 0. \qquad (27)$$

Initial condition 27 represents a system, initially phosphorus-free, into which a piece of phosphorus is placed. The solution to Equation 26 is

$$\frac{C}{C^*} = \frac{K}{\Omega} \int_0^T \operatorname{erfc}\left(\frac{\Omega-1}{2\sqrt{s}}\right) e^{-Ks} ds + \frac{1}{r} \operatorname{erfc}\left(\frac{\Omega-1}{2\sqrt{T}}\right) e^{-KT} \qquad (28)$$

where

$$\Omega = \frac{r}{R_o} = \text{dimensionless distance} \qquad (29)$$

$$T = \frac{tD}{R_o^2} = \text{dimensionless time} \qquad (30)$$

$$K = \frac{kR_o^2}{D} = \text{dimensionless reaction rate constant.} \qquad (31)$$

Figure 46 shows concentration profiles plotted at various dimensionless times for $K = 0.1$. The concentration profile for $T = 100$ is identical to the steady-state profile. Therefore, because the lifetime of a piece of phosphorus is on the order of $T = 10^5$ and steady state is achieved

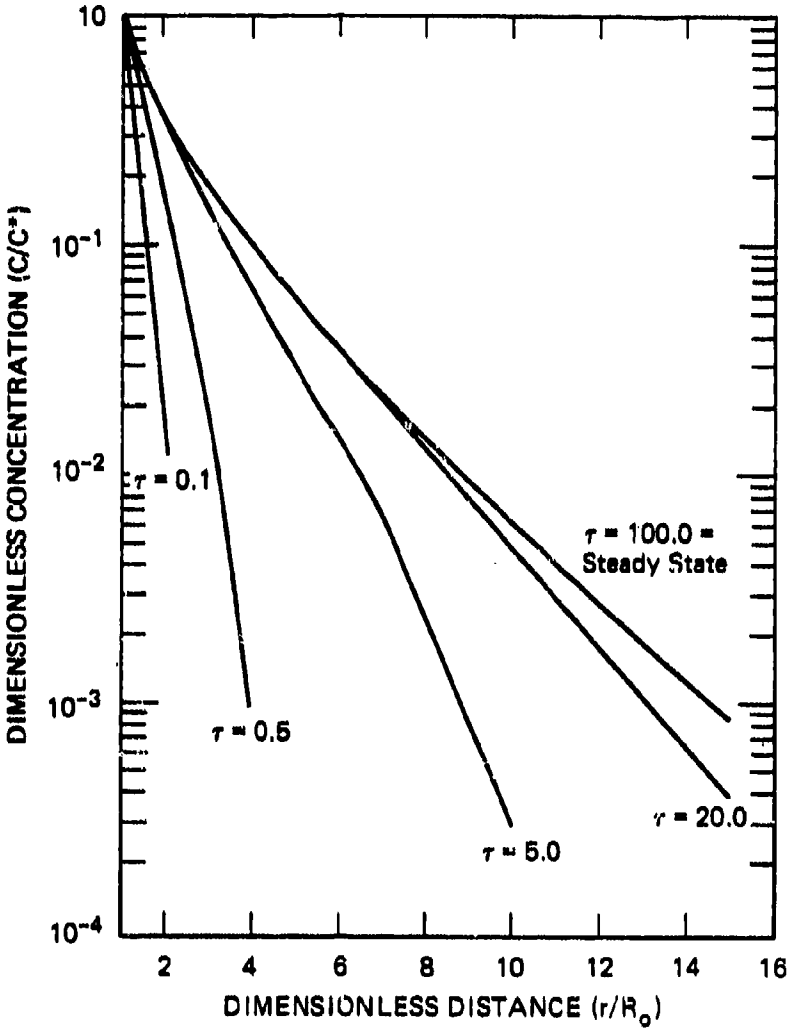

FIGURE 46 TRANSIENT CONCENTRATION PROFILES FOR K = 0.1

by T ~ 100, the quasi-steady-state analysis should be sufficient for this problem.

An analysis for porous red phosphorus submerged in water was performed in a similar manner to the analysis for porous red phosphorus buried in soil. Equations 17, 18, and 19 are used in this case but C_{O_2} is now the oxygen concentration in water, approximately $8 \cdot 10^{-6}$ g/cm^3 at the solubility limit. The first-order reaction coefficient for red phosphorus oxidation in water can be calculated using the initial rate data in Section IV and Equation 19.

$$\lim_{t \to 0} \left(\frac{dM_c}{dt}\right) = -9.6339 \cdot 10^{-9} \frac{g}{sec} = -kaCo_2 \cdot M_{C_o} \qquad (19)$$

$$k = 4.012 \cdot 10^{-7} \frac{cm}{sec}$$

The time required for 95% of a piece of porous red phosphorus to oxidize in well-aerated water is approximately 20 years. As with red phosphorus in soil, a solid piece of red phosphorus will require several thousand years to completely oxidize in water. If an oxide layer forms, the lifetime of red phosphorus will be extended about three orders of magnitude, whether it is porous or solid.

B. Aerosol Modeling

The atmospheric dispersion of phosphorus generated from burning WP/F and RP/BR to produce obscurant smokes depends on several interrelated phenomena that are critical in evaluating the fate of phosphorus in the environment. A smoke plume is formed from a munitions burn as the smoke is carried by the prevailing winds, rising aloft due to the bouyant forces generated from the combustion reactions. Ambient wind speed and atmospheric conditions that influence plume rise and expansion are important factors in determining the downwind phosphorus concentration and deposition of the particles produced from a munitions burn on the ground. The type of terrain will also have a profound effect on the particle deposition of phosphorous smokes.

In addition, aerosol rate processes that occur within the plume affect the dispersion of phosphorus in the environment. Nucleation just beyond the combustion zone provides the source of very fine phosphate particles. These primary particles grow in size by coagulation and the condensation of water. Because deposition is size-dependent, the material deposited will change with the evolving particle size distribution. As the smoke is carried from the burn site, the composition of the particles is transformed by chemical reaction; phosphate polymers, formed during the combustion reactions, are hydrolyzed to phosphate.

To model these processes that affect the atmospheric dispersion of phosphorus, we have incorporated relationships for the expansion of a smoke plume and a correlation for particle deposition onto rough surfaces into the MAEROS computer code (Gelbard, 1982), a simulation of the dynamic aerosol processes for multicomponent systems. This overall model was used to predict the plume concentration, the fraction of material deposited, the change in the particle size distribution, and the change in particle composition due to chemical reaction as a function of distance downwind of the burn site. Simulations for the phosphorus dispersion were performed for several values of each of the key parameters that influence particle deposition to evaluate the sensitivity of the model to these parameters.

1. Theory

The fundamental aerosol dynamic phenomena of nucleation, condensation, and coagulation that govern fine-particle systems are represented by the general dynamic equation (Friedlander, 1977). To solve this equation under general conditions, Gelbard and Seinfeld (1980) introduced a sectionalized representation of the particle size distribution; the continuous distribution of particle-mass concentration is divided into discrete sections where the mass concentration in each section is constant. The result is a histogram of mass concentration as a function of particle size. With this approximation, the general dynamic equation is reduced to a system of ordinary differential equations that can be solved by conventional numerical methods. The

MAEROS computer program (Gelbard, 1982) is based on the sectionalization of the particle size distribution in the general dynamic equation. It provides a simulation with respect to particle size for the evolution of chemical species in an aerosol system undergoing coagulation, condensation, and intraparticle chemical reaction.

To simulate the atmospheric dispersion of phosphorus, the munitions burn time is assumed to be negligible compared to the evolution of the plume, so that the munitions burn is considered to be an instantaneous source of smoke. In addition, the particle concentration is considered to be uniform in the horizontal, x, and vertical, y, directions of the evolving plume (downwind distance is in the Z-direction.) The convective transport in the plume is incorporated into the sectionalized dynamics equations of MAEROS in equation 32 (see Gelbard and Seinfeld, 1980, Equation 50).

$$\frac{dQ_{\ell k}}{dt} = -\frac{1}{A}\frac{dA}{dt}Q_{\ell k} - \frac{L_x}{A}\bar{v}_\ell Q_{\ell k} + \bar{R}Q_{\ell k} \qquad (32)$$

$$+ 1/2\sum_{j=1}^{\ell}\sum_{i=1}^{\ell}\left(\bar{{}^1\beta}_{\ell ji}Q_{jk}Q_i - \bar{{}^1\beta}_{\ell ij}Q_{ik}Q_j\right) - Q_{\ell k}\sum_{j=i}^{m}\bar{{}^2\beta}_{\ell j}Q_j$$

$$+ \bar{G}_{\ell k}Q_\ell - \sum_{i=1}^{s}\left[\bar{{}^2G}_{\ell i}Q_{\ell i}Q_{\ell k} - \bar{{}^2G}_{\ell-1,i}Q_{\ell-1,k}\right] + \bar{{}^3G}_{\ell-1,k}Q_{\ell-1}$$

where $\frac{dQ_{\ell k}}{dt}$ represents the rate of change of the particle mass concentration for section ℓ and component k. For a system consisting of s components and m total sections, m x s ordinary differential equations result.

The first three terms in Equation 32 represent the dilution, deposition, and chemical reaction, respectively. These are specific to the model for the dispersion of phosphorous smokes and each will be discussed in detail later in the report. The 4th and 5th terms are the sectionalized representation of coagulation and the 6th, 7th, and 8th

terms are the sectionalized representation of condensation. The simulation of coagulation and condensation for phosphorous dispersion requires no modification to MAEROS and a thorough description can be obtained in the references cited.

The dilution of the smoke plume as it expands is represented in the first term of Equation 32. Relationships for the plume area, A, as a function of downwind distance, Z, were obtained from a least-squares fit of a power law relationship to Pasquill's empirical correlations for plume dispersion coefficients reported in Seinfeld (1975). The plume dispersion coefficients are given by:

$$\sigma_i = A_i(V_o t)^{\gamma_i} \tag{33}$$

where V_o is the wind velocity. The fitting coefficients A_i and γ_i, which have been established empirically for three types of atmospheric conditions (moderately unstable, neutral, and moderately stable), are presented in Table 31.

Table 31

FITTING COEFFICIENTS FOR THREE ATMOSPHERIC STABILITY CLASSES

	σ_y Vertical Dispersion Coefficient		σ_x Horizontal Dispersion Coefficient	
	A_y	γ_y	A_x	γ_x
Moderately stable	0.134	0.651	0.057	0.928
Neutral	0.402	0.625	0.164	0.883
Moderately unstable	0.0526	1.14	0.328	0.890

Given that the cross-sectional area of the plume is proportional to the product $\sigma_x\sigma_y$, the expression $\frac{1}{A}\frac{dA}{dt}$ becomes $(\gamma_x + \gamma_y)/t$. For a neutral plume, this expression for plume expansion produces a 32-fold

concentration dilution going from 100 m to 1000 m downwind from the source.

Particle loss by deposition on the ground is represented in the second term of Equation 32. This term is the product of the ratio of the horizontal plume width, L_x, to the plume area, A, times the particle mass concentration, $Q_{\ell k}$, and the deposition velocity, $\bar{V}_{d_\ell}$.

The deposition velocity is defined as the deposition flux to the surface divided by the bulk plume concentration and represents an overall mass transfer coefficient that includes the particle deposition mechanisms of diffusion, interception, impaction, and gravitational settling. The deposition velocity depends on particle size. It is high for small particles where diffusional transport predominates, is minimum for particles between 0.1 and 0.3 μm in diameter, and increases rapidly for larger particles as impaction and gravitational settling predominate. This general functionality is exhibited for all rough surfaces, but the magnitude of the deposition velocity depends on the type of surface and can differ by several orders of magnitude.

The general correlation developed by Schack, Pratsinis and Friedlander (1985, in press) was used to compute the deposition velocity in the model for the dispersion of phosphorus. The correlation was obtained from a fit of the available experimental data to various rough surfaces. Profiles of the deposition velocity as a function of particle size are presented in Figure 47 for the three natural surfaces considered, rye grass and crushed gravel (B), and water (C). These profiles were generated for an ambient wind velocity of 3.0 m/sec and include gravitational settling.

The sectional representation of the deposition velocity, derived following the procedure of Gelbard and Seinfeld (1980), becomes:

$$\bar{V}_{d_\ell} = \int_{f(v_\ell)}^{f(v_{\ell+1})} \frac{V_d}{f(v_{\ell+1}) - f(v_\ell)} dv \qquad (34)$$

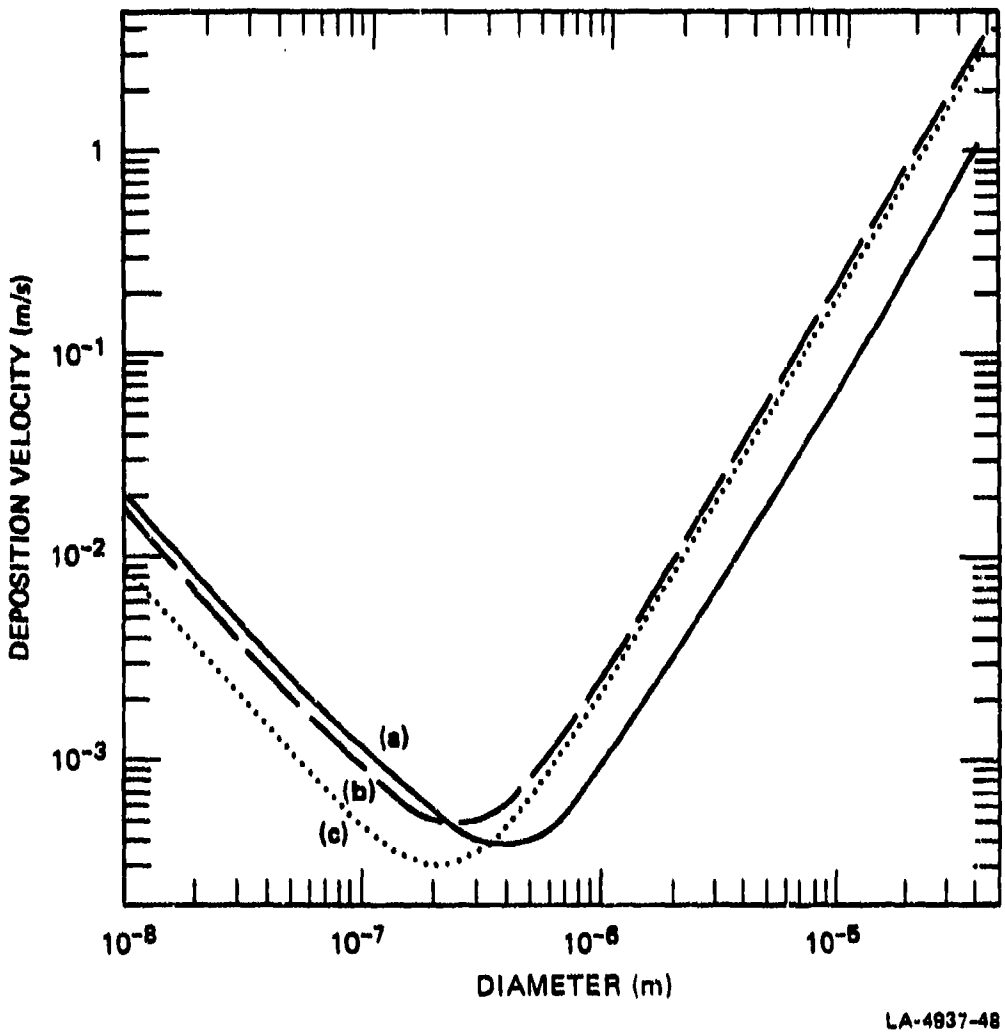

FIGURE 47 PROFILES OF DEPOSITION VELOCITY FOR A PHOSPHORUS SMOKE AEROSOL ON THREE ROUGH SURFACES:

(a) Rye Grass; (b) Crushed Gravel; (c) Water

The correlation for the deposition velocity is integrated over a particle mass, v, mass of section, ℓ, so that the sectional deposition velocity, $\bar{V}_{d_\ell}$, represents an average deposition velocity for section ℓ.

We now discuss the chemical reaction term (third term) in Equation 32. The change in particle compostion due to the hydrolysis of phosphate polymers is modeled as three consecutive first- order reactions with a phosphate monomer formed at each step:

$$P_n \xrightarrow{k_3} P_3 + P_1$$

$$P_3 \xrightarrow{k_2} P_2 + P_1 \qquad (35)$$

$$P_2 \xrightarrow{k_1} P_1$$

The change in chemical composition within the particle due to intraparticle chemical reaction can be related to the change in the composition of the aerosol, $\frac{dQ_{\ell k}}{dt}$ through the sectionalized rate coefficient, $\bar{R}_{\ell k}$, which is in general a function of particle size. However, when it is assumed that the intraparticle reaction rate is a linear combination of first-order terms and that the density of each particle remains constant, the sectionalized rate coefficient equals the intraparticle rate coefficient, k_i, and is independent of particle size.

The system of first-order ordinary differential equations that result from Equation 32 provides a general model for the atmospheric dispersion of phosphorous smokes. The model incorporates particle dilution in an expanding plume, deposition to rough surfaces, and intraparticle chemical reaction. It also includes the dynamic particle growth processes of coagulation and condensation. The growth processes influence the dispersion of phosphorus because particle deposition is such a strong function of particle size.

The simulations of phosphorous smoke dispersion were initiated 1 min downwind from the source, the time that corresponds to the age of the munitions smoke sampled in the scale-model deployment studies. The

initial particle size distribution used in the simulation was obtained from these experimental measurements of munition burns. Measurements were obtained for burns conducted at three humidities. For the simulation, we assumed that water condensation was completed in the 60-sec period prior to sampling; consequently, it was not included in the simulation. The effect of relative humidity on the phosphorus dispersion is therefore reflected only in the initial particle size distribution.

For the base-case simulation, we chose initial values of the key parameters that were typical of conditions that would exist in a field munitions burn. The initial particle distribution was taken to be a log normal distribution having a mass median diameter of 1.3 μm and a standard geometric deviation of 1.8. These values were consistently measured for the particle distribution from the WP/F burns. The initial concentration of 0.3×10^{-3} kg/m^3 was used in the simulation. This concentration is reported to be required to produce an effective obscurant (Berkowitz et al., 1981). Neutral plume expansion coefficients (Table 31) were used for the base-case simulation. The other meterological variables that affect plume dispersion wind speed and plume rise were chosen to be 3.0 m/sec and 10 m, respectively. The munitions-burn rate, determined from the initial concentration, wind speed, and plume expansion by $J_o = C_o V_o A_o$, was computed to be 6.05×10^{-1} kg/sec. Finally, the deposition velocity was computed for a gravel surface.

Profiles of the particle concentration in the plume as a function of downwind distance for the moderately stable, the neutral, and the moderately unstable plume-expansion conditions are presented in Figure 48. The decrease in mass concentration is a result of both dilution and particle loss by deposition. To obtain the fraction of material remaining in the aerosol, the mass flow rate velocity downwind from the source is normalized to the initial source rate. The fraction deposited is computed directly from the fraction remaining. The fractional representation is independent of concentration dilution and of the

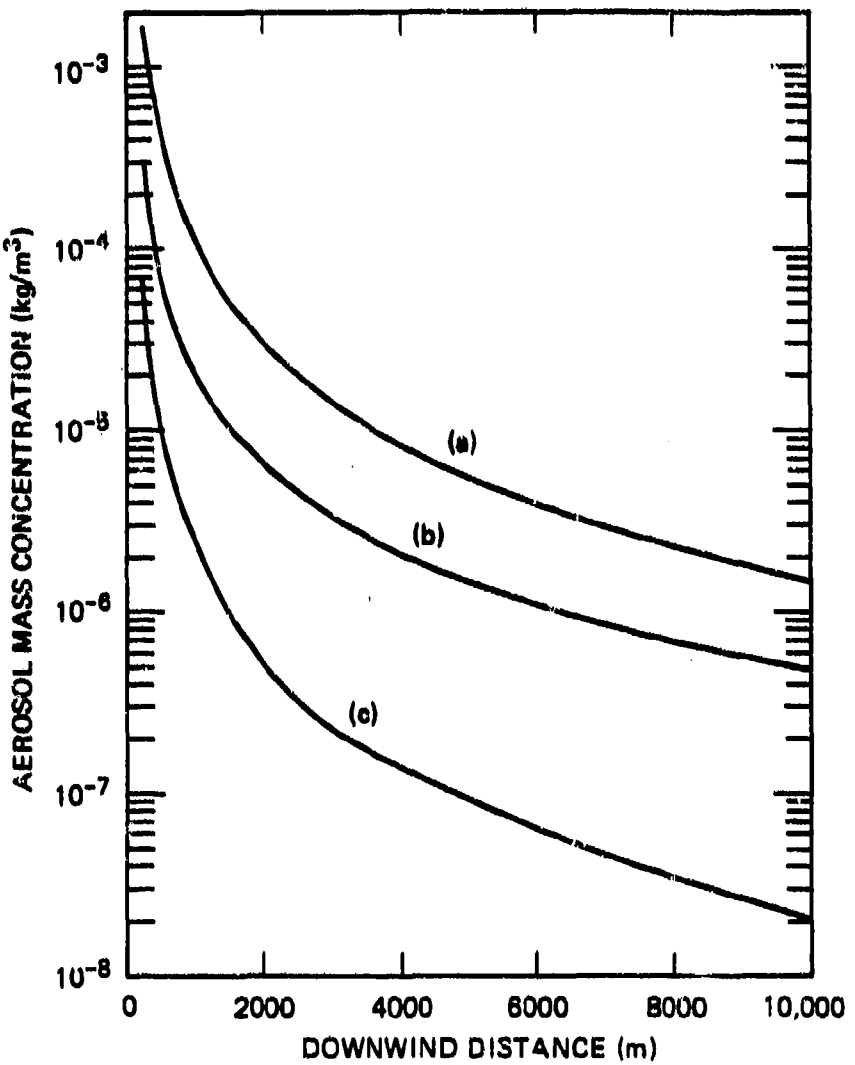

FIGURE 48 PHOSPHORUS AEROSOL CONCENTRATION AS A FUNCTION OF PLUME EXPANSION:

(a) Moderately Stable Plume; (b) Neutral Plume; (c) Moderately Unstable Plume

source-dependent quantities of munitions burn rate and burn period. For the base-case simulation of a neutral plume, the fraction of material in the aerosol and the fraction deposited are given in Figure 49. The particle deposition is rapid early in the simulation but decays with distance as the particle concentration is diluted in the expanding plume. Under these conditions, 66% of the phosphorus burned remains in the aerosol 10,000 m from the burn site.

The sectional representation of the initial and final particle size for the simulation are presented in Figures 50 and 51. Section number, plotted on the x axis, is a function of the log of the particle diameter and covers the diameter range of 0.01 to 40.0 μm. Mass concentration is plotted along the y axis. The initial particle size distribution, Figure 50, is generated from a log normal particle size distribution with mass median diameter of 1.3 μm, a standard geometric deviation of 1.8, and an initial concentration of 3.0×10^{-4} kg/m^3. The final particle size distribution was obtained for the simulation at 10,000 m. Particle concentration in Sections 13, 14, 15, and 16 are depleted in the final distribution relative to the initial distribution because of the preferential deposition of the larger particles. Coagulation appears to have no significance in this case because there is observable difference in the relative quantities of the lower sections, 8, 9, 10, between the initial and final distributions.

Experimental measurements of the composition of phosphorous smokes yielded polymers that contained up to 16 phosphorous molecules. To simulate the hydrolysis of the polyphosphates in the phosphorous smokes, the particle composition was represented by four components--the phosphate monomer, dimer, trimer, and polymer, where polymers greater than 3 were grouped in the polymer component. The experimentally measured composition, used as the initial values for the simulations, were as follows: $P_1 = 24.77\%$; $P_2 = 24.82\%$; $P_3 = 11.44\%$; and $P_n = 38.97\%$. The reaction rate coefficients were determined from measurements of the hydrolysis in aqueous solution. Values for the rate

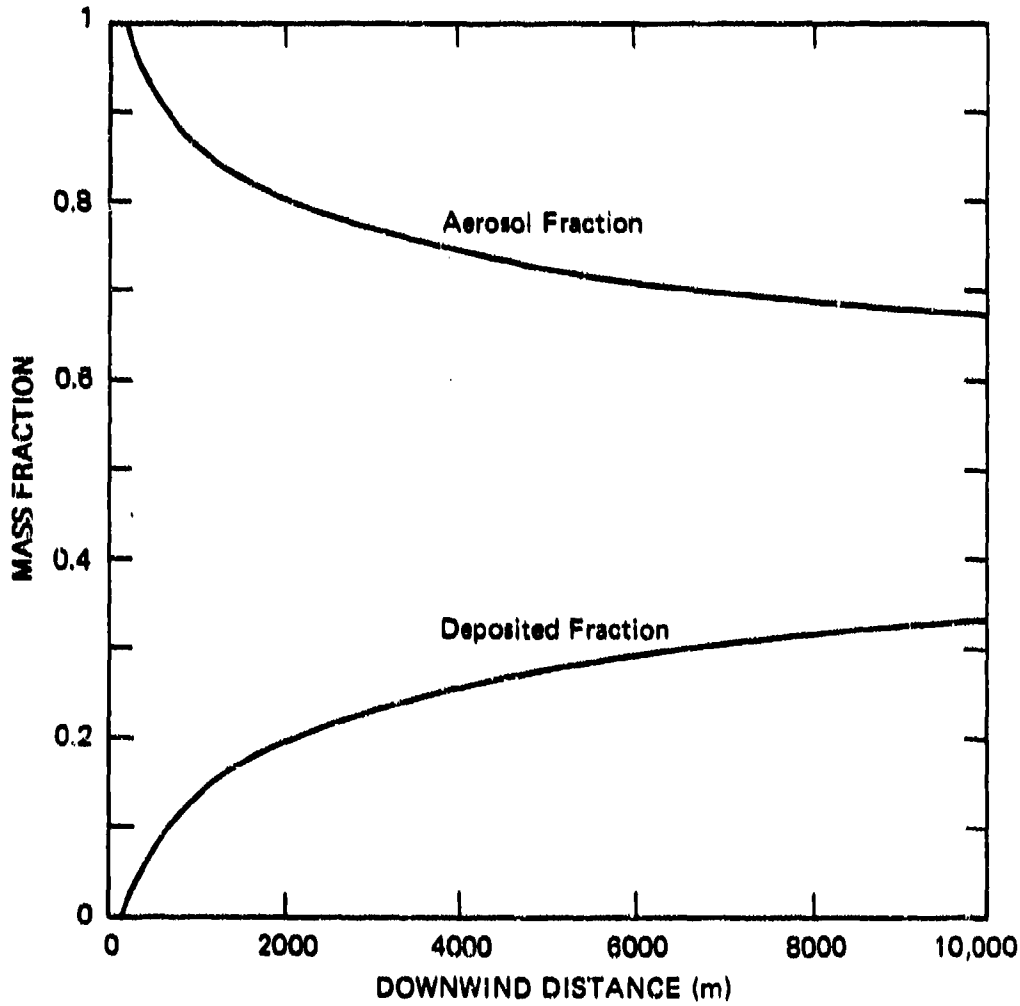

FIGURE 49 PHOSPHORUS DEPOSITION FROM A PLUME

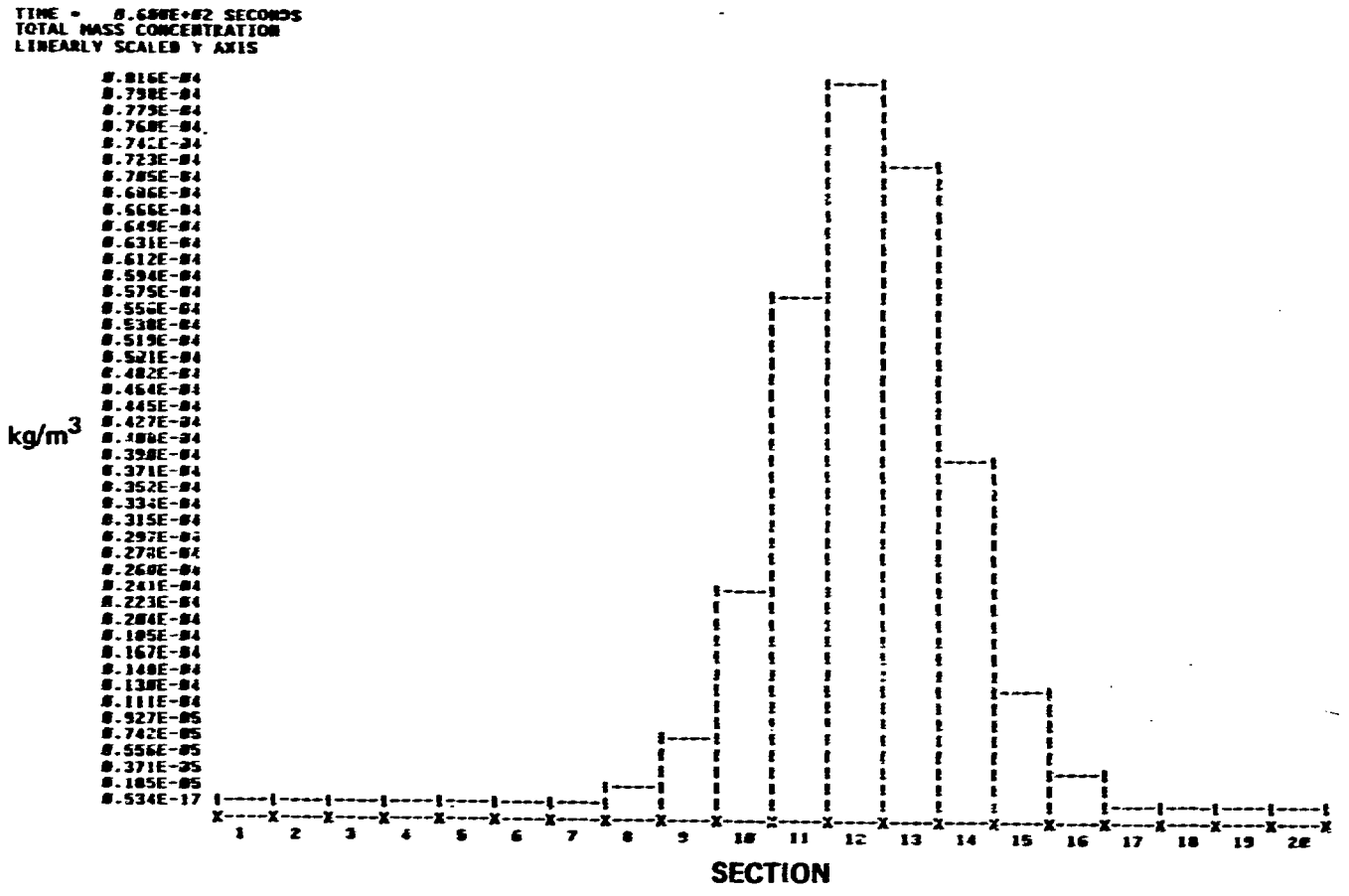

FIGURE 50 INITIAL PHOSPHORUS SMOKE AEROSOL/SIZE DISTRIBUTION FOR $C_O = 0.3 \times 10^{-3}$

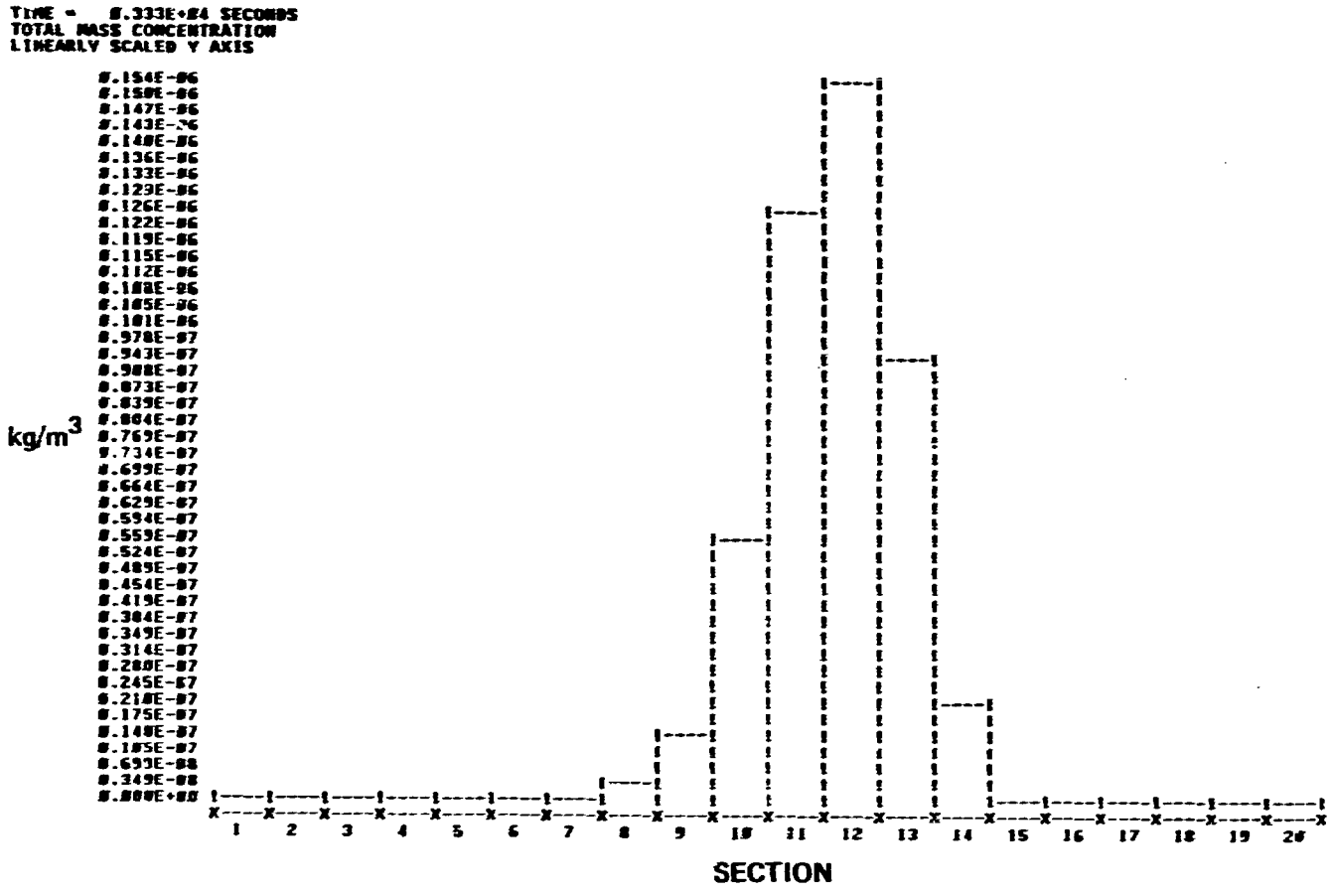

FIGURE 51 FINAL PHOSPHORUS SMOKE AEROSOL PARTICLE SIZE DISTRIBUTION AT 10,000 m

coefficients used in the simulations are as follows: $k_1 = 4.9 \times 10^5$ sec^{-1}.

The evolution of the particle composition as the munitions aerosol is carried downwind is presented in Figure 52. The composition values are reported in mass fractions. The reaction kinetics for the full four days is presented in Figure 53. If it is assumed that the reaction kinetics are the same for the particles deposited on land as for the suspended particles, then this 96-hour simulation of the hydrolysis of phosphate polymers accurately models the fate of these compounds in the environment regardless of whether they are in the aerosol or the deposited form.

Further analysis of the phosphorus dispersion model was conducted to determine the sensitivity of particle deposition to several of the key parameters that influence phosphorus dispersion. The evaluations were performed varying the selected parameter while the base conditions were maintained for the others.

The results for the effect of initial concentration on particle deposition is presented in Figure 54. The fraction of material deposited is independent of concentration until the initial concentration is high enough for coagulation to be significant. Deposition is enhanced as the particles coagulate and grow in size. The effect of coagulation on the final particle distributions at 10,000 m downwind is shown in Figure 55 for an initial concentration of 1.0×10^{-3} kg/m^3 and in Figure 56 for an initial concentration of 1.0×10^{-1} kg/m^3. In Figure 55, material is preferentially depleted in the lower sections 8, 9, 10, and 11, whereas Figure 56 shows a pronounced shift in the distribution toward the right to the larger sized particles. These concentrations at which coagulation is significant are higher than what is preferred in the field since concentrations of 1.0×10^{-3} kg/m^3 have been reported to have undesirable health effects (Berkowitz et al. 1981). Therefore, we conclude that coagulation is an unimportant mechanism in the dispersion of phosphorous smokes except perhaps in the immediate vicinity of the burn site.

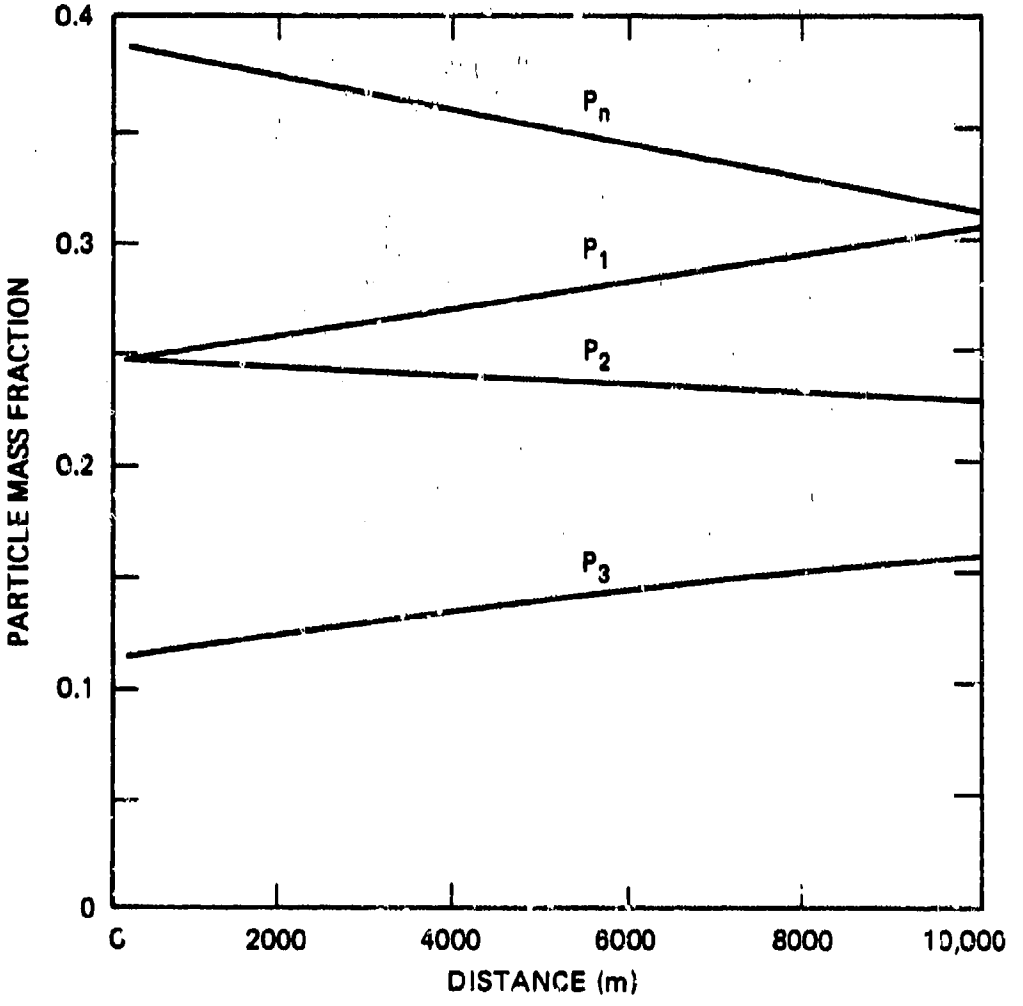

FIGURE 52 PHOSPHATE HYDROLYSIS IN A PLUME

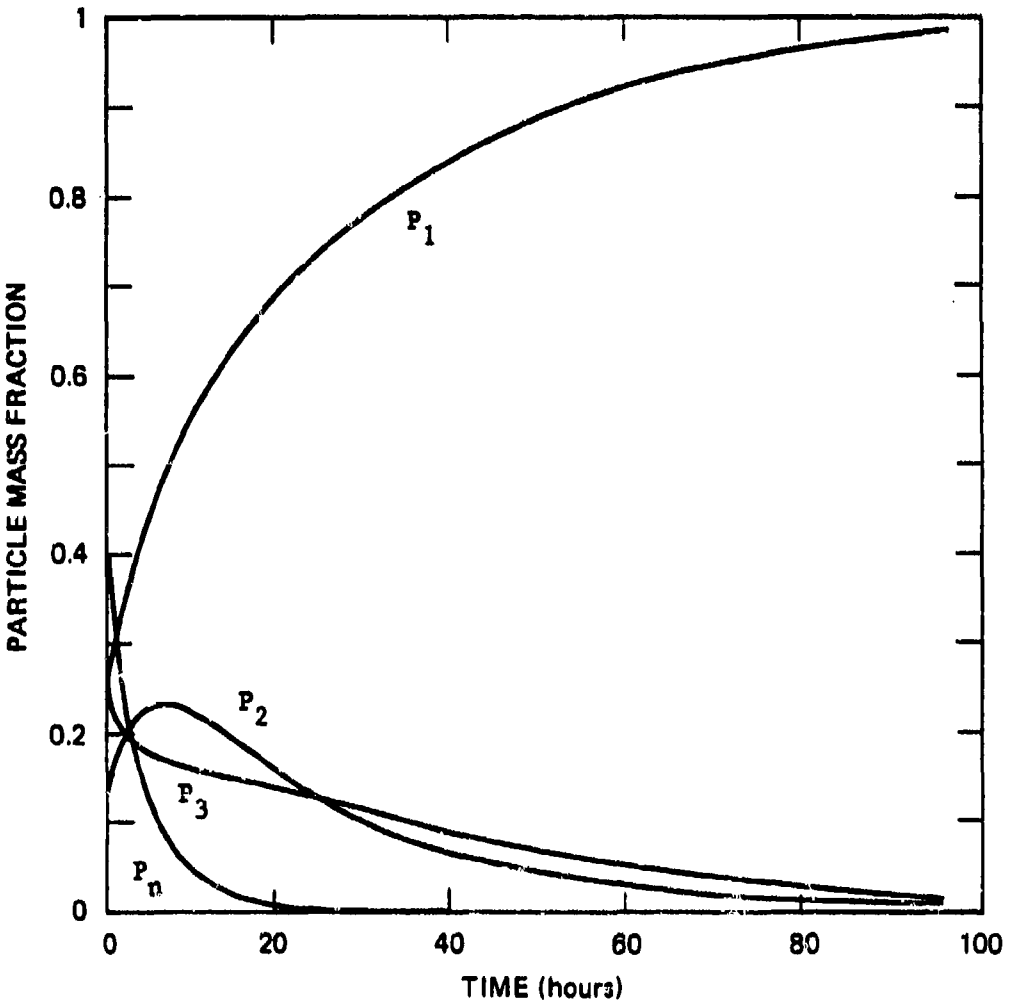

FIGURE 53 SIMULATED PHOSPHATE HYDROLYSIS IN SMOKE AEROSOL

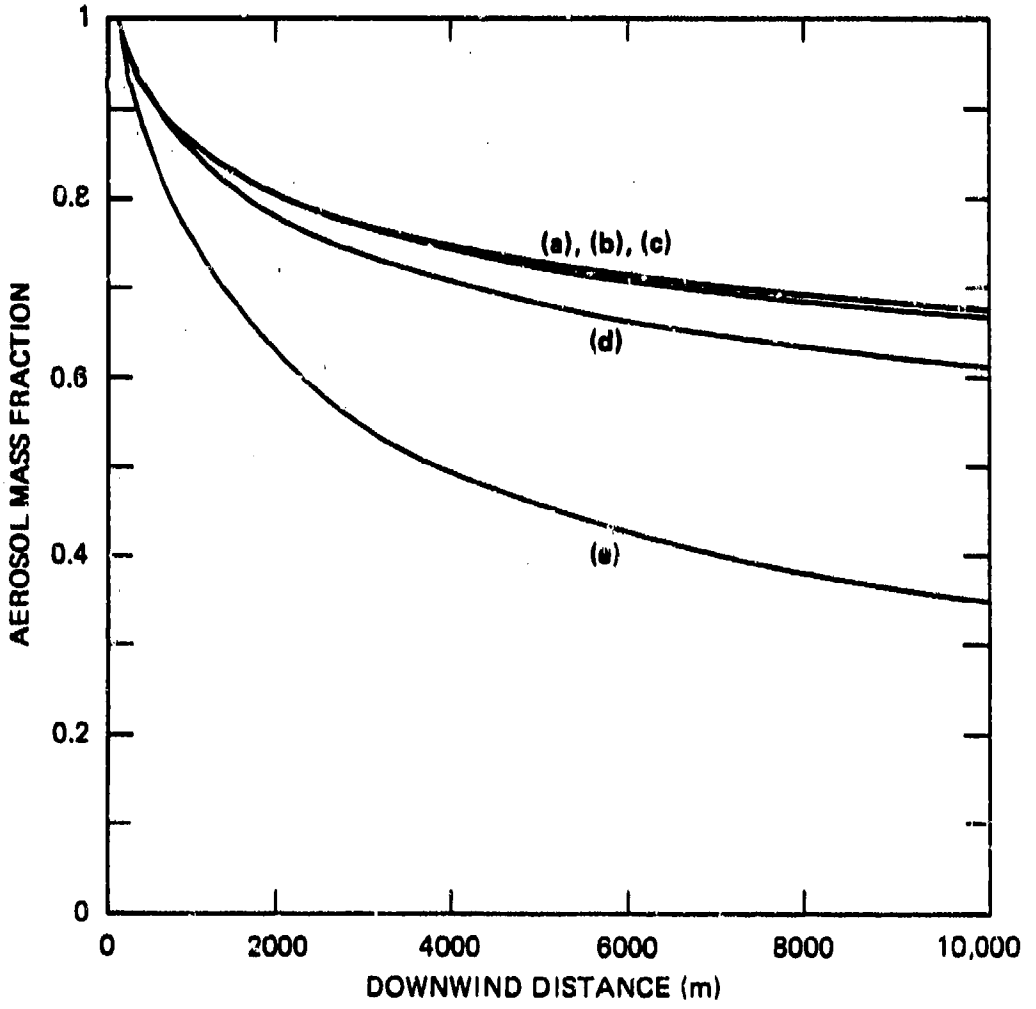

FIGURE 54 PHOSPHORUS SMOKE AEROSOL PARTICLE DEPOSITION AS A FUNCTION OF INITIAL CONCENTRATION

(a) $C_o = 1.0 \times 10^{-3}$ kg/m^3; (b) $C_o = 0.3 \times 10^{-3}$ kg/m^3; (c) $C_o = 1.0 \times 10^{-3}$ kg/m^3; (d) $C_o = 1.0 \times 10^{-2}$ kg/m^3; (e) $C_o = 1.0 \times 10^{-1}$ kg/m^3.

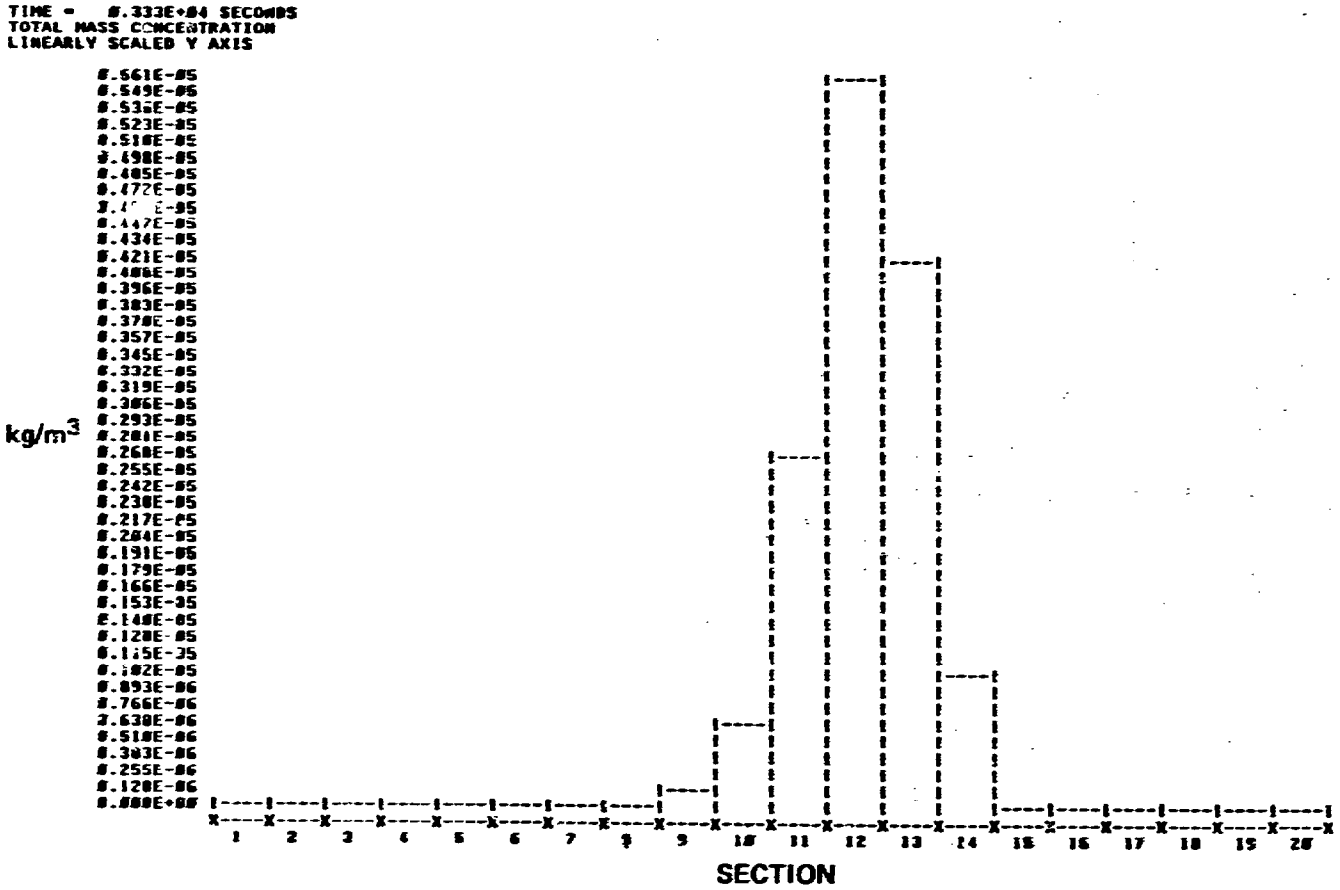

FIGURE 55 FINAL PHOSPHORUS SMOKE AEROSOL PARTICLE SIZE DISTRIBUTION FOR $C_o = 1.0 \times 10^{-3}$ kg/m^3

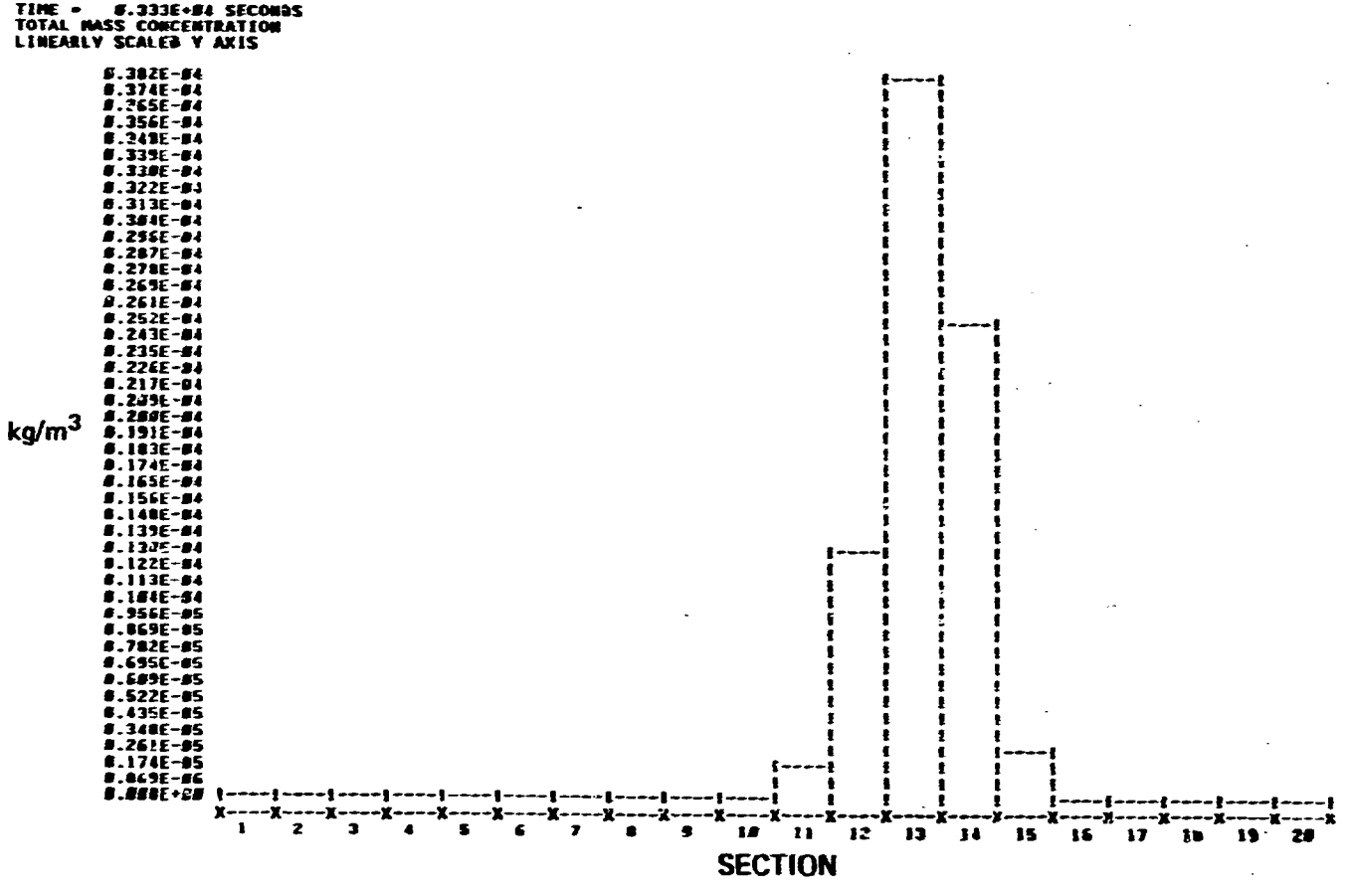

FIGURE 56 FINAL PHOSPHORUS SMOKE AEROSOL PARTICLE SIZE DISTRIBUTION FOR $C_o = 1.0 \times 10^{-1}$ kg/m^3

Simulations were performed varying the coefficients for plume expansion, the wind speed, and the plume rise to evaluate the effect of these atmospheric conditions on the phosphorus dispersion in the environment. The results of the simulation for three conditions of plume dispersion are given in Figure 57. The moderately unstable plume is dispersed more rapidly than the base-case neutral plume, and more material remains in the air. The moderately stable plume, however, is dispersed more slowly, and nearly 50% of the material is deposited by 10,000 m downwind. The initiation of the deposition in the stable plume is delayed until the plume has expanded to intercept the ground.

Results of particle deposition as a function of wind velocity are presented in Figure 58. Curves were generated for wind speeds of 3.0, 6.0, 9.0 m/sec. Although high wind speed dilutes the initial concentration of the plume, particle deposition increased as wind velocity increased because of the enhancement of the deposition velocity. For the high wind speed, 44% of the burned material is deposited by 10,000 m.

The effect of plume rise on the aerosol behavior is presented in Figure 59. Simulations were performed for plumes that were carried aloft 10, 20, and 30 m. Particle deposition is delayed until the plume has expanded to intercept the ground; then roughly similar deposition profiles are produced. Plume rise has little effect on the overall particle deposition; the difference in the deposition fractions between a 10-m and a 30-m plume rise is approximately 8%.

The type of surface and its roughness characteristics has a profound effect on the deposition of particles. Expressions for deposition velocity can be derived from basic principles only for simple roughness elements. These results can be applied to represent an actual-surface through a surface-specific density factor. When this approach is taken, it is found that deposition velocity profiles differ by as much as an order of magnitude for different types of grasses (Davidson et al., 1982). The general correlation for particle deposition developed by Schack et al. (in press) from an analysis of

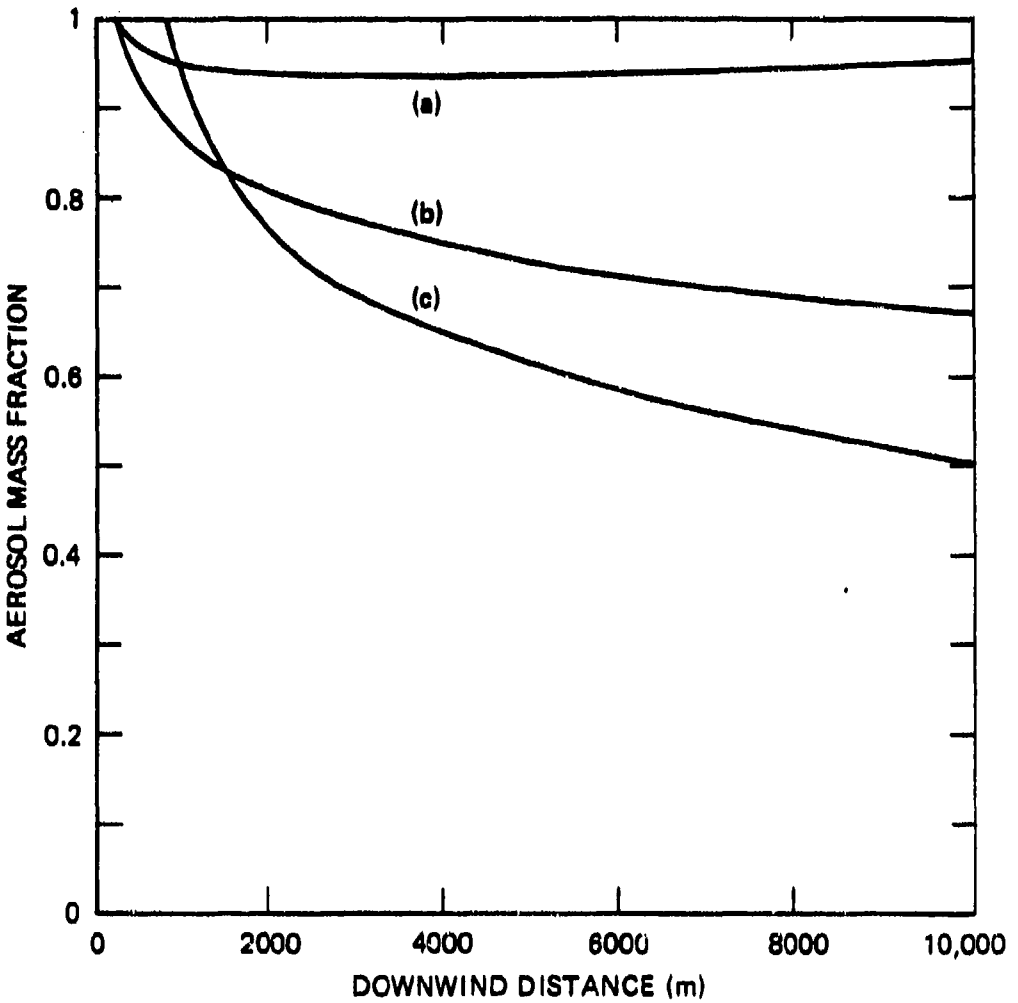

FIGURE 57 PHOSPHORUS SMOKE AEROSOL PARTICLE DEPOSITION AS A FUNCTION OF PLUME EXPANSION

(a) Moderately unstable; (b) Neutral; (c) Moderately stable.

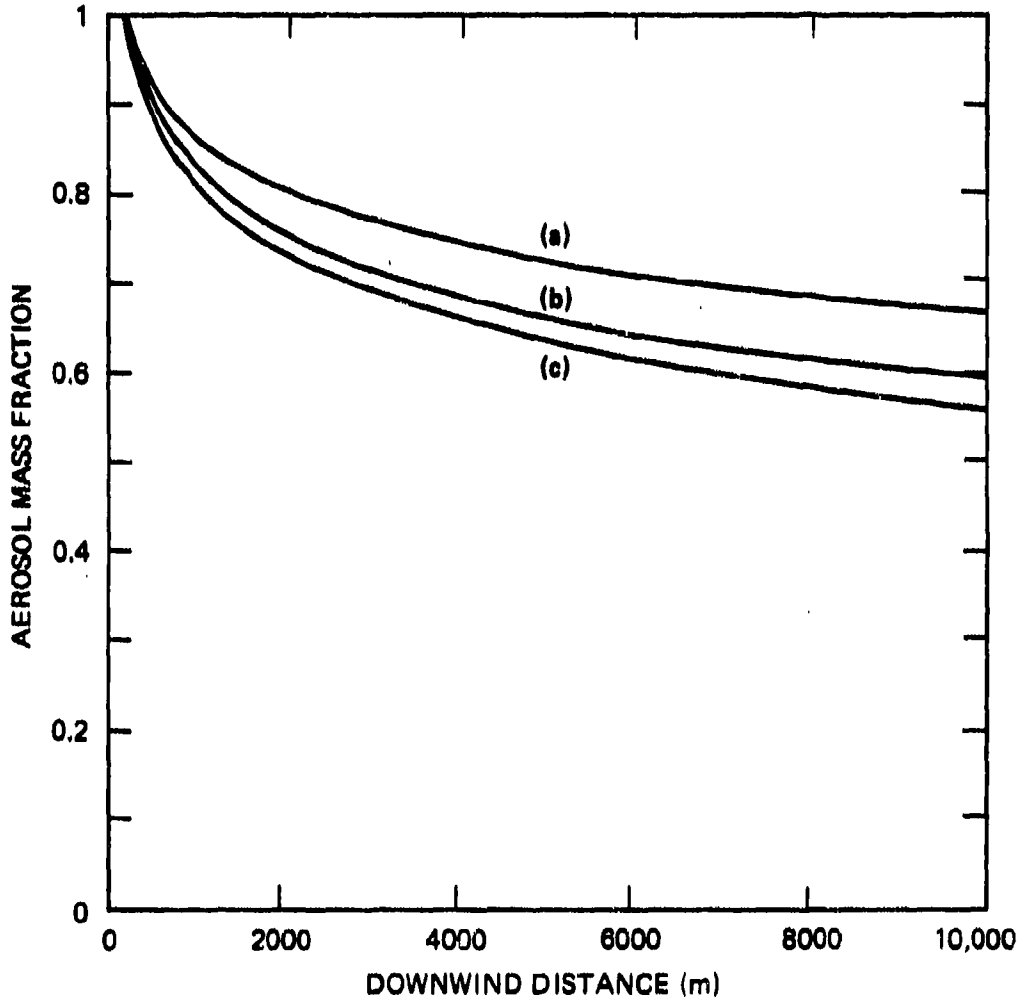

FIGURE 58 PHOSPHORUS SMOKE AEROSOL PARTICLE DEPOSITION AS A FUNCTION OF WIND VELOCITY

(a) V_0 = 3.0 m/s; (b) V_0 = 6.0 m/s; (c) V_0 = 9.0 m/s.

171

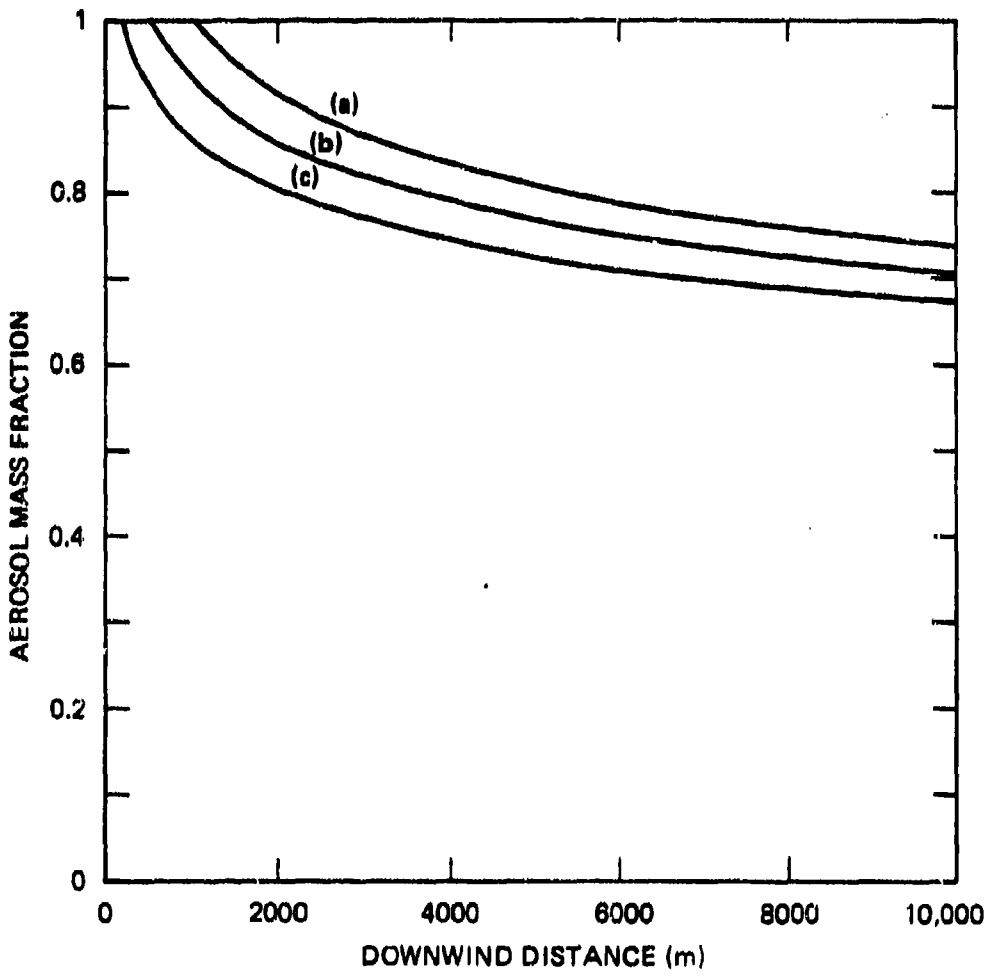

FIGURE 59 PHOSPHORUS SMOKE AEROSOL PARTICLE DEPOSITION AS A FUNCTION OF PLUME RISE

(a) 30-m; (b) 20-m; (c) 10-m.

experimental literature produced deposition velocity profiles for grass, water, and gravel (see Figure 47) that are similar in magnitude. Yet these relatively small differences in deposition velocity produced fairly significant differences in the calculated amount of smoke deposited (Figure 60). The differences in the simulation obtained for grass (11% deposition at 10,000 m) and that obtained for gravel (34%) and water (29%) may be a result of differences in experimental design. The results for gravel and water were obtained from experiments conducted in the same laboratory.

The effect of particle size on the deposition of phosphorous smokes was the final parameter studied. The results, presented in Figure 61, are for simulations wherein the initial log-normal distribution had mass median diameters of 0.5 1.3, and 5.0 μm. Particle size exhibits the most significant effect on the distribution of the material between the aerosol and surface phases of any of the parameters studied. These results illustrate the importance of including the particle growth mechanisms in the plume dispersion model.

2. Summary and Conclusions

The model for the dispersion of phosphorus munitions smokes incorporates correlations of plume expansion and particle deposition into a program for multicomponent aerosol dynamics that includes particle growth by coagulation and condensation. The intraparticle reaction for the hydrolysis of phosphate polymers was also included in the model. Using this simulation, we predicted the downwind aerosol concentration, the fraction of material in the aerosol plume, the fraction of aerosol deposited, the effect of particle growth processes on the particle size distribution, and the change in particle composition due to chemical reaction.

The series of successive first-order reactions used to model the phosphate hydrolysis reduced to a representation that was independent of particle size and plume conditions. Rate constants used in the model are based on experimental findings indicating that the phosphate hydrolysis is complete within four days.

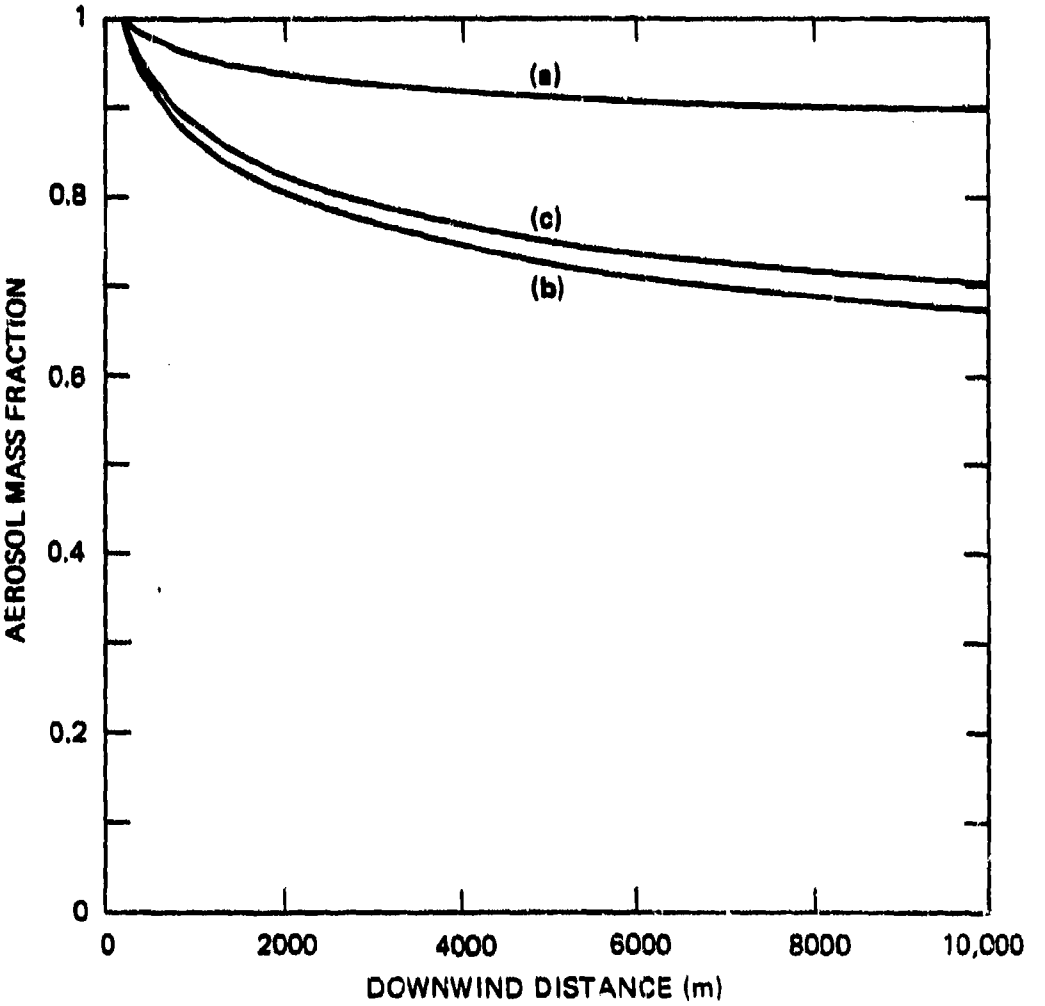

FIGURE 60 PHOSPHORUS SMOKE AEROSOL PARTICLE DEPOSITION TO VARIOUS SURFACES

(a) Rye grass; (b) Crushed gravel; (c) Water.

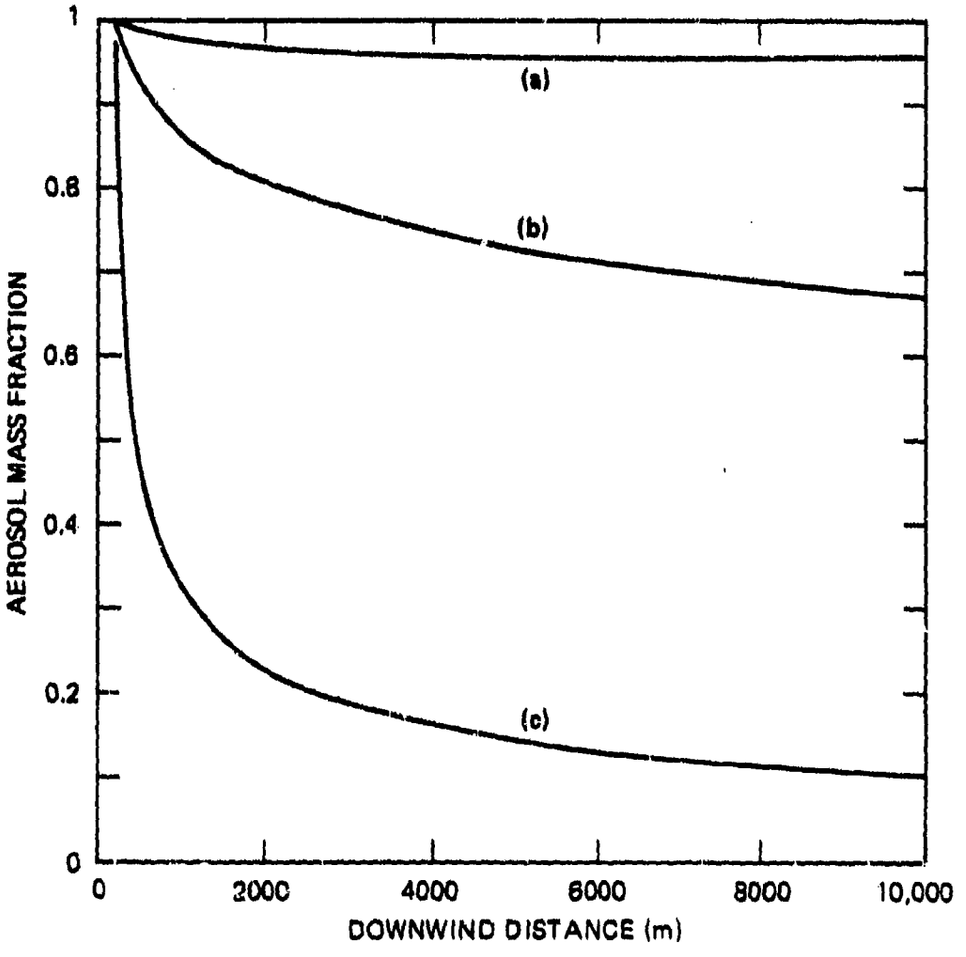

FIGURE 61 PHOSPHORUS SMOKE AEROSOL PARTICLE DEPOSITION AS A FUNCTION OF MASS MEDIAN PARTICLE DIAMETER

(a) $\bar{d}_p$ = 0.5 μm; (b) $\bar{d}_p$ = 1.3 μm; (c) $\bar{d}_p$ = 5.0 μm.

Because the atmospheric conditions and the type of terrain for a munitions burn are variable, the effects of these parameters on phosphorus dispersion were studied. Simulations varying plume expansion, wind speed, plume rise, and type of surface showed that under a wide range of atmospheric and terrain conditions, at least 50% of the aerosol remained in the atmosphere at 10,000 nm downwind.

The simulation was the most sensitive to particle diameter and its influence on deposition velocity. The mass median particle diameter produced from a munitions burn was consistently measured to be between 1.0 and 1.3 μm in diameter. Therefore, unless otherwise specified, the simulations were conducted using an initial mass median diameter of 1.3 μm.

The sensitivity of particle deposition to particle size emphasizes the importance of including the particle growth processes into the phosphorus dispersion model. Coagulation, however, proved to be significant only at concentrations higher than those that are likely to be encountered in the field. Condensation was not included in the model presented in this study. Condensation occurs relatively rapidly and it was assumed to have occurred before the initiation of the simulation, 60 sec downwind from the burn site. The incorporation of condensation into the model also would have presented some numerical difficulties. Because it is the most rapid rate process, it controls the progress of the numerical integration routine. The result is that the simulation becomes inefficient and costly. Further analysis of the effects of condensation on particle deposition can be investigated by experimentallly determining whether the particle size distribution in the plume stabilizes; if it continues to grow, condensation should be incorporated into the model.

The correlation for the deposition velocity is perhaps the weakest component of this model, as evidenced by the fact that theoretically derived expressions and the experimental correlations can give deposition velocities that vary by an order of magnitude. Because the deposition computed by the simulation is sensitive to the deposition

velocity, it should be known fairly accurately. The correlation developed by Schack et al. (in press) is the most suitable available representation of deposition velocity; however, there are difficulties with its application. Deposition experiments are known to scale-up rather poorly, and the results can be dependent on the experimental apparatus. The deposition data used in this model were limited to controlled rough surfaces of a homogeneous composition. A natural terrain is heterogeneous, consisting of a variety of surface types. SRI believes that controlled laboratory deposition studies on heterogeneous surfaces need to be performed so that a more confident prediction of deposition velocity can be obtained.

IX DISCUSSION AND CONCLUSIONS

The use of smoke in military training exercises will deploy many components into terrestrial, aquatic, and atmospheric environments. The major components on a mass basis are the condensed linear polyphosphates. By applying solution-phase chemistry to the aerosol particle, we projected that the linear polyphosphates would undergo acid-catalyzed hydrolysis to orthophosphoric acid, with a half-life of 2 days. That fraction of aerosol that deposits on terrestrial or aquatic surfaces where neutralization can occur will be subjected to both aerobic and anaerobic microbial transformations, which are nutrient-dependent. In soils and water, half-lives of up to 15 days are projected in system a containing at least 1×10^5 organisms/ml (g). The cyclic metaphosphates, which are apparently formed by catalytic events on linear polyphosphates in natural waters, are much more stable to acid hydrolysis and microbial transformations than their linear analogs. However, aerobic and anaerobic bacteria were found to hydrolyze these compounds, with half-lives of 15 to 20 days. This transformation was also observed to be nutrient-dependent.

Phosphorous acid (H_3PO_3) was found to be stable in aerated water but could be oxidized to orthophosphoric acid by microorganisms. Half-lives of 25 to 35 days, including acclimation periods of 15 to 25 days, were observed in two natural water systems. This biotransformation was found to be inversely related to the amounts of extra organic nutrients present in the system, which tended to slow the transformation. However, the transformation still occurred and suggests that the persistence of phosphorous acid will be controlled by microbial populations.

Elemental phosphorus (P_4) in the vapor phase will react extremely rapidly with atmospheric oxygen to produce the phosphorus oxides mentioned above. Thus, the overall fate of P_4 in the vapor phase will be controlled by oxidation and acid hydrolysis to produce orthophosphoric acid. This

reactivity to oxygen minimizes the possibility that any P_4 deposition in terrestrial or aquatic environments will occur from the vapor phase.

Phosphine (PH_3) was observed to be produced from the incomplete combustion of WP/F and from the solid-phase oxidation of RP/BR as a function of relative humidity. Based on its high vapor pressure and low water solubility, PH_3 will rapidly volatilize into the atmosphere. In the atmosphere, PH_3 will be subjected to oxidative transformations resulting from ozone and hydroxyl radical, yielding half-lives of 8 and 5 hr, respectively. In the presence of sunlight, transformation rates are enhanced ($t_{1/2}$ = 2.3 hr) due to interactions with tropospheric agents that are not completely understood. We project, however, that PH_3 will not be a persistent chemical in the environment.

The modeling of the smoke aerosol projected that at least 50% of the aerosol remained in the atmosphere at 10,000 m downwind. Because acid hydrolysis predominates in the aerosol phase, the major component of aerosol deposition after 20 hr will be orthophosphoric acid; in the immediate vicinity of the burn, the heavier particles--including the condensed polyphosphates--could contaminate surrounding environments. Overall, however, the products of WP/F and RP/BR combustion are readily controlled by environmental mechanisms that convert these materials to orthophosphoric acid.

Incompletely combusted WP/F and RP/BR or disposed smoke devices from manufacturing practices were found to persist in terrestrial and aquatic environments for an exceptionally long time. The fate of WP/F or RP/BR buried in soil will be controlled by the diffusion of oxygen through the soil, the diffusion of oxygen through surface-oxide layers that build up on phosphorus, the surface area of the phosphorus, and the depth at which the phosphorus is buried. For a 1-cm^3 piece of white phosphorus buried 12 cm in soil, the lifetime is expected to range from 10 years in the absence of a surface-oxide layer to 10,000 years in the presence of a surface-oxide layer. RP/BR is expected to persist longer due to its slower reactivity with oxygen.

The persistence of WP/F in water is controlled by the readiness of the phosphorus to dissolve into the aqueous phase. Due to the low water solubility of P_4, dissolution is slow and a lifetime of 48 years is projected for a 1-cm-diameter piece of WP. On the other hand, RP/BR has essentially no water solubility and oxidation at the water-solid interface will control the lifetime of RP. On the basis of the slower reactivity of RP with oxygen relative to WP, lifetimes are expected to be in excess of 48 years.

The lifetime of soluble P_4 in the aquatic environment will be controlled by volatilization in shallow or highly turbulent water bodies, a factor overlooked by previous investigators, leading to a wide range of reported rate constants for the loss of P_4 in water. In a stream 1 m deep, the half-life is estimated to be 50 min. As depth increases and turbulence decreases, the persistence of soluble P_4 is controlled by hydrolytic and oxidative processes. These processes occur at approximately equivalent rates, yielding a half-life of 42 hr. These processes, however, can be mitigated by naturally occurring organics that may provide stability to P_4 solutions in water. The exact nature of these stability mechanisms is unknown and caution should be used in estimating persistence of soluble P_4 in deep water bodies with low turbulence.

LITERATURE CITED

Alexander, M. 1977. Introduction to soil microbiology John Wiley & Sons, New York, N.Y. P. 348.

Atkinson, R., W.P.L. Carter, A. M. Winer, and J. N. Pitts (1981) An Experimental Protocol for the determination of hydroxyl radical rate constants. J. Air Poll. Control Assoc. 31 1090.

Atkinson, R., K. R. Darnall, A. C. Lloyd, A. M. Winer, and J. N. Pitts (1979). Kinetics and mechanisms of reactions of hydroxyl radical with organic compounds in the gas phase Adv. Photochem. 11 375.

Batlino, R. and H. L. Clever (1966). The solubility of gases an liquids. Chem. Rev. 66 395-463.

Berkowitz, J. B., G. S. Young, R. C. Anderson, A. J. Colella, W. J. Lyman, A. L. Preston, W. D. Steber, R. G. Thomas, and R. G. Vranka (1981). "Occupational and Environmental Hazards Associated with the Formation and Use of White Phosphorous-Felt and Red Phosphorous-Butyl Rubber Screening Smokes." Arthur D. Little, Final Report, Contract No. DAMD17-79-C-9139.

Bomberger, D. L., J. L. Gwinn, W. R. Mabey, D. Tse, and T. W. Choi (1982). Environmental fate and transport at the terrestrial interface. Chapter 10 in "Fate of chemicals in the environment, ACS Symposium Series 225.

Calvert, J. G. and J. N. Pitts, Jr. (1966). Photochemistry John Wiley & Sons, INc., New York, pp. 780-782, 795-798.

Casida, Jr., L. E. 1980. Microbial oxidation and utilization of orthophosphate during growth. J. Bacteriol. 80:237.

Claussen, W. F. (1951). A second water structure for inert gas hydrates. J. Chem. Phys. 19 1425-1426.

Crutchfield, M. M., C. H. Dungan, J. H. Letcher, V. Mark, J. R. Van Wazer, 1967. P^{31} Nuclear Magentic Resonance. Interscience Publishers, New York.

CRC Press (1973) Handbook of Chemistry and Physics, 54th Edition.

Dainton, F. S. and J. C. Bevington (1945). The oxidation and inflammation of yellow phosphorus. J. Chem. Soc. 377-388.

Davidson, C. I., J. M. Miller, and M. A. Pleskow (1982). The influence of surface structure on predicted particle dry deposition to natural grass canopies. Water, Air and Soil Pollution 18, 25-43.

Fluck, E. (1972) Chemistry of Phosphine. Fortschr. Chim. Forsch. 35 1-64.

Friedlander, S. K. (1977) In: Smoke, Dust, and Haze. John Wiley & Sons, Inc. New York, New York.

Gelbard F. (1982) "MAEROS Users Manual," Sandia National Laboratories, No. SAND BO-0822.

Gelbard F., and J. H. Seinfeld (1980). Simulation of multicomponent aerosols dynamics. J. Coll. Int. Sci. 78, 485-501.

Gill, J. B. and S. A. Riaz (1969). Kinetics and degradation of long chain polyphosphates. J. Chem. Soc. (A) 183-187.

Gilliam, J. W., and E. C. Sample 1968 Hydrolysis of pyrophosphates in soils: pH and biological effects. Soil Sci. 106:352.

Griffith, E. J. and R. L. Buxton (1965). The preparation and properties of the 12-membered ring hexametaphosphate anion. Inorg. Chem. 4 549-551.

Griffith, E. J. and R. L. Buxton (1967). The preparation and properties of tetra-, penta-, hexa-, hepta-, and octaphosphates J. Am. Chem. Soc. 89 2884-2890.

Halmann, M. and I. Platzner (1961). The photochemistry of phosphorus compounds IX photolysis of sodium hydrogen phosphate in aqueous solution. J. Phys. Chem. 70 2281.

Hooper, F. (1973) Origin and Fate of organic phosphorous compounds in aquatic systems. In Griffith E. et al. ed Environmental Phosphorus Handbook. John Wiley & Sons, Inc., New York, N.Y. (p. 179).

Kenaga, E. E. and C. A. Goring (1978). Relationship between water solubility, soil sorption, octanol-water partitioning and bioconcentration of chemicals in biota. In: Third Aquatic Toxicology Symposium, October 17-18, New Orleans. American Society for Testing Materials, Philadelphia.

Leo, A., C. Hansch, and D. Elkins (1971). Partition coefficients and their uses. Chem. Rev. 71 525-616.

Lorenz, K. and R. Zellner (1982). XV Informal Conference on Photochemistry, June 27-July 1, Stanford, CA.

Lynden-Bell. 1969. Nuclear Magnetic Resonance Spectroscopy. Appleton-Century-Crofts Publishers, New York.

MacKay, D., W. Y. Shiu, R.P.L. Sutherland (1979). Determination of air-water Henry's Law constants for hydrophobic pollutants. Environ. Sci. Technol. 13 333-337.

NBS 500 (1952). Circular of the National Bureau of Standards.

Osterheld, R. K. (1972). Nonenzymatic hydrolysis at phosphate tetrahedra. In Topics in Phosphorus Chemistry, Vol. 7. E. J. Griffith and M. Grayson (eds) John Wiley & Sons, New York.

Parnas R., and S. K. Friedlander (1984). Particle deposition by diffusion and interception from boundary layer flows. Aero. Sci. Tech. 3, 3-8.

Peck, H.D., C. L. Liu, A. K. Varma, L. G. Ljungdall, M. Saulczynski, F. Bryant, and L. Carreira (1983). The utilization of inorganic pyrophosphate, tripolyphosphate, and tetrapolyphosphate as energy sources for the growth of anaerobic bacteria. In, Basic Biology of New Development in Biotechnology. A. Hollaender (Ed.), Plenum Press, New York pp 317-348.

Sanderson, R. T. (1971) Chemical Bonds and Bond Energy Academic Press, New York.

Schack C., B. S. Pratsinis, and S. K. Friedlander (in press). A general correlation for deposition of suppended particles from turbulent gases to completely rough surfaces. J. Atmos. Environ.

Seinfeld, J. H. (1975). In: Air Pollution. McGraw-Hill, New York, New York, 260-346.

S. Skinner (1887) Proc. Royal Soc. 42 283.

Small, H. and T. E. Miller (1982). Indirect photometric chromatography. Anal. Chem. 54 462-469.

Stock, A., W. Bottcher, and W. Lenger (1909). Einwirkung von flussigem ammoniak auf die beiden festen phosphorwasserstoffe. Chemische Ber. 42 2853-2857.

Sullivan, J. H., J. D. Putnam, M. A., B. C. Pruitt, J. C. Nichols, and J. T. McClare. 1979. A summary and evaluation of aquatic environmental data in relation to establishing water quality criteria for munitions-unique compounds. Part 3: White Phosphorus. Final Report, U.S. Army Medical Research and Development Command, Contract DAMD17-77-C-7027.

Sutton C. D., and S. Larsen 1964 Polyphosphate as a source of phosphorous for plant Soil Sci. 97-196.

Sutton, C. D., D. Gunary, and S. Larsen 1966. Pyrophosphate as a source of phosphorous for plant:II. Hydrolysis and initial uptake by a barley crop. Soil Sci. 101:199.

Van Wazer, J. R. 1958. Phosphorus and It's Compounds. Vol. I. Interscience Publishers, New York.

Weston, R. E. (1954). The solubility of phosphine in aqueous solution. J. Am. Chem. Soc. 76 1027-1028.

Yalkowsky, S. H. and S. C. Valvani (1980). Solubility and Partitioning I: Solubility of nonelectrolytes in water. J. Pharm. Sci. 64 912.

Yamaguchi, H., T. Nakamara, Y. Hirai, and S. Ohashi (1979) High-performance liquid chromatographic separation of linear and cyclic condensed phosphates. J. Chromatog. 172 131-140.

Appendix A

NOMENCLATURE FOR TERRESTRIAL AND AQUATIC MODELING

A	Area of phosphorus surface
C	Concentration of dissolved phosphorus in water
C_{air}	Concentration of air
C_{O_2}	Concentration of oxygen in soil
C^*	Solubility limit of phosphorus in water
D	Diffusivity of phosphorus in water
D_s	Diffusivity of oxygen in soil
D_{ox}	Diffusivity of oxygen in solid layer
d	Depth below surface phosphorus piece is buried
erfc	Complementary error function
K	Dimensionless reaction rate constant $\frac{kR_o^2}{D}$
k	Reaction rate constant for red phosphorus oxidation or white phosphorus destruction in water
M_C	Mass of phosphorus
M_{C_o}	Initial mass of phosphorus
R	Radius of piece of phosphorus
R_o	Initial radius of piece of phosphorus
r	Radial distance
r^*	Radius of unreacted phosphorus in a piece where a solid layer forms
s	Dummy variable of integration in Equation 17
t	Time
y	Distance
Ω	Dimensionless radial coordinate
ρ	Density
T	Dimensionless time $\frac{tR}{R_o^2}$

Appendix B

DEPOSITION VELOCITY MODEL

Deposition efficiency, η is defined as follows:

$$\eta = \frac{\text{particles/sec depositing on single cylindrical element}}{\text{particles/sec passing through projected cylinder area } d_f h}$$

Deposition efficiency by diffusion (Parnas 1984)

$$\eta_d = 1.88\ Re^{-1/2}\ Sc^{-2/3}$$

$$Re = \frac{U_o d_f}{\nu} \quad Sc = \nu/D$$

where

U_o = velocity
ν = kinematic viscosity
d_f = fiber diameter
D = diffusivity.

Deposition efficiency by interception (Parnas 1984)

$$\eta_I = 0.80\ R^2\ Re^{1/2}$$

$$R = d_p/d_f$$

where

d_p = particle diameter
d_f = fiber diameter

The overall efficiency becomes:

$$\eta = 1 - [(1-\eta_d)\ (1-\eta_I) \approx$$

In terms of the dimensionless mass transfer number (Sherwood No.) for a cylinder

$$\frac{kd_\rho}{D} = \frac{\pi RPe}{\pi} \qquad Pe = \frac{d_f U_o}{D}$$

The mass transfer coefficients to an individual cylinder

$$k = H\frac{U_o}{\pi} \qquad [m/sec]$$

Particle deposition rate to single roughness element

$$J = kA_f C \qquad [kg/sec - element]$$

where

A_f = surface area of element

Flux to roughness surface

$$J_g = \rho_f kA\ C \qquad [kg/m^2\ sec]$$

where

ρ_f = density of roughness elements [elements/m^2]

Filtration deposition velocity

$$V_f = J_f/C = \rho_f kA_f \qquad [m/sec]$$

Overall deposition velocity

$$V_d = V_f + V_s$$

Where V_s is gravitational settling velocity

$$V_s = \frac{\rho_p g d_p^2}{18 \mu} C$$

where

ρ_p = particle density

g = gravitational constant

μ = viscosity

and the slip correction factor is given by:

$$C = 1 + \frac{2\ell}{d_p}\left(1.37 + 0.4 \exp\left|\frac{0.55 d_p}{\lambda}\right|\right)$$

where

ℓ = mean free path.